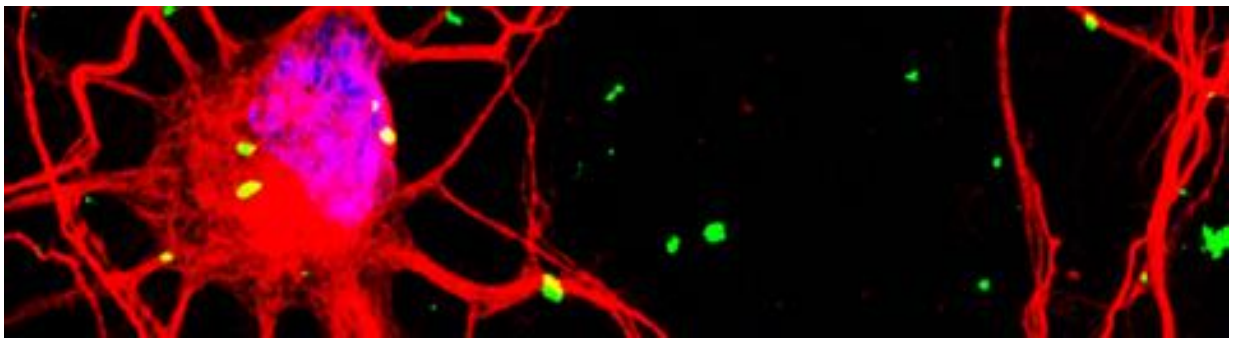

Corso di Dottorato in Neuroscienze
Curriculum Neuroscienze e Neurotecnologie
Ciclo XXXI

ATP6V1A: from organelle acidification to Early Onset Epileptic Encephalopathies

Candidate: Alessandro Esposito
Supervisors: Fabio Benfenati
Anna Fassio

ISTITUTO ITALIANO DI TECNOLOGIA

UNIVERSITÀ DEGLI STUDI DI GENOVA

Contents

1. Introduction

1.1 The vacuolar (H+)-ATPase (V-ATPase)

The vacuolar (H^+) ATPase (v-ATPase) is a large multimeric complex that couples ATP hydrolysis to transport of protons. V-ATPase is composed of 14 subunits organized in two domains : a peripheral V_1 domain that hydrolyses ATP and an integral V_0 domain that translocates protons by a rotary mechanism (Nishi and Forgac, 2002) (Figure 1). V-ATPase is responsible for membrane trafficking processes such as receptor-mediated endocytosis, intracellular trafficking of lysosomal enzymes, and acidification of intracellular organelles in all eukaryotic cells (Forgac 2007; Cotter et al., 2015).

1.2 Structure

As mentioned before, V_1 domain is responsible for ATP hydrolysis. It is composed by eight subunits (A-H) some of which present in more than one copy. V_1 domain includes three copies of subunits A and B, two copies of subunits G and E, one or more copies of subunit H and a single copy of the other subunits (C, D, F) (Figure 1).
The three subunits A and the three subunits B form a hexamer of about 400KDa: They alternate in the hexame, to form a cylinder, in which three ATP-hydrolysis sites are present between A and B subunits. Most of the residues, which participates in the catalytic site, belong to subunit A. In the other interfaces, a binding site for nucleotides is present, and most of the residues which participate in this site belong to subunit B, which seems to have a modulatory role (Nishi and Forgac, 2002). Subunits D and F serve as a rotor that couples the energy derived from ATP hydrolysis to the rotation of subunits in the V_0 domain (Forgac, 2007). Subunits G and E (Ohira et al.,

2006) form two heterodimers (Féthière et al., 2005) which probably interact with subunit C and subunit H respectively (Wilkens et al., 2004) (Zhanga et al., 2006) . Together, they act as a stator, preventing the rotation during ATP hydrolysis.

The integral V_0 domain serves as a proton translocator across the membrane. It is composed of subunits a, d, e, c and c''. There are four or five copies of subunit c and single copies of the remaining subunits (Nishi and Forgac, 2002). Subunits c, c' and c'' are highly hydrophobic, they are arranged to form a proteolipid ring (Wilkens et al., 2004). Each of them contains a buried glutamate (Glu) residue located in transmembrane helix-4 (TM4) of subunit c and c' and TM3 of subunit c''. These Glu residues undergo protonation during proton transport (Nishi and Forgac, 2002). The a-subunit has a hydrophilic N-terminal domain that is oriented towards the cytoplasmic surface, and a C-terminal domain that contains eight or nine transmembrane helices (Nishi and Forgac, 2002). In TM7 there is a buried arginine (Arg) residue also required for proton transport (Nishi et al., 2001).

The V_0 domain also contains subunit d, which provides connection between the V1 domain and the V_0 domain (Iwata et al., 2004) (Figure 1).

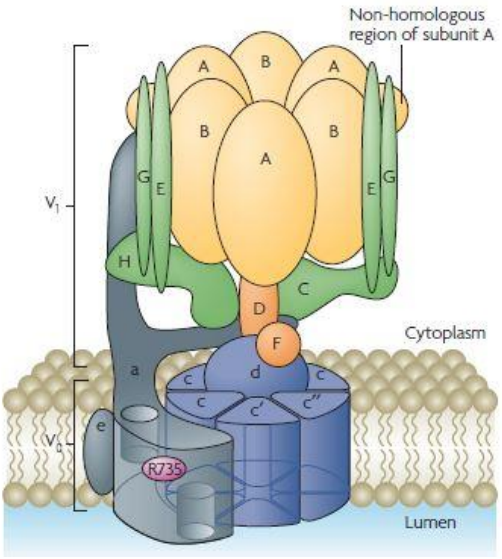

Figure1. Structure of v-ATPase.

The vacuolar (V⁻)ATPase complex is composed of a peripheral domain (V_1, shown in yellow and orange), which is responsible for ATP hydrolysis, and an integral domain (V_0, shown in blue and grey), which is involved in proton translocation across the membrane. The core of the V_1 domain is composed of a hexameric arrangement of alternating A and B subunits, which participate in ATP binding and hydrolysis. The V_0 domain includes a ring of proteolipid subunits (c, c' and c'') that are adjacent to subunits a and e. The V_1 and V_0 domains are connected by a central stalk, composed of subunits D and F of V_1 and subunit d of V_0, and multiple peripheral stalks, composed of subunits C, E, G, H and the N⁻terminal domain of subunit a . Subunit a possesses two hemi-channels and a crucial buried Arg residue (R735), which are required for proton translocation across the membrane. From Forgac, 2007.

1.3 Assembly

V-ATPases are large multi-subunit complexes that operate in multiples intracellular organelles and at plasma membrane. Each component is expressed in the right quantity, correctly assembled in the final enzyme and targeted to the ultimate destination. This is particularly challenging since v-ATPase is made by peripheral and integral components. Indeed, both transcriptional and post-transcriptional mechanisms regulate these processes (Holliday et al., 2014).

In yeast, the assembly of V_0 domain is dependent on a set of dedicated chaperones that reside in the endoplasmic reticulum (ER) (Laurie et al., 2004), such as the integral proteins Vma12 (vacuolar membrane ATPase activity-12), Vma21, the peripheral membrane protein Vma22 and the identified Pkr1 (Graham et al., 1998, Davis-Kaplan et al., 2006). Vma21 appears to promote the assembly of the proteolipid ring in the ER and the binding of subunit d to this complex, through the interaction with subunit c'. It also accompanies V_0 exit from ER. Vma12 and Vma22 interact transiently with a-subunit and mediate its assembly with the proteolipid ring (Graham et al., 2003). Pkr1 increases the efficiency of V_0 assembly and export

(Davis-Kaplan et al., 2006). Homologous of these chaperones have been identified in higher eukaryotes (Per Malkus et al., 2004), but their role in v-ATPase assembly remains to be established (Forgac, 2007)

The translation of V_1 domain subunits happens in the cytoplasm, their assembly can occur in absence of subunit C, provided that all the remaining subunits are present (Kane et al., 2006). There is an alternative route for the assembly of the two domains: subunit A begins to assemble with V_0 subunits (in particular, the a-subunit) before V_0 is completely assembled (Kane et al., 2006). The conditions that might promote one pathway over the other are still unclear. Once the V_0 domain is complete, it is exported to the Golgi apparatus. Here, Vma21 can be recycled back to the ER, and the V0 domain can interact with V_1 domain on the cytoplasmic side: assembly of V_0 complexes can occur either with almost fully assembled V_1 domain (lacking subunit C) plus free subunit C or by assembly with individual V_1 subunits or sub-complexes (Forgac, 2007).

1.4 Proton transport

The v-ATPase rotary mechanism has been studied in bacteria (Imamura et al., 2003) and yeast (Hirata et al., 2003). Protons are first loaded into the V_0 domain (Figure 2a): the cytoplasmic side of a-subunit has an aqueous hemi-channel trough which protons can reach the buried Glu residues in the proteolipid subunits (E137 in subunit c, E145 in subunit c' and E108 in subunit c'') and protonate them as previously proposed for ATP synthase (Steven et al., 2000) (Fillingame et al., 2003) (Figure. 2b). The residues remain protonated as they are subsequently placed in contact with the hydrophobic environment of the bilayer.

Rotation is facilitated by ATP hydrolysis at catalytic sites located on the interface of subunits A and B in the V_1 domain. This hydrolysis drives the rotation of the central rotor (subunit D and F) of V_1 connected to subunits d and the ring of proteolipid subunits of V0 (Figure 2c).

Following rotation, protonated Glu residues reach another aqueous hemi-channel on luminal side of subunit a, from which they enter into the lumen (Figure 2d). For proton transport a crucial buried Arg residue (R735) in transmembrane helix-7 (TM7) of subunit a is absolutely required. Other buried residues of the c-terminal subunit a (H743, E789, R799) line the lumenal hemi-channel trough which protons exit the membrane, thereby making the lumen more acidic (Nishi and Forgac, 2002).

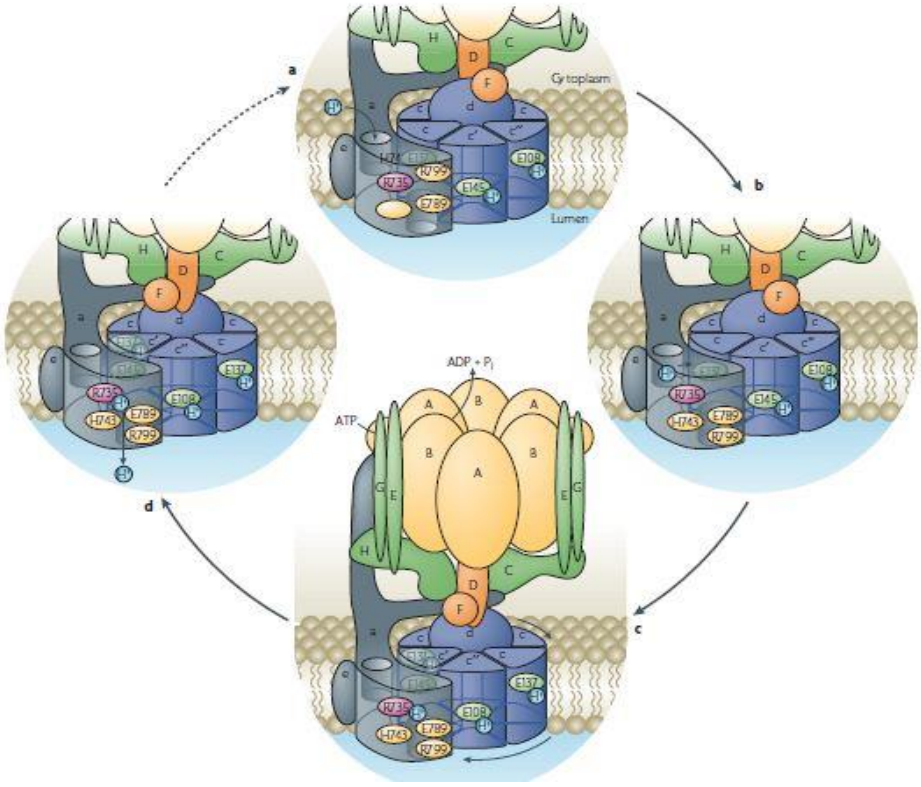

Figure 2: Proton transport cycle.

Protons enter through the a subunit from a hemi-channel on the cytoplasm side (a), and interact with buried Glu residues in the proteolipid subunits (E137 in subunit c, E145 in subunit c' and E108 in subunit c'') protonating them (b). The hydrolysis of ATP on the ctoplasmic side facilitates the rotation of the rotary assembly (subunits D, F, d and the ring

of proteolipid subunit c, c' and c'') which causes active transport of protons (c). Protonated Glu residues reach another aqueous hemi-channel on luminal side of subunit a, from which they can enter the lumen. To enter the lumen, it is important the interaction between protons and the Arg735 residue (d). From Forgac, 2007.

1.5 Functions of v-ATPase

The canonical functions of v-ATPase rely on its ability of pumping H^+ and its function is crucial for the characteristic Ph of each intracellular organelles. V-ATPases-dependent acidification drives various processes as receptor-ligand uncoupling after endocytosis and to activate enzymes such as cathepsins. Additional roles of V-ATPase are the creation of an electrochemical gradient in the secretory vesicles to couple the neurotransmitters transport inside the vesicle and a more recent role in the fusion of these vesicles with the plasma membrane (Figure 3).

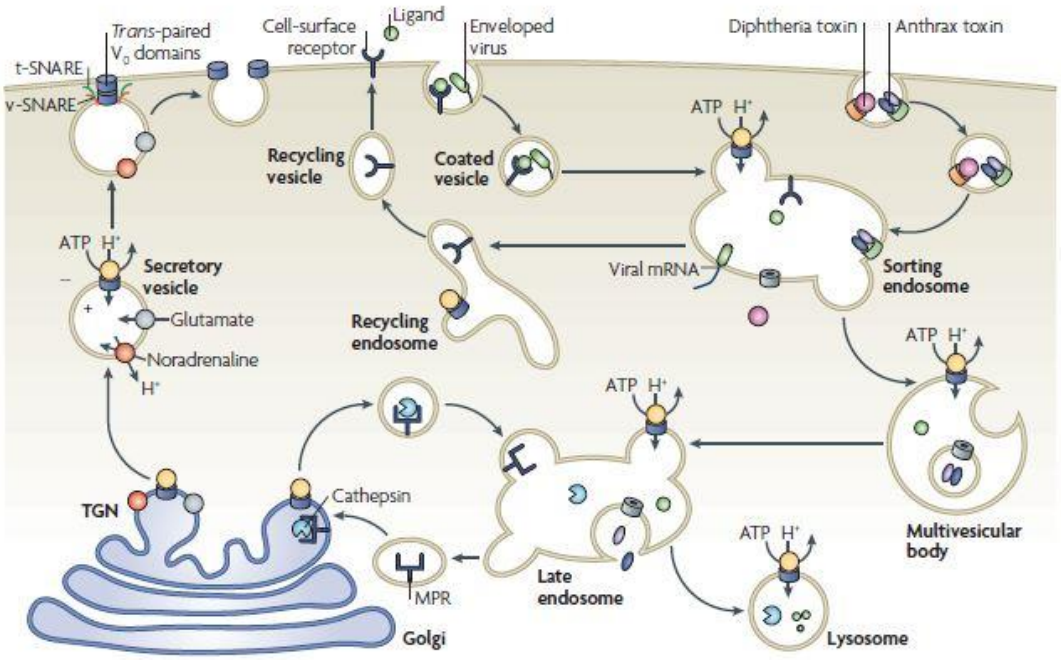

Figure 3: functions and localizations of v-ATPases.

V-ATPase is located on intracellular organelles like sorting endosome, multivesicular body, lysosome, late endosome, secretory vesicle. V-ATPase can acidify intracellular organelles and this process is necessary for their function. From Forgac, 2007

1.6 Membrane Traffic

Extracellular ligands can be internalized by receptor-mediated endocytosis from the plasma membrane and trafficked to the sorting endosome (Maxfield et al., 2004). Here v-ATPases generate acidic pH, which drives the uncoupling of internalized ligand-receptor complexes (Forgac, 2007). This facilitates the recycling of unoccupied receptors to the plasma membrane and targeting of ligands to the lysosome for degradation through multivesicular bodies (MBVs, also known as "endosomal carrier vesicles") (Maxfield et al., 2004). Formation of MVBs is also dependent on lumenal acidic pH (Clague et al., 1994).

Acidification of late endosomes by the v-ATPase is also important in intracellular trafficking of newly synthetized lysosomal enzymes from the Golgi to lysosomes. These enzymes have a Mannose-6-phosphate tag recognized by their receptor in the Trans-Golgi network (TGN) which allows the delivery of the complex to the late endosomes (Ghosh et al., 2003). Here, low pH provided by v-ATPases causes the release of the inactive enzyme and the recycling of the receptor to the TGN. Progression to the acidic lysosome results in a conformational change of the enzyme and thus its activation. The low pH also triggers conformational changes in proteins, making them more susceptible to proteolytic degradation. Within these compartments, v-ATPases provide the necessary proton gradient to drive coupled transport of small molecules and ions. Therefore, breakdown products of macromolecules, such as amino acids, are effluxed from the lysosome into the

cytoplasm by H^+/amino acid cotransporters using the proton gradient generated by v-ATPases (Hinton et al., 2009).

Moreover, the proton and membrane potential gradients established by the v-ATPases are used to drive the uptake of small molecules, such as neurotransmitters, as it will be discussed in follow section (1.8.1).

Furthermore, since v-ATPase interacts with actin (Vitavska et al., 2003), it has been speculated that the v-ATPase promotes the regulation of cytoplasmic G-actin pool, as well as crosslinking and stabilization of actin into filaments (Vitavska et al., 2005). By connecting vesicles to actin filaments, the v-ATPase is thought to play a role in vesicular sorting and transport during exocytosis and recycling (Maxson et al., 2014).

1.7 Membrane fusion

One novel function of v-ATPase is membrane fusion. There are evidences of the transmembrane electrochemical H^+ gradient requirement for fusion of synaptic or secretory vesicles (Poëa-Guyon et al., 2013). However, subsequent studies have pointed out a structural role of the v-ATPase, largely based on yeast vacuolar fusion experiments (Peters et al., 2001). It was proposed that, following soluble NSF attachment protein receptor (SNARE)-mediated docking, the V_0 domains of two adjacent membranes form a trans-complex, thereby creating a fusion pore that aids vesicle fusion through a mixing of the highly hydrophobic proteolipid subunits of the two V0 domains. Subsequent experiments in synaptic vesicle release in Drosophila neurons (Hiesinger et al., 2005) and fusion cuticle-containing vesicles of epidermal cells (Liegeois et al., 2006) in *C. elegans* suggest that this mechanism is not only restricted to the yeast's vacuole. However, the debate is still ongoing, with some groups supporting the original conclusion, namely the acidification, rather than the formation of the fusion pore the main role of v-ATPase in vesicle fusion.

1.8 V-ATPase in neurons

Despite the ubiquitous role in pH homeostasis and intracellular signaling pathways, the v-ATPase complex is expressed at high levels in neurons where it plays additional and unique roles in neurotransmitter loading into synaptic vesicles and in the regulation of synaptic transmission (Morel and Poëa-Guyon, 2015; Bodzeta et al., 2017).

One of the major roles of v-ATPases in neurons is to provide the electrochemical potential, acidic and positive inside the synaptic vesicle (SV), that contributes to the loading of the SVs with neurotransmitters by specific vesicular transporters (Edwards et al., 2007). Debated findings have suggested that v-ATPase membrane domain (V_0) also contributes to $Ca2^+$-dependent transmitter release via a direct role in vesicle membrane fusion (Morel and Poëa-Guyon, 2015).

1.8.1 Energy coupling

In neurons, neurotransmitters (NTs) are synthesized, stored and released in highly specialized domains, the nerve terminals, where they are accumulated in synaptic vesicles by specific transporters (Edwards et al., 2012).

V-ATPases are present in the membrane of every synaptic vesicle in one or two copies (Stadler and Tsukita 1984; Yamagata et al., 1989) and they generate a large electrochemical proton gradient with pH around 5.5 inside the synaptic vesicles (Michaelson et al., 1980; Füldner et al., 1982). Acidification of synaptic vesicles by v-ATPase energizes the accumulation of neurotransmitters in these organelles and is therefore required for efficient synaptic transmission.

The filling of synaptic vesicles with neurotransmitter depends on the energy stored in a H^+ electrochemical gradient ($\Delta\mu H^+$) produced by the v-ATPase. $\Delta\mu H^+$ in turn comprises both a chemical gradient ($\Delta\mu H$) and membrane electrical gradient ($\Delta\psi$), and the transport of all classical transmitters into synaptic vesicles depends on these gradients.

Pharmacological inhibition of v-ATPase activity blocks neurotransmitter loading without affecting neurotransmitter release from already loaded vesicles (Poëa-Guyon et al., 2013) as seen blocking neurotransmitter transporters.

From pharmacological and biochemical data, it has been estimated that only one or two molecules are present per synaptic vesicle (Takamori et al., 2006), laying emphasis on the strategic position of this large protein complex in the functional control of loading and, possibly, of exocytosis of SVs.

1.8.2 Synaptic vesicle fusion

Neurotransmitter release by synaptic vesicle exocytosis proceeds in several steps:

The neurotransmitter is internalized, accumulated and stored in synaptic vesicles (SVs), by specific transporters that use the large electrochemical proton gradient generated by v-ATPase as described above (Edwards et al., 2012). It is generally assumed that all the vesicles in the nerve terminals are filled with NT, but it could also not to be the case, especially under sustained synaptic activity. SVs acquire competence for release, entering in the releasable pool, through the docking and priming steps (Imig et al., 2014). As in intracellular membrane fusion events, this involves SNARE proteins that associate in a tight SNARE complex: VAMP2 (also named synaptobrevin-2), the v-SNARE protein anchored at synaptic vesicle membrane, forms a trans-complex with two SNARE proteins of the presynaptic membrane (t-SNAREs): syntaxin-1 and SNAP-25. The soluble protein Munc-18

binds sintaxin-1 in its closed conformation, and remains attached during the complex formation, controlling the proper SNARE complex assembly (Südhof et al., 2009). In addition, SNARE complex assembly is also controlled by Munc-13, which binds proteins in the active zone (the specialized portion of the presynaptic plasma membrane where synaptic fusion takes place), helping in positioning the synaptic vesicle in close proximity to voltage-gated calcium channels (Südhof et al., 2012).

The calcium-influx, generated by the arrival of the Action Potentials (APs), triggers neurotransmitter release from primed vesicles via the action on additional proteins as synaptotagmins and complexins. Synaptotagmins are calcium-binding synaptic vesicle proteins that associate with SNARE complex and clamp it until the calcium-binding. Complexins are small soluble proteins that binds to the assembled SNARE complexes and act as synaptotagmin cofactors (Südhof et al., 2009). Upon calcium entry, synaptotagmins trigger membrane fusion. The two lipid bilayers merge at the contact site, and then an aqueous pore (the fusion pore) opens, connecting the synaptic vesicle lumen with the extracellular space, allowing neurotransmitters to be released. Expansion of the fusion pore makes the synaptic vesicle completely fuse. Alternately, the fusion pore may close without expanding, a process called kiss-and-run. The nature of the fusion pore, purely lipidic or containing proteolipids or proteins, is still unknown.

In recent times, some works support the hypothesis the hydrophobic V_0 v-ATPase membrane domain could be involved in membrane fusion (Peters et al., 2001) and neurotransmitter release (Morel et al., 2011).

As noted above, at nerve terminals v-ATPase is present both on synaptic vesicle membrane and on the pre-synaptic membrane. The functional significance of its expression at pre-synaptic plasma membrane is a matter of debate, even if it has been

recently shown to be involved in stimulation-dependent alkalinization of the cytoplasm, which may regulate endocytosis (Zhang et al., 2010).

The V_0 membrane domain of the v-ATPase was shown to interact with proteins that are involved in exocytosis: the SNAREs and calmodulin in its calcium-bound form and this would regulate the SNARE complex assembly (Wang et al., 2014).

VAMP-2 associates with V_0 via its membrane-proximal region, and this interaction excludes subunits of the V_1 catalytic sector. A VAMP-2 binding site has been demonstrated in c-subunit, in the loop between the transmembrane domains 3 and 4, which is exposed to the cytosol after dissociation of V_1. This interaction does not affect the formation of the SNARE complex, it occurs probably as a cis complex within the same membrane. The stoichiometry estimated is 1:1 thus the c-subunit hexamer could potentially bind six v-SNARE (Di Giovanni et al., 2010).

An interaction of V_0 with the t-SNARE syntaxin-1 has also been reported (Hiesinger et al., 2005; Wang et al., 2014), in agreement with data from yeast (Peters et al., 2001). Syntaxin-1 appears to bind to coiled-coils domains at the N-terminus of the a1 Drosophila orthologue (Hiesinger et al., 2005).

This interaction could occur either as a trans complex formed by a vesicular V_0 and syntaxin-1 in the presynaptic membrane, therefore, concerning a limited number of already docked synaptic vesicles, or as a cis-complex within the presynaptic plasma membrane, unrelated to secretory vesicles. The functional relevance of the latter remains to be elucidated.

V_0 was also shown to interact with Ca2+/calmodulin (Peters et al., 2001; Wang et al., 2014) via a calmodulin-binding site in the a-subunit. Calmodulin is a small, ubiquitous Ca2+-dependent regulator of cell biological processes. During prolonged stimulations, calmodulin bound to Munc-13 proteins promoting synaptic vesicle priming and replenishment of the readily releasable pool of vesicles. Priming might

also include calmodulin binding to SNAREs (Di Giovanni et al., 2010). Like complexins, calmodulin bound to VAMP-2 seems to act as a clamp that can be removed by synaptotagmin (Di Giovanni et al., 2010). By interacting with calmodulin, subunit a1 can regulate the formation of SNARE complexes (Wang et al., 2014). Instead Bodzeta et al. provide direct evidence, that unlike reported previously, v-ATPase does not play a direct role in SV fusion. Instead, v-ATPase modulates release upstream of docking to facilitate fusion of fully acidified and hence, neurotrasmitter-loaded SVs. Their results demonstrate that : (1) under resting conditions, the cytosolic V_1 domain binds with low affinity to the V_0 membrane sector of SVs at presynaptic boutons; (2) the binding equilibrium between assembled and disassembled state of the v-ATPase is shifted toward the assembled state on non-acidified SVs, (3) SV fusion competence is decreased upon locking v-ATPase in an assembled state; and (4) SVs with attached V1 in principle undergo robust release when enough time is granted for docking and priming (Bodzeta et al., 2017).

1.8.3 V_0-ATPase as a sensor of luminal pH

Based on the studies on secretory granules and their exocytosis in PC12 cells (Poëa-Guyon et al., 2013), it has also been proposed a role for the V_0 domain as a sensor of the luminal pH. Dissipating the intra-granular pH gradient was associated with an inhibition of exocytosis, and this appears correlated with the V_1-V_0 association status in secretory granules. It probably concerns a priming step that confers the competence for release, before the formation of trans-SNARE complexes. At acidic pH, V_1 would dissociate from V_0, allowing it to interact with the exocytotic complex. V_0 could also allow the exocytotic machinery to discriminate fully loaded an acidified vesicles from

vesicles undergoing neurotransmitter reloading (Poëa-Guyon et al., 2013; Morel and Poëa-Guyon, 2015).

Summarizing, v-ATPases might control neurotransmitter storage and release: in a V_1-V_0 conformation, v-ATPase translocates protons and energizes the accumulation of neurotransmitter within synaptic vesicles (Edwards et al., 2007).

When synaptic vesicles are filled with neurotransmitter, the proton electrochemical gradient is no longer dissipated and V0 could behave as an intravesicular pH sensor.V0 changes its conformation and V1 is released. V0 is now competent to participate in the regulation of SNARE complex assembly. A single c-subunit hexamer present in the vesicle could function as scaffolding to organize higher order SNARE assemblies optimal for fusion. The v-SNARE VAMP2 interacts with the proteolipid c-subunits and the t-SNARE syntaxin-1 with the N-terminal cytosolic domain of the a-subunit. These interactions, which might be regulated by calmodulin and calcium, occur during the priming-docking step allowing synaptic vesicles to enter the readily releasable pool.

Finally, V0 might facilitate lipid mixing and the formation of the fusion pore during the fusion step: the hexameric V0 c-subunit is potentially a pore-forming structure, although it does not function as such during proton transport. However, another possibility is that upon interaction between t-SNARE and v-SNARE, the energy of this zipping is enough to pull apart V0 subunits, and lipids could infiltrate with full collapse fusion (El Far et al., 2011) (Figure 4).

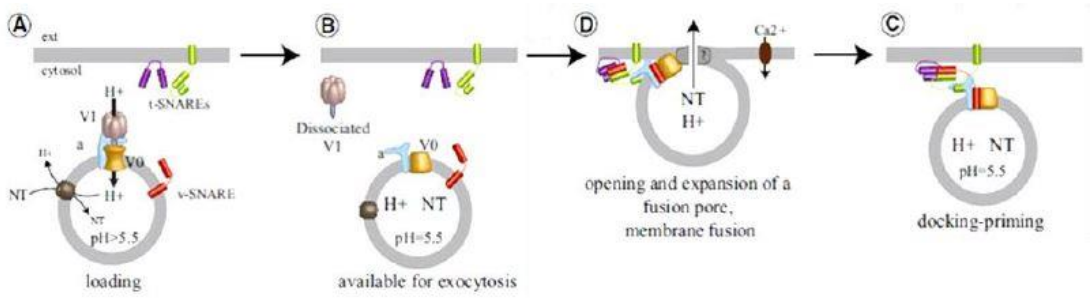

Figure 4: possible roles of V_0 subunit in synapse:

A, in association with V_1, V_0 translocates protons inside the synaptic vesicle to energize neurotransmitter influx. B, when synaptic vesicle is filled with neurotransmitters, V_0 acts as pH sensor, changing conformation and causing the release of V_1. C, V_0 could participate in the regulation of SNARE complex assembly. D, finally, upon calcium influx, V_0 could facilitate lipid mixing and the formation of the fusion pore. Modified from Morel et al. 2015

1.8.4 V-ATPase and diseases

In humans, a redundant set of subunits is encoded by 22 autosomal genes, allowing the composition of diverse v-ATPase complexes with specific properties and tissue expression. Among these, only six have been associated to several recessive disorders, including distal renal tubular acidosis and hearing loss (ATP6V1B1 and ATP6V0A4) (Karet et al., 1999; Stover et al., 2002), osteopetrosis, with macrocephaly, progressive deafness, blindness, hepatosplenomegaly, and severe anemia (ATP6V0A3) (Kornak et al., 2000; Frattini et al., 2000), cutis laxa, a systemic disorder with severe neurological impairment featuring structural brain abnormalities, severe delay, and seizures (ATP6V0A2, ATP6V1E1 and ATP6V1A) (Fischer et al., 2012; Van Damme et al., 2017) (Table1). Two allelic dominant disorders, Zimmermann-Laband syndrome type 2, featuring facial dysmorphisms and intellectual disability (Kortum et al., 2015) and a form of congenital deafness with anonyochia, have also been described (ATP6V1B2) (Yuan et al., 2014).

Gene	Phenotype	OMIM number	Inheritance	Reference
ATP6V1A	Cutis laxa, autosomal recessive, type IID (ARCL2D)	617403	AR	Van Damme et al., 2017
ATP6V1B1	Renal tubular acidosis with deafness (dRTA)	267300	AR	Karet et al., 1999
ATP6V1B2	Deafness, congenital, with onychodystrophy, autosomal dominant (DDOD)	124480	AD	Yuan et al., 2014
	Zimmermann-Laband syndrome 2 (ZLS2)	616455	AD	Kortum et al., 2015
ATP6V1E1	Cutis laxa, autosomal recessive, type IIC (ARCL2C)	617402	AR	Van Damme et al., 2017
ATP6V0A2	Cutis laxa, autosomal recessive, type IIA (ARCL2A)	219200	AR	Kornak et al., 2008 Fischer et al., 2012
	Wrinkly skin syndrome (WSS)	278250	AR	Kornak et al., 2008
ATP6V0A3	Osteopetrosis, autosomal recessive 1 (OPTB1)	259700	AR	Kornak et al., 2000 Frattini et al., 2000
ATP6V0A4	Renal tubular acidosis, distal, autosomal recessive (RTADR)	602722	AR	Smith et al., 2000 Stover et al., 2002

AR: Autosomal Recessive, AD: Autosomal Dominant.

Table1. V-ATPase subunits associated with human disorders

1.9 Early onset Epileptic encephalopathies

Developmental brain disorders (DBDs) are a group of severe conditions characterized by developmental brain dysfunctions and manifesting with different and often concomitant neuropsychiatric symptoms such as intellectual disability, behavioral abnormalities, motor defects and seizures. The physio-pathological landscape of neurodevelopmental disorders implicates a range of biological mechanisms including channelopathies, transcriptional dysregulations, impaired DNA repair/remodelling and metabolic defects. Early onset epileptic encephalopathies (EOEEs) are severe DBDs in which cognitive, sensory, and motor development is impaired by recurrent clinical seizures and/or major interictal paroxysmal activity during the neonatal or the

early infantile periods. They are characterized by rapid deterioration of brain function with progressive disturbance of cognitive, sensory or motor function (Nabbout et al., 2003). EOEEs are genetically heterogeneous disorders: over 100 genes have been suggested to be involved in the etiology of these syndromes (Lemke et al.,2012). Many EOEE cases are sporadic, occurring in patients with no family history of seizures or epilepsies (Allen et al., 2013). Sporadic cases are commonly caused by autosomal dominant *de novo* mutations in genes encoding neuronal proteins. Next-generation sequencing (NGS) has contributed to the identification of many monogenic epilepsy syndromes. Moreover, information emerging from NGS studies allows to better understand mechanisms of these pathologies, progressively delineating specific entities previously gathered under the generic definition of epileptic encephalopathies (Mei et al., 2017). In addition to many genes coding for ion channels , there is also a significant group of genes coding for synaptic proteins, suggesting a prominent role of synaptic dysfunction in the pathophysiology of EOEEs (Table2)

Gene	Inheritance
DNM1	AD
GABRA1	AD
GABRB1	AD
GABRB3	AD
STXBP1	AD
SYNJ1	AR
TBC1D24	AR

Table2. Genes coding for synaptic proteins associated with epileptic encephalopathies

AD Autosomal Dominant; AR Autosomal Recessive.

2. Aim of the study

The aim of the study is to analyze the functional consequences of the novel pathogenic mutations in *ATP6V1A* described in patients with EOEE. As experimental models we employed transfected HEK293 cells and patients' lymphoblasts to assess the effects of the mutations on the stability of ATP6V1A protein and on organelle acidification; transfected primary neurons to assess neuronal development and connectivity.

3 Abstract

Our collaborators at Meyer Children's Hospital of Florence have identified, through whole exome sequencing, *de novo* heterozygous mutations in *ATP6V1A*, encoding the A subunit of v-ATPase, in four patients with developmental encephalopathies with epilepsy. The aim of my PhD project is to analyze the functional consequences of the novel pathogenic mutations described in EOEE in v-ATPase function, in neuronal development and synaptic mantainance. During my PhD i addressed the impact of p.Asp349Asn and p.Asp100Tyr mutations on ATP6V1A expression and function by analysing HEK293T cells overexpressing ATP6V1A and patients' lymphoblasts. The p.Asp100Tyr mutant was characterized by reduced expression level due to increased degradation. Conversely, no significant decrease in expression and clearance was observed for the p.Asp349Asn mutant. In HEK293T cells overexpressing either pathogenic or control variants, the p.Asp349Asn mutation significantly increased Lysotracker fluorescence with no effects on EEA1 and LAMP1 expression. Conversely, the p.Asp100Tyr mutation decreased both Lysotracker fluorescence and LAMP1 levels, leaving EEA1 expression unaffected. Both variants impaired v-ATPase recrutiment to autophagosomes. Parallel experiments performed on patients'

lymphoblasts using the ratiometric Lysosensor probe revealed a decrease in the pH of endocytic organelles for the p.Asp349Asn mutation and a reduced expression of LAMP1 with no effect on the pH for the p.Asp100Tyr mutation. The data demonstrate a gain of function for the p.Asp349Asn mutation characterized by an increased proton pumping in intracellular organelles, and a loss of function for the p.Asp100Tyr mutation with decreased expression of ATP6V1A and reduced levels of lysosomal markers.

I also expressed p.Asp349Asn and p.Asp100Tyr in rat hippocampal neurons and confirm significant and opposite effects in lysosomal labeling. However, both mutants caused a similar defect in neurite elongation accompanied by a loss of excitatory inputs, revealing that altered lysosomal homeostasis markedly affects neurite development and synaptic connectivity, uncovering a novel role for v-ATPase in neuronal development.

This study provides evidence that *de novo* heterozygous *ATP6V1A* mutations cause a developmental encephalopathy with a pathomechanism that involves perturbations of lysosomal homeostasis and neuronal connectivity.

4 Materials and methods

ATP6V1A constructs

We synthesized wild-type (w.t.) and mutant (p.Asp100Tyr and p.Asp349Asn) human *ATP6V1A* cDNAs *in vitro* and cloned in pLVX-IRES-mCherry vector by Biomatik (Cambridge, Canada). We performed Sanger sequencing of all constructs to check the correct inserts orientation and validate their sequence. For silencing *ATP6V1A* we used Origene constucts (Catalog. number TL314568).

Cell culture and transfection

Human Embryonic Kidney-derived 293T (HEK) cells were maintained at 37°C in a humidified 5% CO_2 incubator in in DMEM (Life Technologies) supplemented with 10% FBS, 2 mM L-glutamine and 1% Penicillin-Streptomycin. Cells were transfected with Lipofectamine 2000 (Life Technologies) according to the manufacturer's instructions. HEK cells were starved by medium withdrawal for 2 hrs. Lymphoblatsts were prepared by infecting lymphocytes obtained from patients and their parents with the Epstein-Barr virus (EBV) *in vitro* using standard protocols and maintained in RPMI 20% FBS, 1 mM L-glutamine and 10 mM D-glucose. Primary cortical neurons were prepared from E18 brains of Sprague Dawley (SD) rats as previously described (Verstegen et al. 2014). Neurons were transfected using Lipofectamine 2000 at 7 or 14 days in vitro (DIV) and analysed three days after transfection.

Western blotting

Protein lysates from HEK, lymphoblast and neuronal cultures were extracted in lysis buffer (50 mM Tris [pH 7.5], 150 mM NaCl, 0.1% SDS, 1% Nonidet P40, 0.2 mM phenylmethylsulfonyl fluoride, 2 μg/ml pepstatin, and 1 μg/ml leupeptin
) and then separated by SDS-PAGE and assayed by immunoblotting with the following primary antibodies: anti-ATP6V1A (1:1000; #ab137574, Abcam), anti-ATP6V0D (1:1000; #ab155594, Abcam) anti-ATP6V1B2 (1:2000; #ab73404, Abcam), anti-LAMP1 (1:1000; #ab24170, Abcam), anti-EEA1 (1:5000; #610457, BD Bioscience, USA), LC3B (1:1000; #7543 Sigma-Aldrich), p62 (1:1000, #P0067 Sigma-Aldrich), anti-GAPDH (1/1000; #SC-25778, Santa Cruz Biotechnology), anti-VAMP2 (1:1000; #104202; Synaptic Systems, Gottingen, Germany); anti-V-GLUT1 (1:1000; #135304; Synaptic Systems) anti-PSD95 (1:1000; #SC- 32290, Santa Cruz

Biotechnology). anti-vGAT (#131004; Synaptic Systems), anti NMDA R2B (#ab28373; Abcam) and anti-Gephyrin (#147 011; Synaptic Systems). Bafilomycin A1was from Tocris Bioscience (Cookson, USA)

Degradation assay

HEK cells were transfected with ATP6V1A wild type (w.t.), ATP6V1A Asp349Asn or ATP6V1A Asp100Tyr and treated with 10 µg/ml of cycloheximide (C4859, Sigma-Aldrich) 24 hrs after transfection. Cells were lysed at different times after cycloheximide addition and analysed by Western Blotting. Protein level is expressed with respect to ATP6V1A content in the cells collected at time zero and treated with vehicle (DMSO).

Immunocytochemistry and fluorescence microscopy

Transfected primary cortical neurons or HEK cells were fixed in 4% paraformaldehyde in PBS, permeabilized in 0.1% Triton X-100, blocked with 2% FBS /0.05% Tween-20 in PBS and incubated with the various antibodies in blocking solution. Samples were mounted in ProLong Gold antifade reagent with DAPI (#P36935, Thermo-Fisher Scientific). Capture of confocal images was performed using a laser scanning confocal microscope (SP5, Leica) with a 40X or 63X oil-immersion objective. For LAMP1 (1:200, #L1418 Sigma-Aldrich) and EEA1 (1:500; #610457, BD Bioscience), ATP6V1B2 (1:200, #SAB1405501 Sigma-Aldrich) and LC3B (1:200, #2775 Cell Signalling) labeling, each image consisted of a stack of images taken through the z-plane of the cell. The colocalization of ATP6V1B2 and LC3B signals was analysed using the ImageJ intensity correlation analysis plugin to calculate Pearson's correlation coefficient. For Lysotraker Deep Red (Molecular Probes/Life Technologies) experiments, HEK cells were incubated with 200 nM Lysotraker for 1 hr, whereas neurons were incuated with 50 nM Lysotraker for 30

min, at 37 °C in culture medium, immediately fixed and analysed within 12 hrs. Images were taken at either epifluorescence (Olympus 1X81) or confocal (SP5, Leica) microscope in a single plane not to fade the fluorescent signal. Settings were kept the same for all acquisitions within each experiment.

Measurement of endo-lysosomal pH

Endo-lysosomal pH was measured using a ratiometric pH indicator dye, Lysosensor Yelllow/Blue dextran (LYB-dx, Molecular Probes/Life Technologies), a dual excitation dye that allows pH measurement in endocytic organelles independently of dye concentration. Lymphoblasts (4×10^6) were incubated for 3 hrs at 37 °C with 0.5 mg/ml of LYB-dx in culture medium. Cells were divided into five samples, four to perform the calibration curve and one for the measures. To obtain a pH calibration curve, cells were resuspended with MES calibration buffer solution (5 mM NaCl, 115 mM KCl, 1.2 mM $MgSO_4$ and 25 mM MES, pH ranging from 3.7 to 7.6) containing 10 μM monensin (Sigma-Aldrich) and 10 μM nigericin (Sigma-Aldrich). For the pH measures, cells were resuspended in MES calibration buffer solution pH 7.7 in the absence of ionophores. Emission scans were collected at 450 nm and 528 nm with the Luminescence Spectrometer LS 50 (Perkin Elmer), using excitation at 360 nm and emission/excitation bandwidths set to 4 nm. Calibration data (ratio 450/528) were fitted to a linear regression with the software GraphPad Prism5 and the sample ratios converted into absolute pH values by interpolation in the calibration function.

Sholl analysis

Neurons were plated at low density (80 cells/mm^2), transfected at 7 DIV and analysed at 10 DIV. For analysis, neurons were fixed in 4% PFA, in PBS and decorated with βIII tubulin antibody (1:1000, #MMS-435P Covance) followed by Alexa 488

secondary antibody to unequivocally distinguish neuronal cells. The extent of neurite arborization was evaluated using the Sholl analysis as previously described (Falace et al. 2010). Concentric circles with radii increasing at regular 10 µm steps were centered to the cell body and the number of intersections was automatically evaluated with the Image J/Sholl analysis plug-in.

Synapse quantification

Neurons, plated at low density as described above, were either transfected at 14 DIV and analysed at 17 DIV or treated at 17 DIV with 200 nM leupeptin for 3 hrs (#EI8, MerckMillipore; Goo et al., 2017). To measure excitatory synapses, neurons were labeled with anti-V-GLUT1 (1/500, #135304; Synaptic Systems) and anti-Homer1 (1/200, #160011; Synaptic Systems) antibodies. To measure inhibitory synapses, neurons were labeled with anti-V-GAT (1/500, #131004; Synaptic Systems) and anti-Gephyrin (#147 011; Synaptic Systems) antibodies. Confocal images were acquired with a laser scanning confocal microscope (SP5 Upright, Leica) with a 40X oil-immersion objective. Each image consisted of a stack of images taken through the z-plane of the cell. Confocal microscope settings were kept the same for all scans in each experiment. The colocalization analysis was performed by evaluating the labeling of the VGLUT1/Homer1 and v-GAT/Gephyrin synaptic protein couples. Colocalization puncta with areas of 0.1-2 μm^2 were considered *bona fide* synaptic boutons. Synaptic boutons along Cherry-positive neurites were manually counted on 30 µm puncta starting from the cell body.

5 Results

5.1 Mutations in v-ATPase subunit A in patients with developmental encephalopathy

Through whole exome sequencing of a large cohort of children with neurodevelopmental disorder of presumed genetic origin, our collaborators have identified four different *de novo* missense mutations of the ATP6V1A gene in children with developmental encephalopathy featuring mental retardation and seizures,. All four *de novo* mutations caused missense substitutions at evolutionarily conserved amino acid positions (Figure 5) and were predicted to be damaging by *in silico* methods.

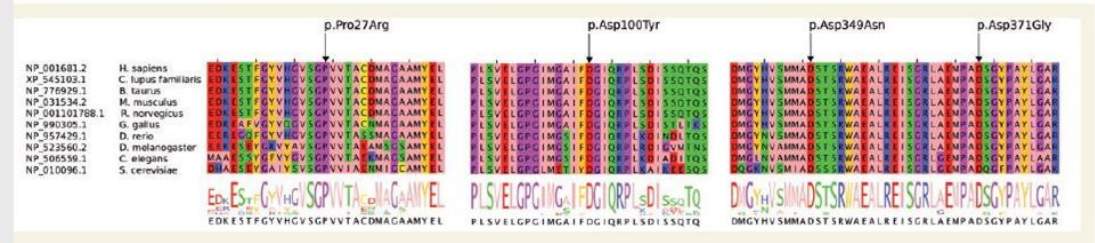

Figure 5. Multiple sequence alignment between human ATP6V1A and orthologous sequences.
Residues affected by the missense substitutions are indicated by black arrows.

5.2 Clinical findings

Clinical findings observed in the four Patients are summarised in Table 1.

Table I Summary of clinical features in four patients carrying *ATP6V1A* mutations

	Patient			
	1	2	3	4
Origin/sex	Caucasian/F	Asian/M	Caucasian/F	Latino/M
Age at follow-up	14 years	8 years	8 years	11 years
ATP6V1A mutation	c.298G>T (p.Asp100Tyr) *de novo*	c.1045G>A (p.Asp349Asn) *de novo*	c.1112A>G (p.Asp371Gly) *de novo*	c.80C>G (p.Pro27Arg) *de novo*
Clinical diagnosis	Infantile onset epileptic encephalopathy	ID/epilepsy	ID/epilepsy	Infantile onset epileptic encephalopathy
Head circumference	At birth: 32 cm = 3rd %ile (−1.9 SD); at 12 years: 44.5 cm ⩽ 1st %ile (−7 SD): microcephaly	At birth: 33 cm = 10th %ile (−1.2 SD)	Unknown	At 12 months: 43.5 cm = 1st %ile (−2.2 SD); at 11 years: 49 cm ⩽ 1st %ile (−3.2 SD): microcephaly
Age/symptoms at first clinical presentation	11 months, hypotonia, developmental delay, seizures	1 month, developmental delay, jerky movement	2 years 6 months, developmental delay, seizures	7 months, hypotonia, developmental delay
Epilepsy	+	+	+	+
Age at seizure onset	11 months	2 years 10 months	2 years 6 months	11 months
Seizures types	Convulsive seizures during fever at onset, then infantile spasms, tonic, focal clonic, focal occipital	Convulsive seizures during fever at onset, then focal occipital	Convulsive seizures during fever at onset, then generalized tonic-clonic	Convulsive seizures during fever at onset, then spasms, tonic, clonic and myoclonic
Interictal EEG	Slow background, diffuse and multifocal epileptiform discharges	Posteriorly dominant, multifocal epileptiform discharges	Anteriorly predominant multifocal epileptiform discharges	Slow background, diffuse and multifocal epileptiform discharges
Brain MRI	Hypomyelination, mild brain and cerebellar atrophy	Normal at 7 years	Normal at 7 years	Mild atrophy at 1 years 5 months and 3 years 7 months
Clinical phenotype at last follow-up	Profound delay, non-verbal, no visual fixation, hypotonic/dyskinetic quadriparesis, non-ambulatory, early puberty (9 years).	Moderate ID (FSDQ: 53), poor language, headache, amelogenesis imperfecta diagnosed at 3 years, optic atrophy	Moderate ID, poor language, mild dysmorphic features (wide forehead, deep set eyes, beaked nose), behavioural abnormalities with autistic traits, wide based gait, hypotonia	Profound delay, non-verbal, no visual fixation, coloboma of the iris, hypotonic/dyskinetic quadriparesis, non-ambulatory

F = female; FSDQ = full scale developmental quotient; ID = intellectual disability; M = male; N/A = not available.

In brief, early manifestations, observed in all patients, were developmental delay and febrile seizures, evolving to encephalopathies with profound delay, hypotonic/dyskinetic quadriparesis, intractable multiple seizure types and severe diffuse epileptiform EEG abnormalities in two patients [patient 1(p.Asp100Tyr) and patient 4(p.Asp371Gly)] and to moderate delay with milder epilepsy and focal/multifocal EEG abnormalities in the other two [patient 2(p.Asp349Asn) and patient 3(p.Asp371Gly)].

Furthermore, the MRI images of the four patients can be seen below (Figure 6 to Figure 10) :

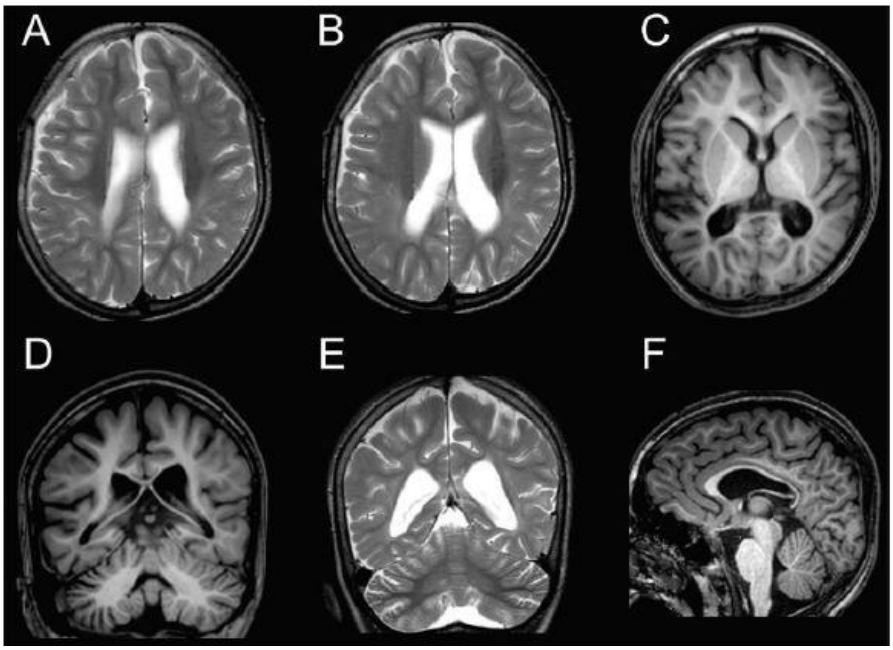

Figure 6. Patient 1 (p.Asp100Tyr)

A-F shows six cuts of magnetic resonance imaging of the brain at 11 years of age. Note the ventricular dilatation, with signs of mild cortical and cerebellar atrophy, a thin corpus callosum and hypomyelination in the posterior brain regions.

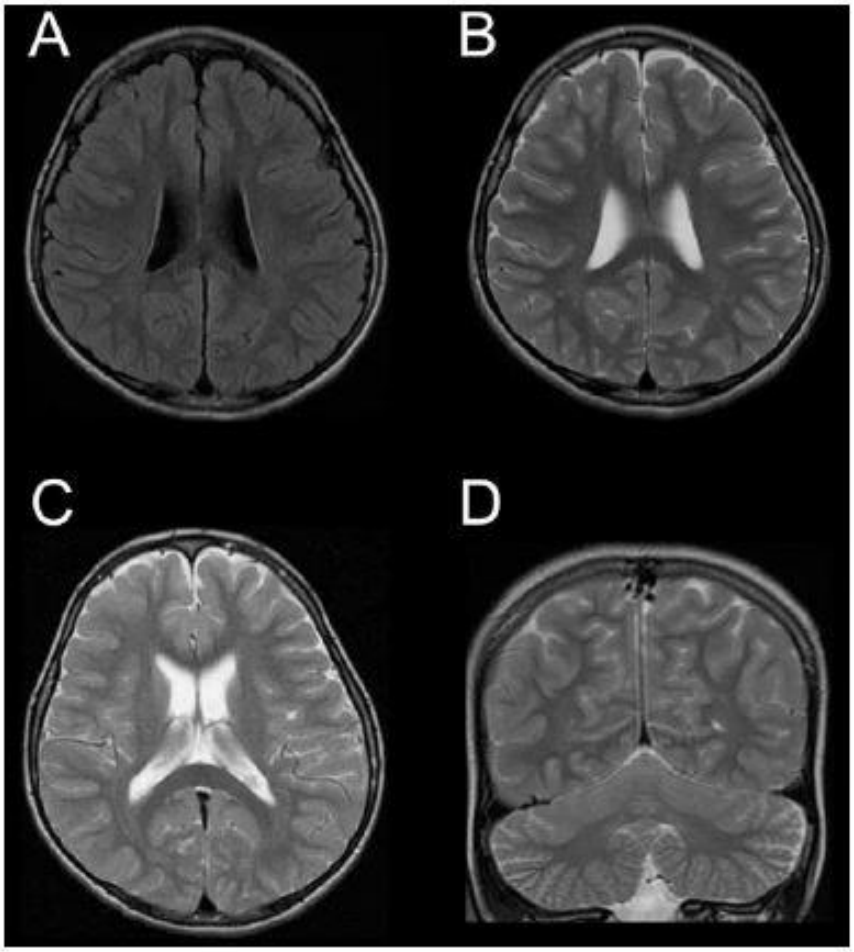

Figure 7. Patient 2 (p.Asp349Asn)

Figures A-D shows four magnetic resonance imaging pictures of the brain at 7 years of age. Brain MRI at 7 years of age was normal.

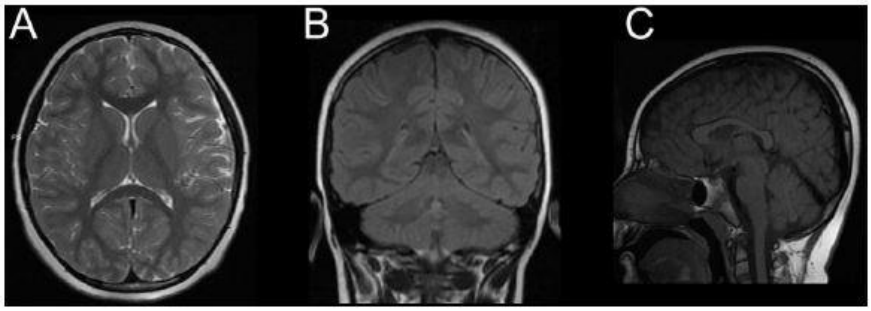

Figure 8. Patient 3 (p.Asp371Gly)

Figures A-C show three magnetic resonance imaging pictures of the brain at 7 years of age. These images show no brain abnormality.

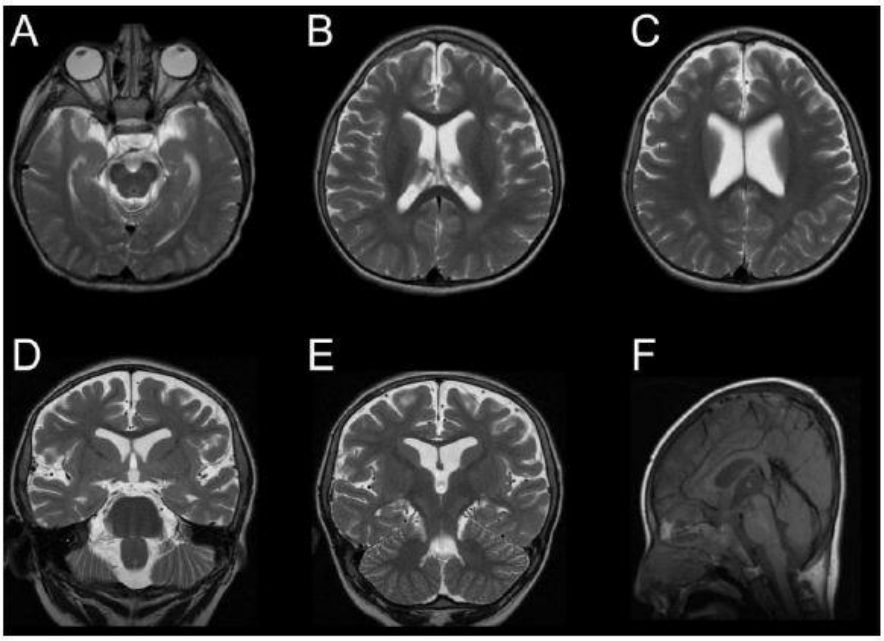

Figure 9. Patient 4 (p.Asp371Gly)

Figures A-F shows six magnetic resonance imaging sections of the brain at 4 years of age. Note mild ventricular dilatation, with signs of mild cortical and cerebellar atrophy, a thin corpus callosum, hypomyelination in the posterior brain regions and plagiocephaly.

5.3 Structural consideration of the v-ATPase mutations

Our collaborators mapped the mutation sites of human ATP6V1A onto the crystal structure of the V_1 domain from a prokaryotic homologue, *Enterococcus hirae* v-ATPase. All the identified mutations fall into the A subunit of the V_1 domain (Figure 10A).

Pro12 (Pro27 in human ATP6V1A) resides in the type I β-turn that is a part of the interaction interface between subunits A and B. Because the substitution of a proline residue with an arginine residue affects the main-chain conformation of the β-turn, the mutation may perturb the A-B interaction (Figure 10 A, B).

Asp85 (Asp100 in human ATP6V1A) makes a hydrogen bond with Arg89, a guanidium group which makes van der Waals contacts with adjacent hydrophobic side chains (Figure 10 B). As a result, the side chain of Asp85 is closely surrounded by hydrophobic residues, and its replacement with a bulkier tyrosine residue quite likely causes steric hindrance and destabilizes the protein folding.

Asp329 (Asp349 in human ATP6V1A) is located near a nucleotide-binding site (Figure 10 B) and its side chain is involved in water-mediated coordination with a magnesium ion, which plays a critical role in the ATPase activity (Figure 10 B). Thus, the Asp329Asn mutation possibly impairs the catalytic function.

Asp351 (Asp371 in human ATP6V1A) is located at the interface among A, B and D subunits (Figure 10 A). The D subunit rotates within the A3B3 core along with the ATP hydrolysis, and thus the rotation process may be affected by the Asp351Gly mutation. The mutation sites were also mapped on the cryo-EM structure of the human homologue v-ATPase from the eukaryotic *S. cerevisiae*. As shown in Figure 10 B, the mapped mutation sites in the *S. cerevisiae* structure overlap with those of the *E. hirae*, suggesting that the predicted impact of the mutations on the prokaryotic structure is also valid for the eukaryotic orthologues.

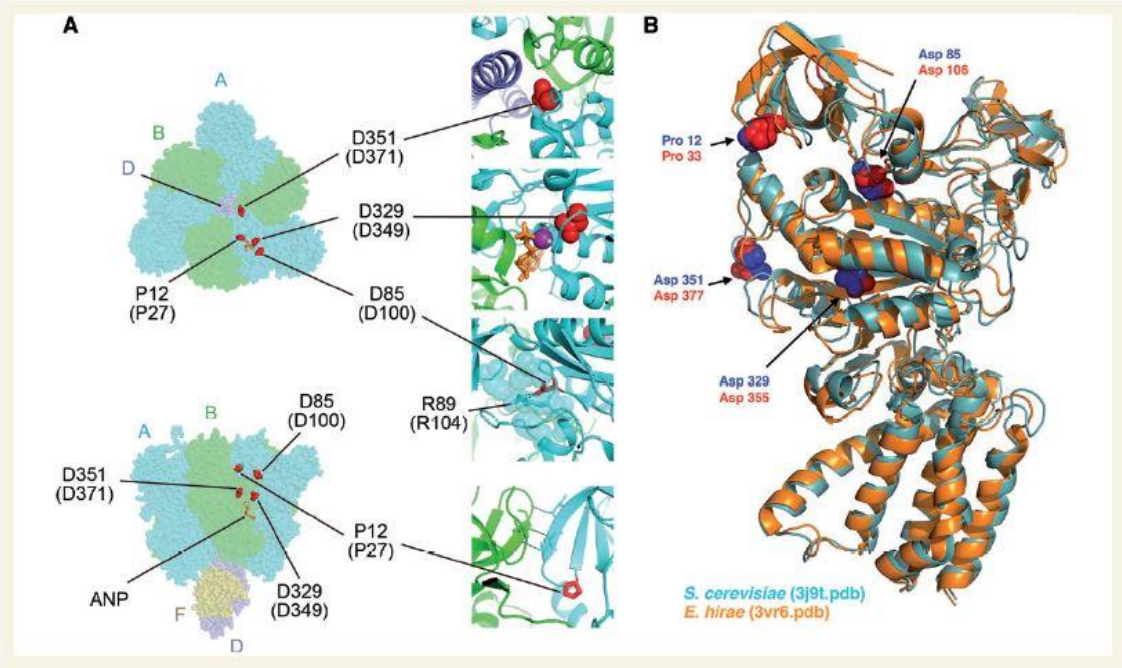

Figure 10. Structural mapping of the missense mutations in the V-ATPase.

(A) Left: Crystal structure of the V1 domain from E. hirae v-ATPase in a nucleotide-bound state, viewed from the extracellular side (top) and the membrane plane (bottom), shown as the sphere representation. The A, B, D and F subunits are coloured in cyan, green, violet and brown, respectively, and residues at the mutation sites are coloured in red. The non-hydrolyzable ATP analogue ANP (phosphoaminophosphonic acid-adenylate ester) is depicted as orange sticks. Right: Magnified views of the mutation sites presented in the ribbon model. Pro12 and Asp85 are depicted as red sticks, and Arg89, which makes a salt bridge with Asp85, is shown as sticks with translucent spheres. Some side chains of hydrophobic residues around Arg89 are shown as translucent spheres, and magnesium ion and its coordinated water molecules are depicted as a purple sphere and small grey dots, respectively. Black dotted lines indicate hydrogen bonds. Amino acid numbers in parentheses correspond to those of human ATP6V1A. (B) Crystal structures of the A subunit from E. hirae (orange) and the cryo-EM structure of the A subunit from S. cerevisiae (cyan, PDB code 3J9T) V-ATPase. Mutation sites are shown as spheres and coloured in red for S. cerevisiae and blue for E. hirae.

5.4 Effects of ATP6V1A mutations on protein expression and stability

We addressed the impact of p.Asp349Asn and p.Asp100Tyr mutations on the ATP6V1A expression and stability by analysing HEK cells overexpressing ATP6V1A using a mammalian vector, driving the expression of the protein under the active human cytomegalovirus immediate early promoter (*P*CMV IE) as well as the expression of a cherry fluorescent tag to visualize transfected cells. Cells were transfected with vectors driving the expression of the wild type or mutant. Immunocytochemistry of transfected cells coupled with quantitative Western blot analysis showed a decreased expression of both ATP6V1A mutants that reached significance only for the p.Asp100Tyr variant, and no overt subcellular mislocalisation of both p.Asp100Tyr and p.Asp349Asn mutants with respect to wild type ATP6V1A (Figure11). The expression of the molecular partner, ATP6V1B2, was not modified either by p.Asp100Tyr or p.Asp349Asn mutation (Figure 11 B).

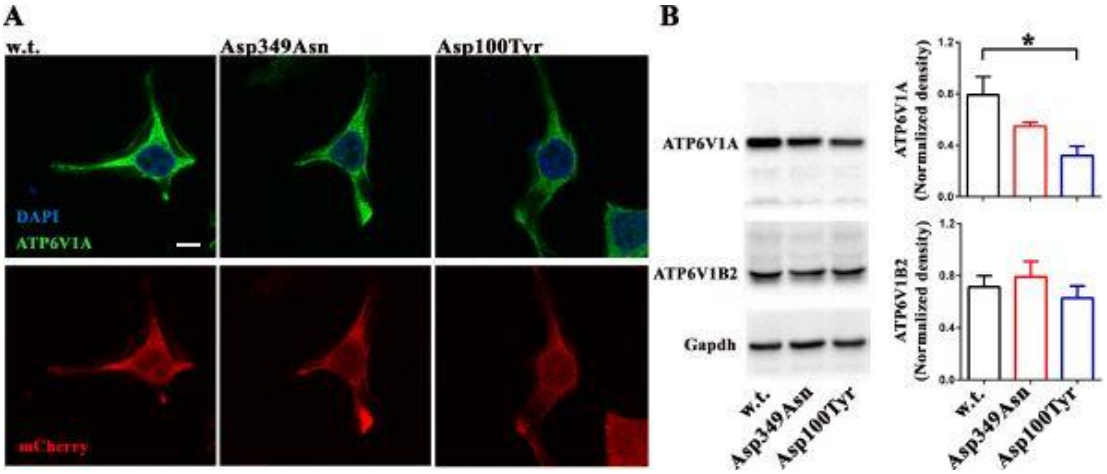

Figure 11. Impact of ATP6V1A mutations on protein expression.

(A) Representative images of HEK cells transfected with vectors coding wild-type ATP6V1A (w.t.), Asp349Asn ATP6V1A (Asp349Asn) or Asp100Tyr ATP6V1A (Asp100Tyr) variants. ATP6V1A immunolabelling, DAPI nuclear stain and Cherry reporter fluorescence are shown. Scale bar = 10 µm. (B) Representative western blot (left) from HEK cells transfected

*as above and lysed 24 h after transfection. ATP6V1A and ATP6V1B2 intensities were quantified by densitometric analysis with respect to GAPDH intensity (right). Data are means ± standard error of the mean (SEM) from five independent experiments. *, p<0.05 versus wild-type; Kruskall-Wallis/Dunn's tests.*

To investigate the stability of ATP6V1A protein, we performed a degradation assay by treating transfected HEK cells with the protein synthesis inhibitor cycloheximide for various times. Compared to the wild type isoform, both mutant ATP6V1A isoforms were less stable, although degradation was significantly increased only for the p.Asp100Tyr variant (Figure 12).

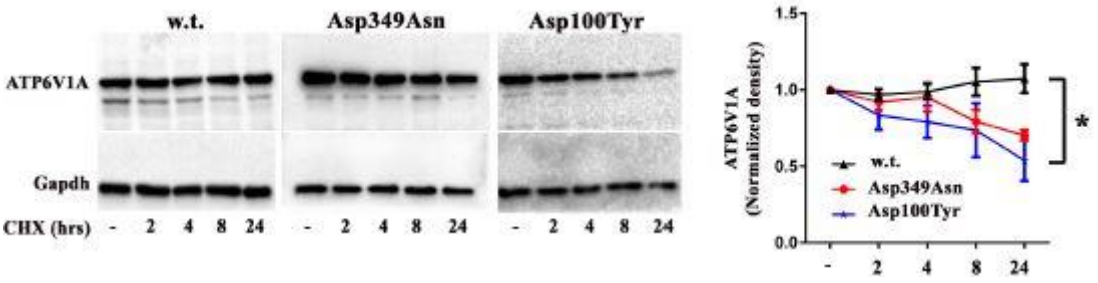

Figure 12. Impact of ATP6V1A mutations on protein stability.

*Left: Representative western blots of HEK cell lysates stained with anti-ATP6V1A antibody and anti-Gapdh as loading control. Cells were transfected with wild-type, Asp349Asn or Asp100Tyr ATP6V1A variants and incubated with cycloheximide for 2, 4, 8, 24 h or vehicle (DMSO; 24 h) as a control (–). Right: Densitometric analysis of ATP6V1A intensity with respect to GADPH expressed in percent of control samples without cycloheximide. Data are means ± SEM from four independent experiments. The areas under the respective curves were compared using the Kruskal-Wallis/Dunn's tests. *, p<0.05 versus wild-type.*

We next asked whether these findings could also be observed in patients' cells. To this aim, we analyzed the expression of endogenous ATP6V1A protein in patients' lymphoblasts and compared it with the respective healthy parents' cells (Figure 13).

While the expression of ATP6V1A and ATP6V1B2 was not modified in Asp349Asn proband's cells with respect to his healthy mother's cells, a significant decrease of ATP6V1A, but not ATP6V1B2, expression was observed in Asp100Tyr proband's cells. These data are in full agreement with the results in HEK cells and with the structural analysis prediction of a folding defect in the p.Asp100Tyr mutant (see Figure 10A) that may enhance its degradation.

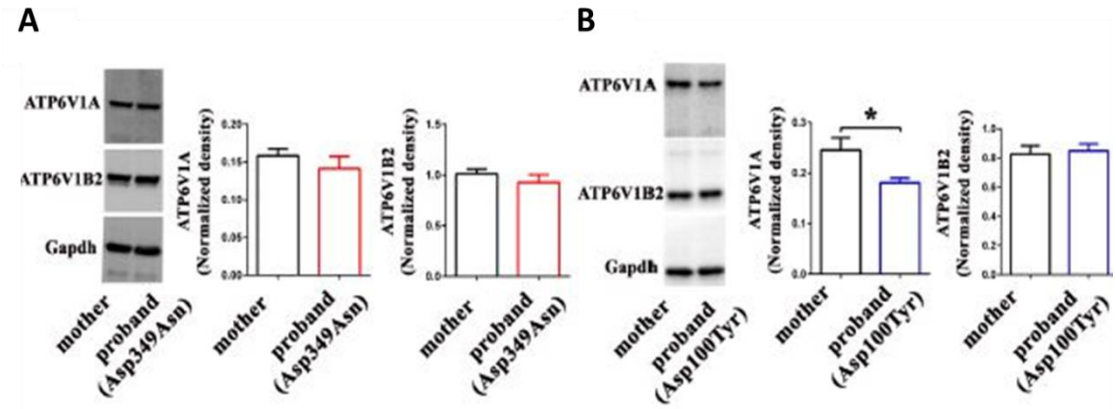

Figure 13. Analysis on ATP6V1A mutations in patients' cells.

*(A) Representative western blot from lymphoblast lysates (30 μg) of patient affected by the Asp349Asn mutation (proband) and the healthy mother. (B) Representative western blot from lymphoblast lysates (30 μg) of patient affected by the Asp100Tyr mutation (proband) and the healthy mother. In A and B, ATP6V1A and ATP6V1B2 intensity were quantified by densitometric analysis with respect to GADPH. Data are means ± SEM from four independent experiments. *, p<0.05; Mann Whitney U-test.*

5.5 ATP6V1A mutations result in lysosomal abnormalities

To examine the impact of the p.Asp349Asn and p.Asp100Tyr mutations in the regulation of pH homeostasis, we employed the Lysotraker probe to qualitatively evaluate intracellular acidic organelles. Before evaluating the pH of transfected cells, we validate the use of the sensor in our experimental model. To do this, we incubated

HEK293T with 200nM of LysoTracker for one hour, then we performed immunocytochemistry experiments. As shown in Figure 14, Lysosomes (Lamp-1 positive puncta),correctly accumulated lysotracker signal.

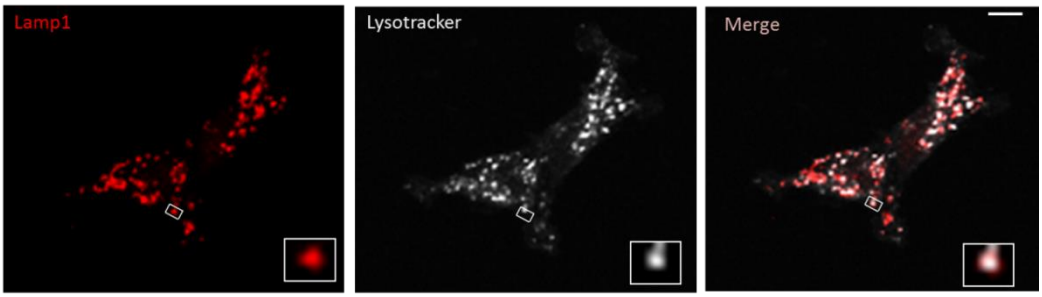

Figure 14. Validation of lysotracker protocol

Representative images of HEK293 cells treated with LysoTracker deep red probe and immunolabeled with Lamp1. Scale bar = 10 µm. Merge panel indicates lysotracker signal is accumulated in lamp1 positive acidic organelles (lysosomes).

Moreover we incubated HEK293T with 200nM of LysoTracker for one hour, then we added Bafilomycin 100nM, an inhibitor of v-ATPase, for an extra hour. As shown in Figure 15, there is a significant decrement of LysoTracker intensity in cells treated with Bafilomycin, indicating that, by blocking v-ATPase, the intensity of signal declines.

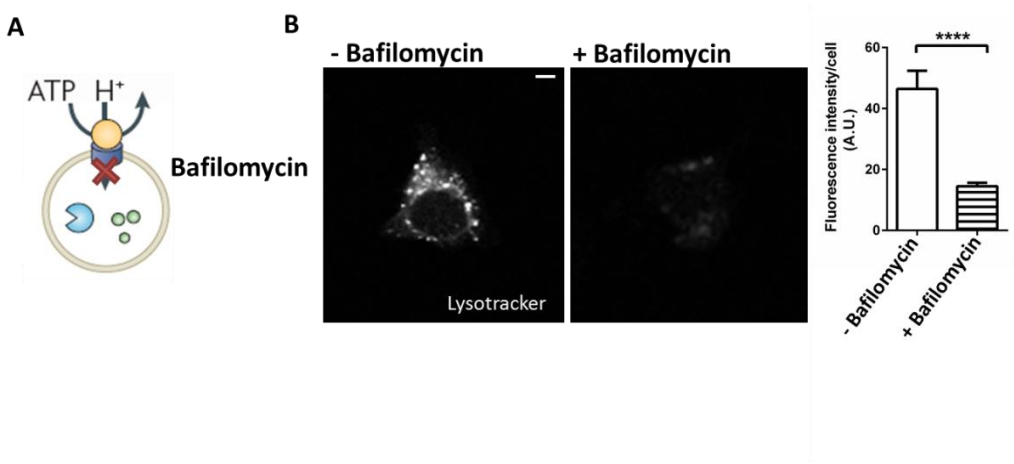

Figure 15: Bafilomycin, blocking v-ATPase activity, decreases lysotracker intensity

*(A) Cartoon showed how bafilomycin blocks v-ATPase activity. (B) Representative images of HEK293 cells labeled with LysoTracker deep red and LysoTracker deep red plus Bafilomycin. Graph shows quantification of fluorescent intensity from 17 cells for experimental group expressed as mean ± SEM. ****p<0.0001 with Student't test. . Scale bar = 10 μm.*

We next analysed the impact of the p.Asp349Asn and p.Asp100Tyr mutations in the regulation of pH homeostasis in HEK cells overexpressing either pathogenic or wild type ATP6V1A variants. Interestingly, the p.Asp349Asn mutant showed an increased Lysotracker fluorescence intensity, while the p.Asp100Tyr mutant showed a decreased Lysotraker fluorescence intensity (Figure 16).

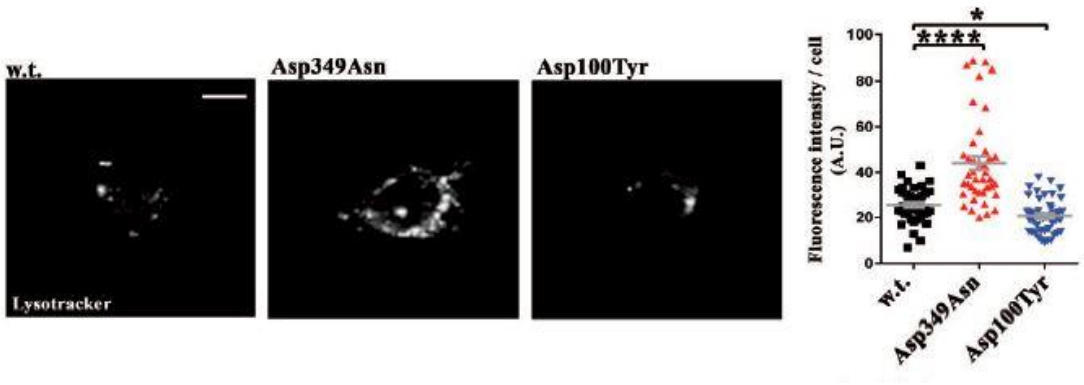

Figure 16. Effect of ATP6V1A pathogenic variants on pH homeostasis

*Left: Representative images of HEK cells transfected with wild-type ATP6V1A (w.t.), Asp349Asn ATP6V1A (Asp349Asn) or Asp100Tyr, ATP6V1A (Asp100Tyr) variants and incubated with LysoTracker (200 nM, 1 h). Right: LysoTracker fluorescence intensity was quantified in 38 (wild-type), 41 (Asp349Asn) and 45 (Asp100Tyr) cells from three independent experiments. Individual data and means ± SEM are shown. *, p<0.05, ****p<0.0001 versus wild-type; Kruskall-Wallis/Dunn's tests. Scale bar = 10 μm.*

The Lysotraker signal monitors both the actual pH of acidic organelles, namely endosomal and lysosomal compartments, and their relative abundance within the cell.

Thus, we analyzed in parallel the expression of the endosomal and lysosomal markers, EEA1 and LAMP1, respectively. Whereas EEA1 expression was unaltered in HEK cells expressing wild type ATP6V1A or either pathogenic variants, the p.Asp100Tyr mutant was associated with a significant decrease of LAMP1 expression evaluated by single-cell immunocytochemistry (Figure 17).

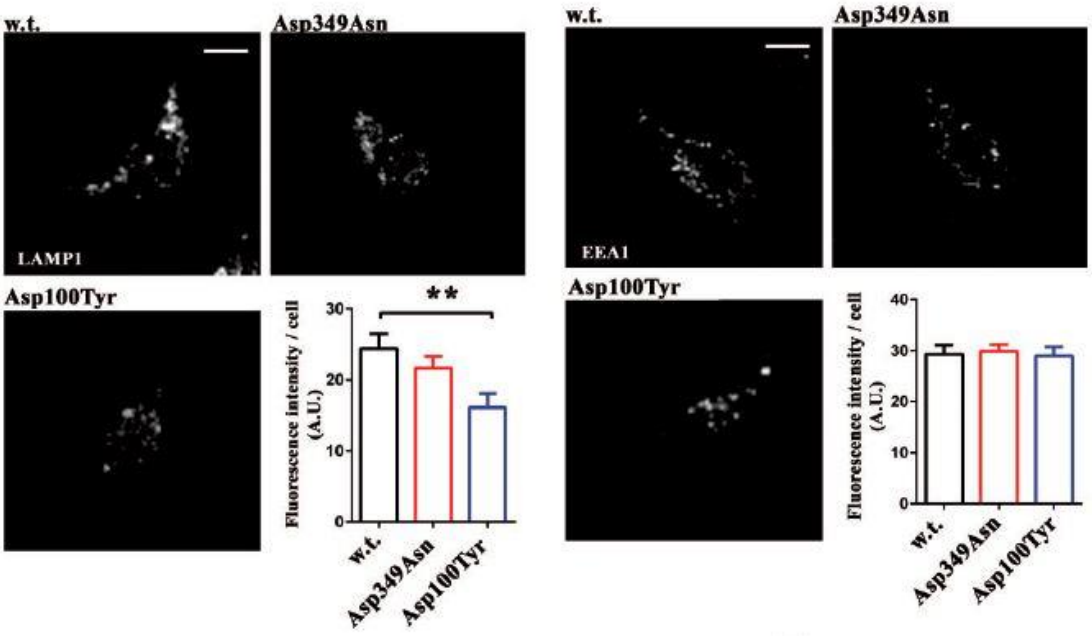

Figure 17. Effects of ATP6V1A mutations on endo-lysosomal markers.

*Representative images and densitometric quantification from HEK cells transfected as above and immunolabelled with LAMP1 (left) or EEA1 (right). Histograms show quantification of signal intensity. Data are means ± SEM of 24–33 cells per experimental condition, from three independent experiments. ** $p<0.01$ versus wild-type Kruskall-Wallis/ Dunn's tests. Scale bar = 10 μm.*

The data suggest that the p.Asp349Asn mutant exacerbates the acidic pH of the intracellular organelles, while the p.Asp100Tyr mutant leads to a decreased expression of LAMP1-positive lysosomal structures. Lysosomes also fuse with autophagosomal structures to generate autolysosomes and v-ATPase is responsible for the acidification of autolysosomal organelles. We therefore asked whether pathogenic ATP6V1A variants affect v-ATPase translocation to LC3-positive

phagosomal structures. To this aim, we measured the colocalization between the v-ATPase subunit ATP6V1B2 and LC3 in HEK cells expressing wild type ATP6V1A or either pathogenic variants. Both p.Asp100Tyr and p.Asp349Asn resulted in a decreased colocalization coefficient with respect to wild type ATP6V1A (Figure 18). However, the activation of the autophagic flux by cell starvation-was slightly impaired by the p.Asp100Tyr mutation and substantially unaffected by the p.Asp349Asn mutation (Figure 18).

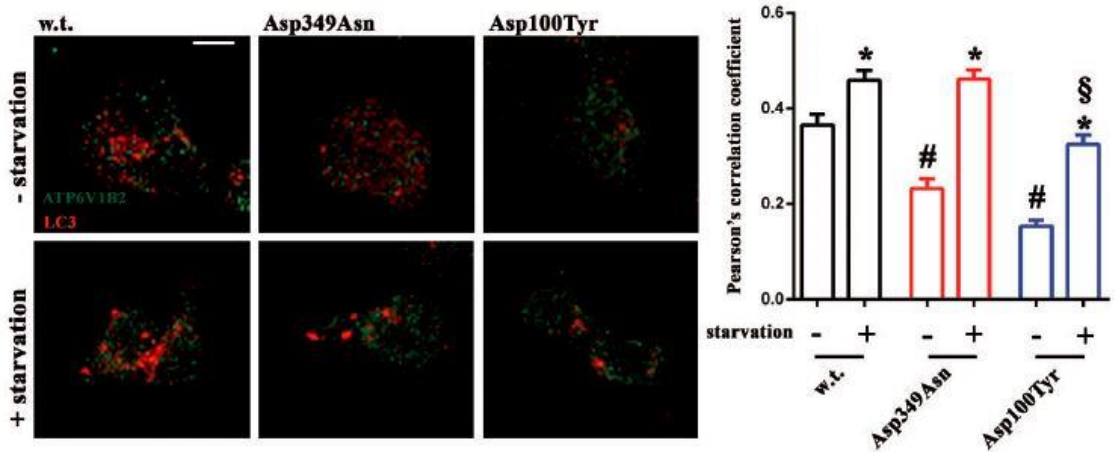

Figure 18 Effects of ATP6V1A mutations on v-ATPase recruitment to autophagosomes. *Representative images from HEK cells transfected as above and immunolabeled with ATP6V1B2 and LC3B under control conditions or after starvation for 2 hrs. Graph shows the quantification of ATP6V1B2 and LC3B colocalization using ImageJ software to determine the Pearson's correlation coefficient. Data are means ± SEM of 30 cells per experimental condition. *, p<0.05 versus respective control; #, p<0.001 versus non-starved w.t.; §, p<0.001 versus starved w.t.. Data were analyzed by two-way ANOVA/ Bonferroni's tests. Scale bar = 10 μm.*

No significant changes in LC3II/LC3I ratio and p62 accumulation were observed in both experimental groups (Figure 19). The data suggest a significant impact of the two mutations on the recruitment of the v-ATPase to LC3-positive autolysosomal

structures, with a slight impairment of the autophagic flux only for the Asp100Tyr mutation.

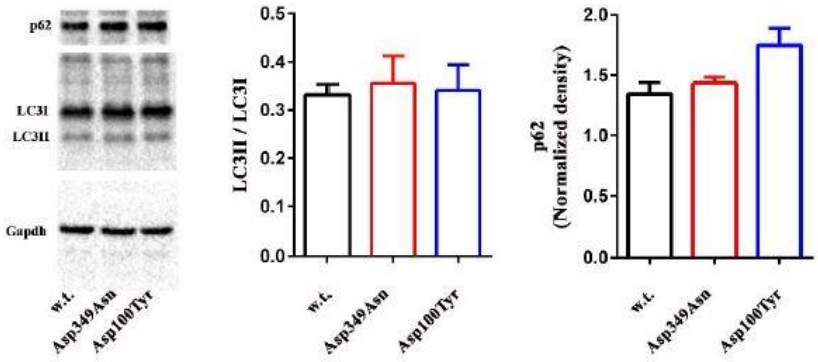

Figure 19. Evaluation of LC3I/LC3II and p62 expression in HEK cells expressing wild type and pathogenic variants of ATP6V1A.
Representative western blots from HEK cells treated as above. Immunoreactive bands for p62, LC3I, LC3II and Gapdh (loading control) are shown (left panel). Densitometric quantification of the LC3II/LC3I ratio and of p62 levels normalized to gapdh are shown (right panels). Data are means ± SEM of 5 experiments.

To verify whether the alteration in lysosomal pH and levels of lysosomal markers were also present in patients, we subjected patients' lymphoblasts to the same analysis. Experiments using the ratiometric pH probe Lysosensor Yelllow/Blue dextran (LYB-dx), revealed a significant reduction in endocytic organelle pH in the Asp349Asn patient's lymphoblasts when compared to his healthy mother's lymphoblasts, in the absence of any change in the expression of LAMP1 and EEA1 (Figure 20 A).

Conversely, while the pH of endocytic organelles was not modified in the Asp100Tyr patient's lymphoblasts, a significant reduction in LAMP1 expression was observed (Figure 20 B, C).

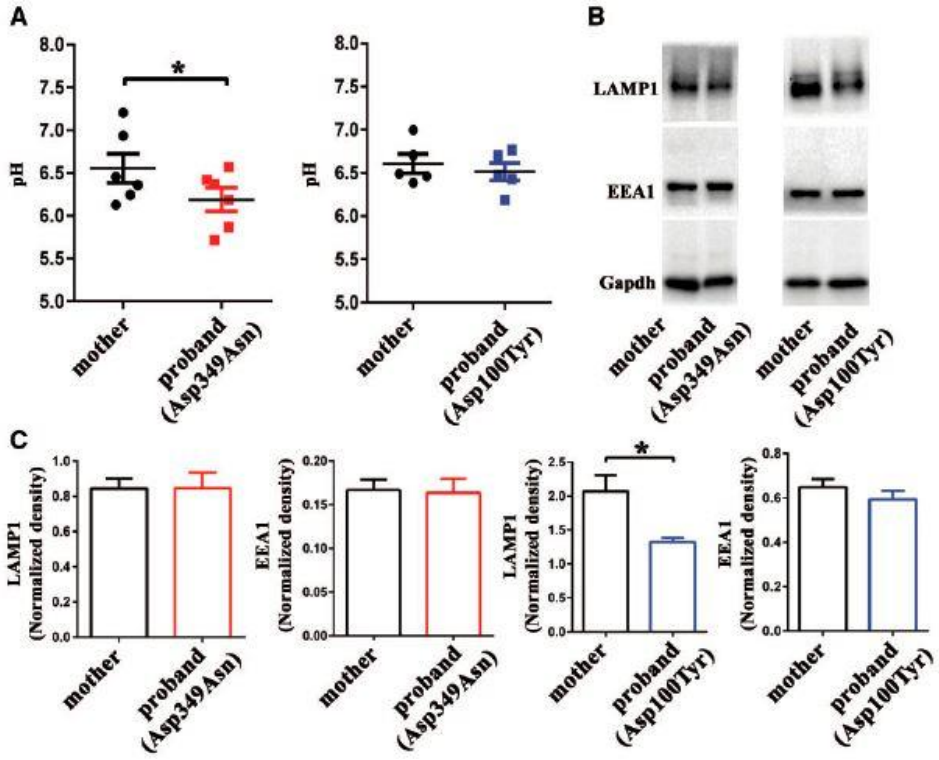

Figure 20. Effects of ATP6V1A mutations on intracellular organelle pH and endo-lysosomal markers in patients' cells

*A, Quantification of endocytic organelle pH in lymphoblasts from patients (probands) bearing either p.Asp349Asn (red) or p.Asp100Tyr (blue) mutation and the respective healthy mothers (black). Individual data and means± SEM of 5-6 independent measurements are shown. *p<0.05; Wilcoxon matched pairs signed rank test. B, Representative western blot from lymphoblast lysates (30 µg) as defined above. LAMP1, EEA1 and Gapdh as loading control is shown. C, LAMP1 and EEA1 immunoreactivities were quantified by densitometric analysis and normalized to Gapdh. Data are means ± SEM from four independent experiments. *p<0.05; Mann-Whitney U-test.*

Taken together these data suggest a gain-of-function effect for the p.Asp349Asn mutation, characterized by an increased proton pumping into intracellular organelles, and a loss-of-function effect for the p.Asp100Tyr mutation associated with defects in lysosomal compartments.

5.6 ATP6V1A mutations impact on neuronal pH homeostasis and neuronal development

In view of the neurodevelopmental phenotype observed in the four patients carrying the *de novo* heterozygous *ATP6V1A* mutations, we investigated whether the effects on lysosomal homeostasis observed in HEK cells and patient-derived lymphoblasts were recapitulated in neurons. To address this question, we transiently expressed ATP6V1A and the pathogenic mutants in rat hippocampal neuronal cultures and evaluated intracellular acidic organelles by Lysotraker staining at the neuronal soma. As shown in Figure 21, neurons overexpressing p.Asp349Asn resulted in a significantly higher Lysotraker staining as compared to wild type ATP6V1A-expressing neurons. On the opposite, p.Asp100Tyr ATP6V1A overexpression induced a significant loss of Lysotraker staining. Thus, the expression of the two mutants in neurons precisely phenocopies the effects observed in cell lines, suggesting that such an alteration in pH and lysosomal homeostasis also occurs in brain cells.

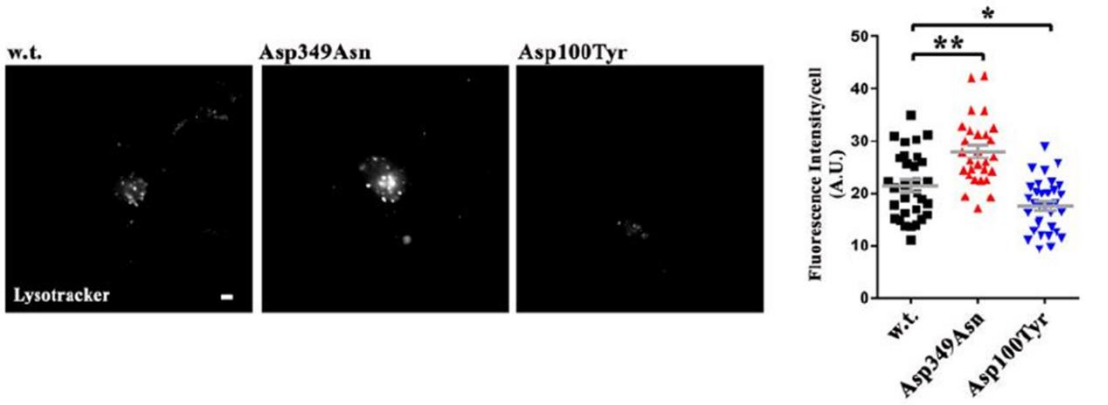

Figure 21. Effect of ATP6V1A mutations on pH homeostasis in primary hippocampal neurons.

*Left: Representative images of rat hippocampal neurons transfected with wild-type (w.t.), Asp349Asn (Asp349Asn) and Asp100Tyr (Asp100Tyr) ATP6V1A variants at 7 DIV and incubated with LysoTracker (50 nM, 30 min) at 10 DIV. Right: LysoTracker fluorescence intensity was quantified in 31 (wild-type), 28 (Asp349Asn) and 33 (Asp100Tyr) neurons from two independent preparations. Individual data and means ± SEM are shown. *p<0.05, **p<0.001 versus wild-type; Kruskall-Wallis/Dunn's tests. Scale bar = 10 µm.*

To investigate cellular correlates of the patients' neurodevelopmental delay and explore whether the defects in Lysotraker signal have an impact on neuronal development, we transfected rat hippocampal neurons at 7 DIV and analyze neurite elongation at 10 DIV by Sholl analysis. The analysis revealed a similar and significant loss of neurite arborization for both p.Asp349Asn- and p.Asp100Tyr-expressing neurons, indicating that both pathogenic variants significantly affect the outgrowth and branching of neuronal processes during development (Figure 22).

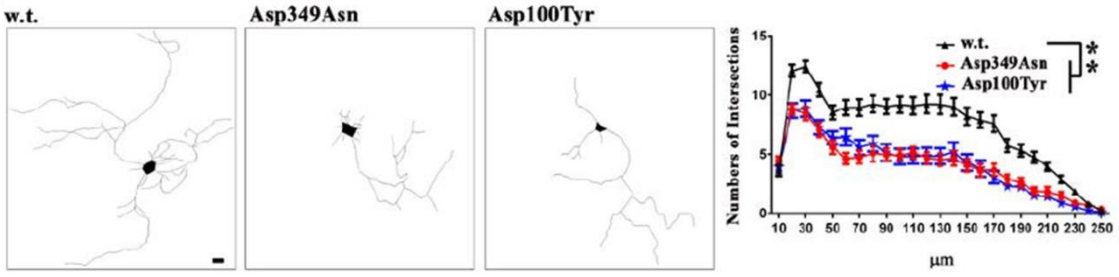

Figure 22. Effect of ATP6V1A mutations on development in primary hippocampal neurons.

*Left: Representative neurite traces of 10 DIV neurons transfected as in A. Right: Sholl analysis of neurite arborization as a function of distance from the soma. Data are means ± SEM of 29–33 neurons for experimental group from three independent preparations. ** p<0.01 versus wild-type; Kruskall-Wallis/Dunn's tests Scale bar = 20 µm.*

5.7 ATP6V1A mutations affect synapse formation in primary neurons

In developing neurons, neurite elongation is followed by synapse formation and stabilization. v-ATPase is a fundamental protein component of synaptic vesicles, where it allows neurotransmitter loading and regulates synaptic transmission (Takamori et al., 2006, Takamori, 2016). Moreover, acidic lysosomes have been recently described at excitatory postsynaptic sites (Goo et al., 2017; Padamsey et al., 2017). Accordingly, the expression of the v-ATPase V_1 subunits, ATP6V1A and ATP6V1B2, was found to increase in parallel with *in vitro* neuronal maturation and synaptogenesis along with the expression of pre- and post-synaptic markers (Figure 23).

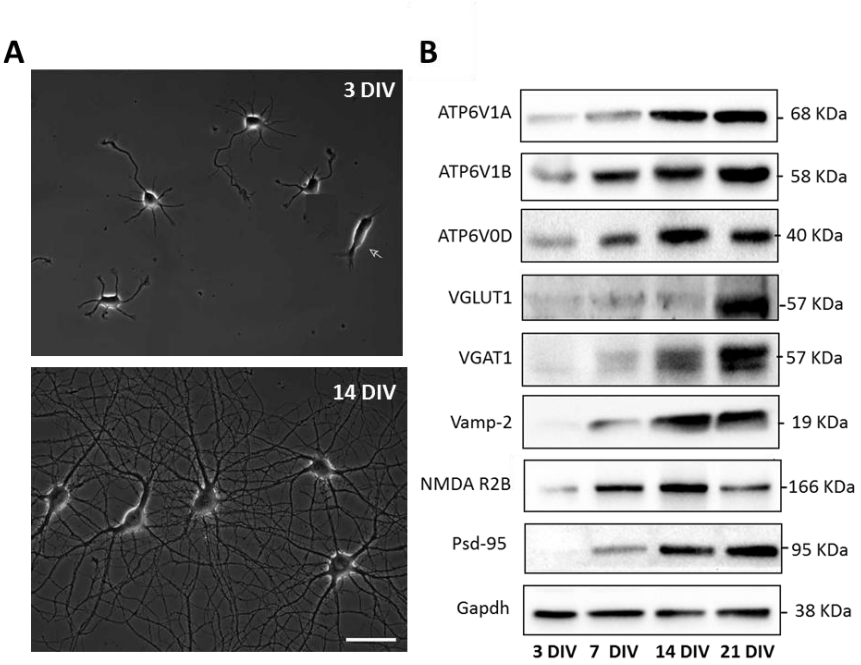

Figure 23. Expression of v-ATPase subunits in developing neurons.

A. (Top) Representative rat hippocampal neurons, cultured on PLL, at DIV 3. (Bottom). Representative rat hippocampal neurons, cultured on PLL, at DIV 14. Scale bar = 90 μm. B Representative western blot of rat hippocampal neuron lysates stained with: v-ATPase subunits, pre-synaptic

markers, post-synaptic markers at different days in vitro (DIV). Gapdh was used as loading control.

To study the effects of ATP6V1A mutants on synapse formation, we transfected hippocampal neurons at 14 DIV and analyzed synapse density at 17 DIV. Excitatory synaptic contacts were visualized by double immunostaining with the excitatory presynaptic marker VGLUT1 and the excitatory postsynaptic marker Homer1 to unambiguously identify mature excitatory synapses. Synapse counting at 30 µm distance from the cell body revealed a significant loss of excitatory synaptic connections for p.Asp349Asn and p.Asp100Tyr overexpressing neurons, suggesting that both pathogenic variants dramatically impair the formation and maintenance of excitatory synapses (Figure 24).

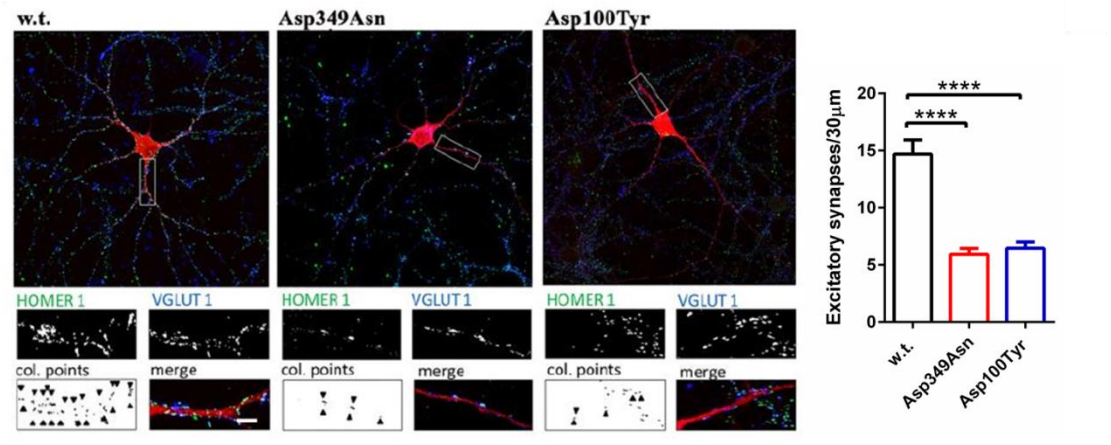

Figure 24. Effect of ATP6V1A mutations on excitatory synaptic connectivity in primary hippocampal neurons.

Left panels: representative images of hippocampal neurons transfected with wild-type ATP6V1A (w.t.), Asp349Asn ATP6V1A (Asp349Asn) or Asp100Tyr ATP6V1A (Asp100Tyr) variants (top) at 14 DIV and analyzed at 17 DIV. White rectangles indicate proximal dendrites shown at high magnification in the bottom panels. Excitatory synaptic boutons were identified by double immunostaining for VGLUT1 (blue) and Homer1 (green). The colocalization panels (col. points) highlight the double-positive puncta (black), marked by

*arrowheads, corresponding to bona fide synapses. The merge panels show positive puncta along transfected branches. Scale bar, 10 µm. Right panel: quantitative analysis of synaptic puncta counted on 30-µm branches starting from the cell body. Data are means ± SEM of 27-28 neurons per experimental condition, from 3 independent preparations. ****p<0.0001 versus w.t.; One-way ANOVA/Bonferroni's tests.*

We further investigated the formation of inhibitory synapses. Neurons were transfected as above at 14 DIV and analyzed for synapse formation at 17DIV. Inhibitory synaptic contacts were visualized by double labeling with presynaptic marker v-GAT and postsynaptic marker Gephyrin, specific for inhibitory pre and post synaptic compartements. Co-localization puncta, representing mature GABAergic synapses, along transfected neurites, were automatically counted in the three experimental conditions. Unlike excitatory synapses, the number of inhibitory synapses was not affected by the expression of pathogenic variants (Figure 25).

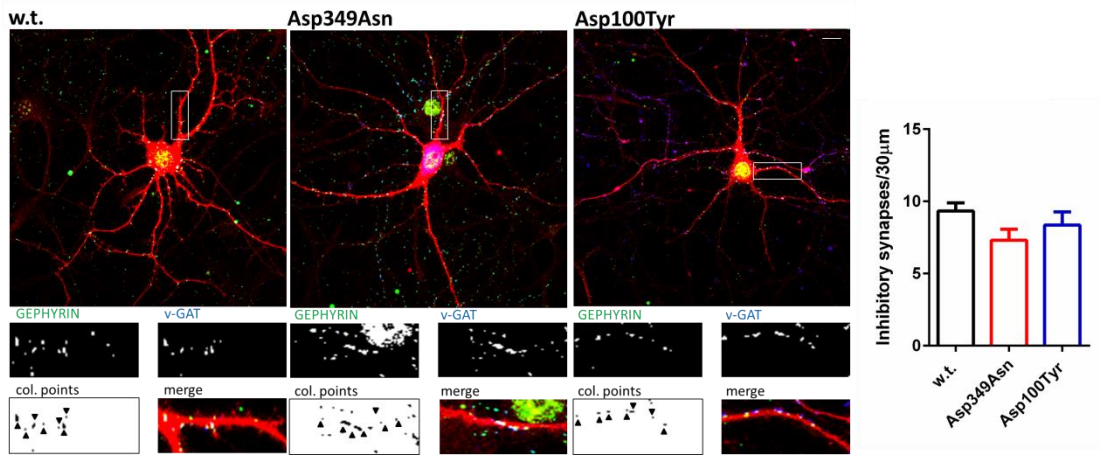

Figure 25. Effect of ATP6V1A mutations on inhibitory synaptic connectivity in primary hippocampal neurons.

Left panels: representative images of hippocampal neurons transfected with wild-type ATP6V1A (w.t.), Asp349Asn ATP6V1A (Asp349Asn) or Asp100Tyr ATP6V1A (Asp100Tyr) variants (top) at 14 DIV and analyzed at 17 DIV. White rectangles indicate proximal dendrites shown at high magnification in the bottom panels. Inhibitory synaptic boutons were identified by double immunostaining for v-GAT (blue) and Gephyrin (green). The

colocalization panels (col. points) highlight the double-positive puncta (black), marked by arrowheads, corresponding to bona fide synapses. The merge panels show positive puncta along transfected branches. Scale bar, 10 µm. Right panel: quantitative analysis of synaptic puncta counted on 30-µm branches starting from the cell body. Data are means ± SEM of 27-28 neurons per experimental condition, from 3 independent preparations. One-way ANOVA/Bonferroni's tests.

Interestingly, when we inhibited lysosomal function, treating hippocampal neurons with the lysosomal enzyme inhibitor leupetin , we found a similar effects on the density of excitatory synaptic contacts (Figure 26).

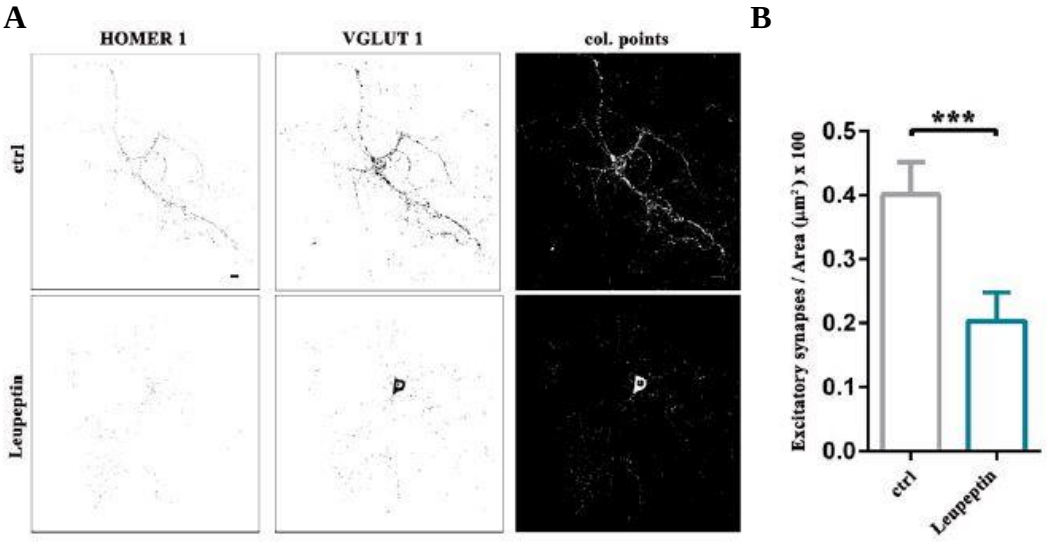

Figure 26. Effects of leupeptin on the density of excitatory synapses.

*A: Representative images of hippocampal neurons at 14 DIV analyzed at 17 DIV under control conditions (ctrl) or treated with 200 µM leupeptin. Synaptic contacts were identified by double immunostaining for VGLUT1 and Homer1. The colocalization panels (col. points) highlight the double-positive puncta (white), corresponding to bona fide synapses. Scale bar, 10 µm. B: Quantitative analysis of the density of excitatory synapses. Data are means ± SEM of 19 neurons per experimental condition, from 3 independent preparations. ***p<0.001 versus ctrl.; Mann-Whitney U-test.*

The fact that leupeptin phenocopied the effects of the ATP6V1A pathogenic variants on synapse formation indicates that this effect may result from an alteration in lysosomal homeostasis that can be perturbed by both lysosome abundance or lysosomal pH.

This is the first evidence of an effect of v-ATPase in synapse formation and suggests that pH homeostasis plays a fundamental role in the proper pre/postsynaptic coupling and that the pathogenic mutation possibly affect synaptogenesis in patient's brain.

We therefore studied the physiological role of *ATP6V1A* on neuronal development and synaptogenesis employing mRNA silencing strategy to model loss ATP6V1A expression in neuronal cell culture.

The day of neuronal culture preparation (0 DIV) a suspension of dissected neurons were nucleofected either with a short-hairpin RNA(Sh-ATP6V1A), or its scrambled version (Scr-ATP6V1A) together with the TurboGFP as gene fluorescent report. We tested the effective knockdown of the protein by western blot analysis. We revealed a strong decreased expression of ATP6V1A at 5 DIV in Sh-ATP6V1A transfected neurons in respect to both not transfected and Scr-ATP6V1A transfected cells (Figure 27 A). We also tested the knockdown of the protein also transfecting hippocampal neurons at 14 DIV and analyzed ATP6V1A expression level at 17 DIV using an antibody anti-ATP6V1A suitable for immunocytochemistry (ICC) (Figure 27 B). Also with ICC experiments, we revealed a strong decreased expression of ATP6V1A in Sh-ATP6V1A transfected neurons in respect to Scr-ATP6V1A transfected cells.

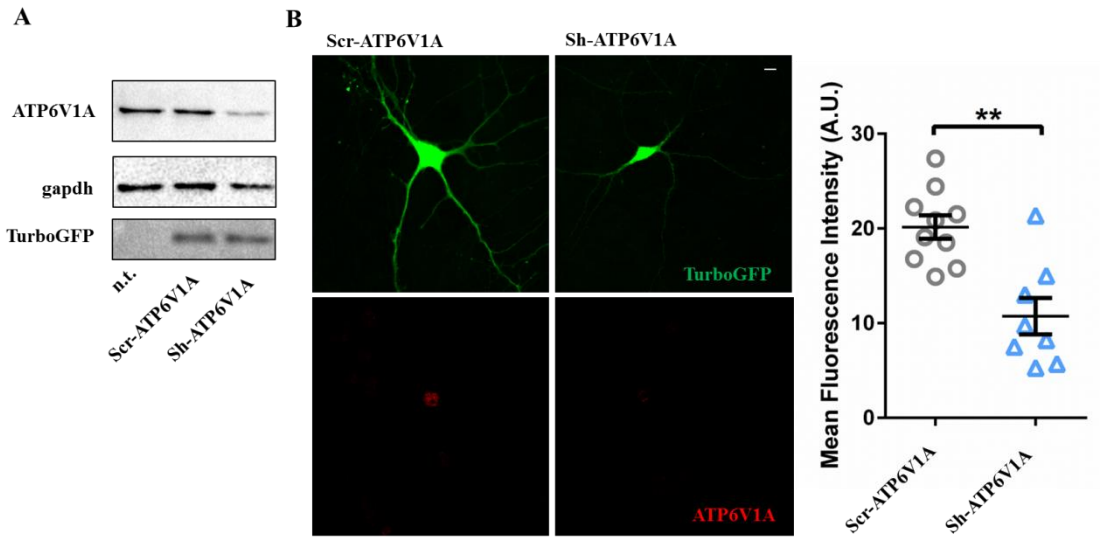

Figure 27. Evaluation of ATP6V1A knock down.

*(A) Representative western blots showing the effective ATP6V1A silencing in rat hippocampal neurons at 5DIV.(B) Representative images of rat hippocampal neurons transfected with Scr-ATP6V1A and Sh-ATP6V1A at 14 DIV and analysed at 17 DIV. Mean fluorescence intensity was quantified in 10 (Scr-ATP6V1A) and 8 (Sh-ATP6V1A) neurons. Individual data and means ± SEM are shown., **p<0.001 versus Scr-ATP6V1A, unpaired t test with Welch's correction. Scale bar = 20 µm.*

In view of the phenotype observed modelling the mutation found in the four patients with EOEE, we investigated whether the effects on lysosomal homeostasis were recapitulated in neurons silenced for ATP6V1A expression. We transiently silenced ATP6V1A in rat hippocampal neuronal cultures and evaluated intracellular acidic organelles by Lysotraker staining at the neuronal soma. As shown in Figure 28, neurons in which ATP6V1A was knocked down showed a significant loss of Lysotraker staining. Thus, the loss of ATP6V1A in neurons resulted an alteration in pH and lysosomal homeostasis.

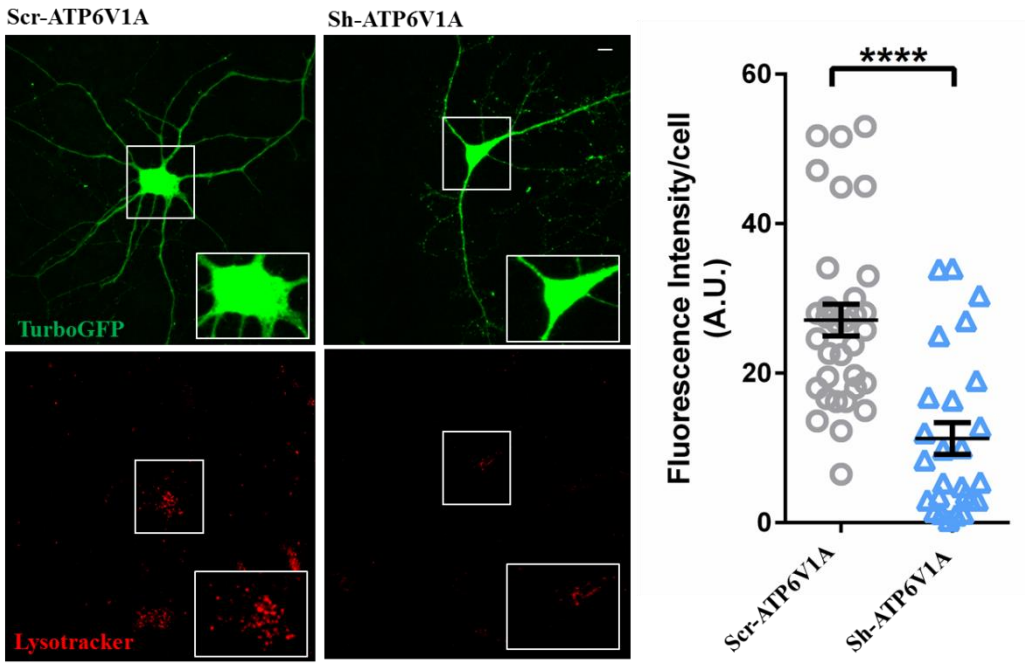

Figure 28. Effect of ATP6V1A knock down on pH homeostasis in primary hippocampal neurons.

*Left: Representative images of rat hippocampal neurons transfected with Scr-ATP6V1A and Sh-ATP6V1A at 14 DIV and incubated with LysoTracker (50 nM, 30 min) at 17 DIV. Right: LysoTracker fluorescence intensity was quantified in 33 (Scr-ATP6V1A) and 26 (Sh-ATP6V1A) neurons from three independent preparations. Individual data and means ± SEM are shown.****p<0.0001 versus Scr-ATP6V1A, unpaired t test with Welch's correction. Scale bar = 20 μm.*

To investigate if the defects on Lysotraker signal have an impact on neuronal development, we transfected rat hippocampal neurons at 14 DIV and analyze neurite elongation at 17 DIV by Sholl analysis. The analysis revealed a similar and significant loss of neurite arborization observed with p.Asp100Tyr (the mutation impacting on ATP6V1A expressing level Figure 22) expressing neurons, indicating that the loss of ATP6V1A protein, causing an alteration on lysosomal homeostasis and pH, significantly affects the outgrowth and branching of neuronal processes during development (Figure 29).

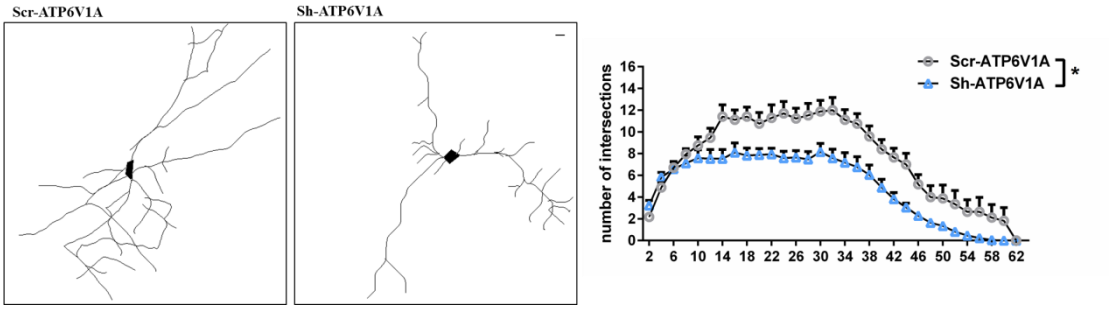

Figure 29. Effect of ATP6V1A loss of expression on development in primary hippocampal neurons.

*Left: Representative images of rat hippocampal neurons transfected with Scr-ATP6V1A and Sh-ATP6V1A at 14 DIV and analyzed at 17 DIV Right: Sholl analysis of neurite arborization as a function of distance from the soma. Data are means ± SEM of 17 neurons for experimental group from three independent preparations. * p<0.01 versus Scr-ATP6V1A; unpaired t test with Welch's correction. Scale bar = 20 µm.*

A disfunction of lysosomal homeostasis and pH can impact on the autophagy being the lysosome the final destination for the engulfed materials of the autophagic process.

Since the loss of ATP6V1A in neurons caused an alteration in pH and lysosomal homeostasis, we assessed the effect of ATP6V1A loss of expression on autophagic flux, by analyzing LC3II expression by western blot analysis. We transiently knocked down ATP6V1A in rat hippocampal neuronal cultures and analyzed the level of LC3II. We revealed a strong increased level of LC3II in Sh-ATP6V1A transfected neurons in respect to Scr-ATP6V1A transfected cells (Figure 30 A). Moreover ICC experiments revealed a strong increased expression of p62 in Sh-ATP6V1A transfected neurons in respect to Scr-ATP6V1A transfected cells (Figure 30 B).

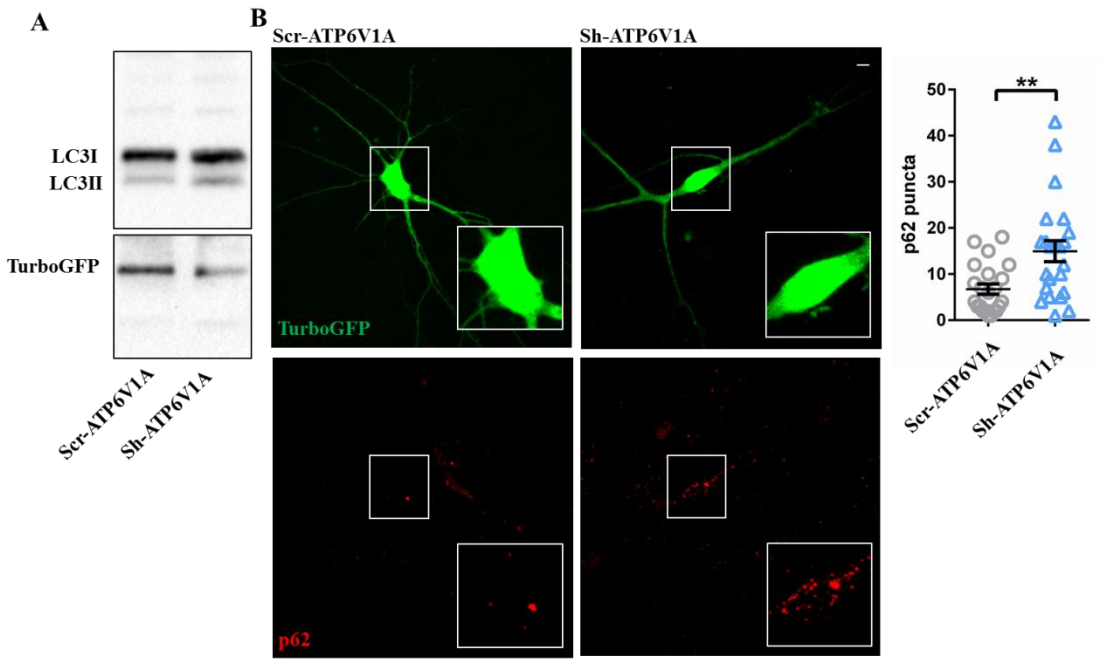

Figure 30. The effect of ATP6V1A knock down on autophagic flux in primary hippocampal neurons.

*(A) Representative western blots showing the increased level of LC3II in Sh-ATP6V1A rat hippocampal neurons compared to Scr-ATP6V1A. (B) Representative images of rat hippocampal neurons transfected with Scr-ATP6V1A and Sh-ATP6V1A at 14 DIV and analysed at 17 DIV. P62 puncta were quantified in 22 (Scr-ATP6V1A) and 23 (Sh-ATP6V1A) neurons from three independent preparations. Individual data and means ± SEM are shown., **p<0.001 versus Scr-ATP6V1A, unpaired t test with Welch's correction. Scale bar = 20 µm.*

These data suggest that the loss of ATP6V1A in neurons caused a block of autophagic flux.

How does this autophagic impairment impact on the excitatory synaptic boutons? To answer this question we investigated the effects of ATP6V1A loss of expression on synapse formation. We transfected hippocampal neurons at 14 DIV and analyzed synapse density at 17 DIV. Excitatory synaptic contacts were visualized by double immunostaining with the presynaptic marker VGLUT1 and the postsynaptic marker Homer1 to unambiguously identify mature excitatory synapses. Synapse counting at

30 µm distance from the cell body revealed a significant loss of excitatory synaptic connections in neurons transfected with Sh-ATP6V1A compared to Scr-ATP6V1A, suggesting that the loss of expression of ATP6V1A significantly impairs the formation and the maintenance of excitatory synapses (Figure 31).

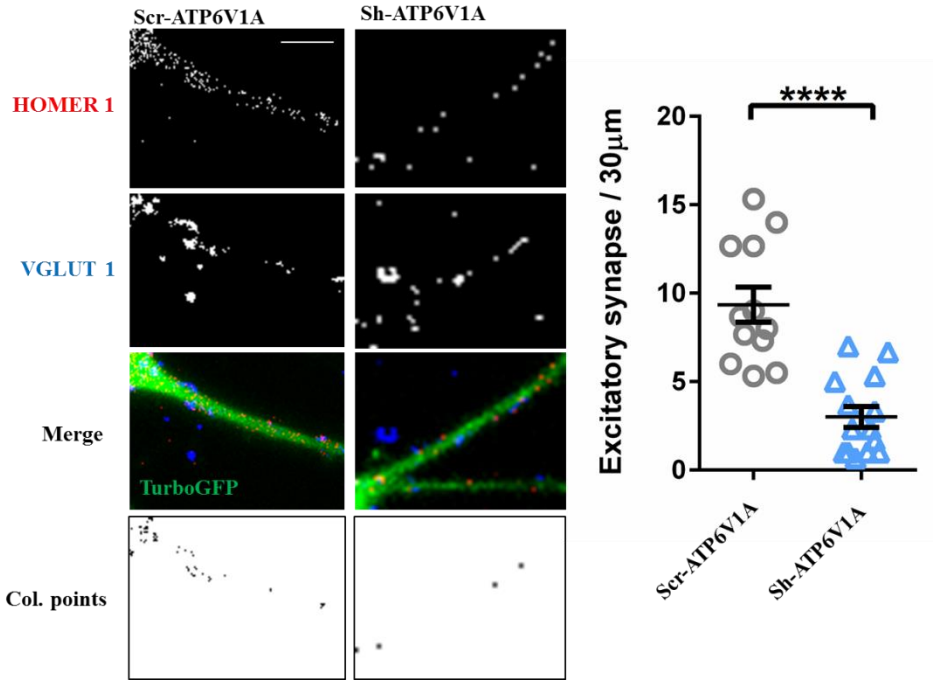

Figure 31. Effect of ATP6V1A loss of expression on excitatory synaptic connectivity in primary hippocampal neurons.

*left panels: representative images of proximal dendrites of hippocampal neurons transfected with Scr-ATP6V1A and Sh-ATP6V1A at 14 DIV and analyzed at 17 DIV. Excitatory synaptic boutons were identified by double immunostaining for VGLUT1 (blue) and Homer1 (Red). The colocalization panels (col. points) highlight the double-positive puncta (black), marked by arrowheads, corresponding to bona fide synapses. The merge panels show positive puncta along transfected branches. Scale bar, 10 µm. Right panel: quantitative analysis of synaptic puncta counted on 30-µm branches starting from the cell body. Data are means ± SEM of 12-14 neurons per experimental condition, from 3 independent preparations. ****p<0.0001 versus Scr-ATP6V1A.; unpaired t test with Welch's correction.*

We showed the loss of ATP6V1A in neurons caused a block of autophagic flux (Figure 30). To associate that the decreased level of excitatory synaptic boutons, caused by the loss of expression of ATP6V1A, is due to an impairment of the autophagic flux, we used bafilomycin, an inhibitor of the vacuolar ATPase, which blocks the fusion of autophagosomes with lysosomes leading to an accumulation of autophagosomal structures (Yamamoto et al., 1998), to inhibits autophagic flux. Cultured primary cortical rat neurons were exposed to 300nM of bafilomycin for 8h and interestingly this treatment significantly increased LC3II and p62 signals phenocopies the results obtained with the knocked down ATP6V1A (Figure 32 A). Moreover, cultured primary cortical rat neurons were exposed to 100nM of bafilomycin for 1h and interestingly this treatment significantly decreased the number of excitatory synapses phenocopying the results obtained with the knocked down ATP6V1A (Figure 32 B) and demonstrating that the loss of ATP6V1A blocks autophagic flux and this effect causes a rearrangement of excitatory synapses.

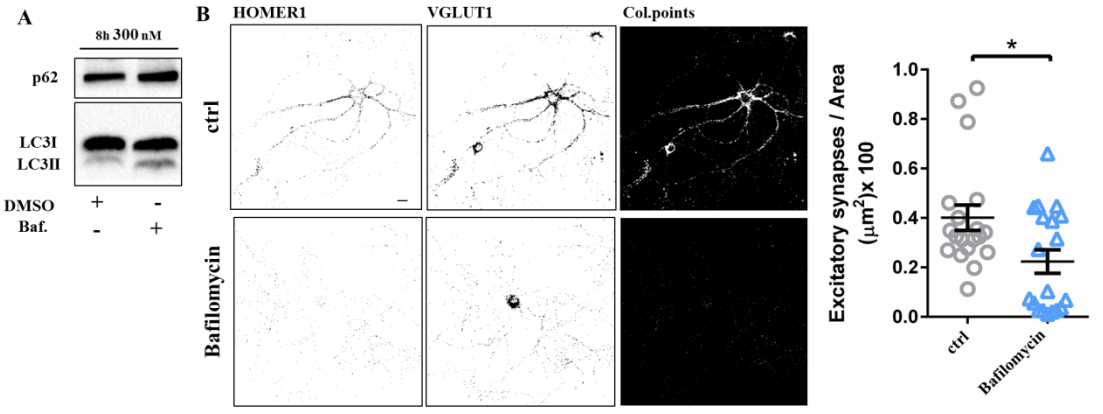

Figure 32. Block of autophagic flux on the density of excitatory synapses.

A: representative Western Blot showing the increased level of LC3II and P62, in lysates of neurons exposed to 300 nM bafilomycin for 8h compared to neurons treated with DMSO as control. B: left panels: Representative images of hippocampal neurons at 17 DIV under control conditions (ctrl) or treated with 100 µM bafilomycin. Synaptic contacts were identified by double immunostaining for VGLUT1 and Homer1. The colocalization panels

*(col. points) highlight the double-positive puncta (white), corresponding to bona fide synapses. Scale bar, 10 µm. Right panel: Quantitative analysis of the density of excitatory synapses. Data are means ± SEM of 19 neurons per experimental condition, from 3 independent preparations. *p<0.05 versus ctrl.; Mann-Whitney U-test.*

6 Discussion

The phenotypic features observed in the four patients reported here can be typically described as developmental encephalopathies with epilepsy and subsumed as *ATP6V1A* encephalopathy, although a larger number of observations is necessary to figure out the whole phenotypic spectrum. However, gathering a large series might require a long time since *ATP6V1A* mutations are very rare as they had not emerged before in large cohorts with epileptic and developmental encephalopathies (Allen et al. 2013, Appenzeller et al. 2014; Developmental Disorders Study 2017) and we could only identify four of them through WES studies on 1498 probands collected in three centers in Europe, Asia and the USA.

Pathogenicity of the *de novo* p.Pro27Arg, p.Asp100Tyr, p.Asp349Asn and p.Asp371Gly variants could be established based on their occurrence in four patients with a developmental encephalopathy with epilepsy, their causing substitutions at highly evolutionarily conserved amino acid positions, their predicted highly damaging consequences emerging from *in silico* methods and the high intolerance of the *ATP6V1A* gene to variations. Accordingly, structural modelling allowed to localise the mutated sites in regions of ATP6V1A responsible for either the proper folding of the subunit (p.Asp100Tyr), the interaction with the V_0 B subunit (p.Pro27Arg) or the catalytic function of the v-ATPase complex (p.Asp349Asn, p.Asp371Gly).

The many genes that have been associated with such complex developmental epilepsy conditions have revealed the pathogenic role of mutations affecting diverse molecular pathways that regulate ion channel functioning, membrane excitability, synaptic plasticity, neurotransmitter release, postsynaptic receptors, transporters, cell metabolism, and many formative steps in early brain development such as the proliferation and migration of neuronal precursors, dendritogenesis, synaptogenesis, cell and glial biology (Guerrini and Noebels, 2014).

Our experimental work on the p.Asp100Tyr and p.Asp349Asn missense substitutions indicates that *ATP6V1A* mutations cause functional defects in v-ATPase physiology with alterations of lysosomal homeostasis associated with abnormal neuritogenesis and excitatory synaptic density.

The main function of v-ATPase is proton transport and acidification of intracellular organelles, in particular lysosomes that have critical requirements for pH. The functional experiments performed on the p.Asp100Tyr mutation, causative of the more severe phenotype, demonstrated an increased degradation with impaired expression of ATP6V1A and a lower lysosomal abundance. This was also associated with a decreased recruitment of v-ATPase by autophagosomes under basal and starvation conditions, suggesting a potential impairment of the autophagic flux, as recently described in patients with mutation in the accessory v-ATPase subunit ATP6AP2 (Rujiano et al. 2017). Conversely, p.Asp349Asn, representative mutation for the milder phenotypes, resulted in decreased endo-lysosomal pH, with no effects on either expression of the mutant protein or lysosomal abundance, pointing to a gain of function effect. This variant slightly impairs v-ATPase translocation to autophagosomes under basal, but not starvation, conditions, suggesting that the formation of autolysosomes is preserved. These functional findings were supported

by structural modeling results, predicting that the p.Asp100Tyr mutation decreases protein stability, whereas p.Asp349Asn affects the catalytic activity of v-ATPase.

When modeled in hippocampal neurons, these pathogenic mutations produced the same significant and divergent effects on lysosomal intensity and endo-lysosomal pH that were observed in cell lines and probands' lymphoblasts, demonstrating the significance of the phenomena for the central nervous system. Moreover, in primary neurons, both p.Asp100Tyr and p.Asp349Asn mutants induced significant and comparable defects in dendrite development and excitatory synapse formation.

This is the first evidence of an effect of v-ATPase in synapse formation and suggests that pH homeostasis plays a fundamental role in the proper pre/postsynaptic coupling and that the pathogenic mutation possibly affect synaptogenesis in patient’s brain.

Considering the emerging role of excitatory/inhibitory balance in epileptic encephalopathy, we further measured GABAergic synapse formation in analogous system. Surprisingly both p.Asp100Tyr and p.Asp349Asn mutants did not affect the development of inhibitory synapses. This result suggests that either Glutamatergic synapse formation is more sensible to pH variation or that GABAergic synapse formation was already completed in the time frame we selected for the experiments. We favor the first hypothesis because western blot analysis revealed a drastic increase of both GABAergic (v-GAT) and glutamatergic (V-GLUT) presynaptic marker between 14 and 18 days in vitro, suggesting that the time interval was proper for both synaptic type. Interestingly, differences in vesicular pH between excitatory and inhibitory synapses have been recently reported: GABAergic synaptic vesicles exhibit a higher resting pH than glutamatergic synaptic vesicles (Egashira et al., 2016), and this difference may be at the basis of the observed phenotype.

The neuronal phenotype of both mutants demonstrates a previously unexplored role of the v-ATPase in the processes of neuronal development and connectivity. As these

effects were phenocopied by leupeptin, a known inhibitor of lysosomal function, it is tempting to speculate that alterations in lysosomal homeostasis can bring about impairments in dendritogenesis and excitatory synapse formation. This hypothesis is also supported by recent reports on novel roles of lysosomes at the synapse for the turnover of synaptic proteins, as well as for the plasticity of dendritic spines (Sambri et al., 2017; Padamsey et al., 2017; Goo et al., 2017). Although the precise molecular mechanisms through which the described *de novo* mutations result in a developmental encephalopathy with epilepsy remain to be clarified, we here propose a role of alteration of lysosomal homeostasis as a novel pathogenic mechanism for epileptogenic developmental encephalopathy. Further work is needed to clarify the role of v-ATPase in brain development and to precisely establish the cellular signaling pathways that can be altered by loss of lysosomal homeostasis.

Next generation sequencing studies have demonstrated that sporadic developmental disorders associated with epilepsy, once considered potentially recessive in nature, often arise from *de novo* mutations of dominant genes and that the same gene can be associated with a broader phenotypic spectrum than originally believed (Mei et al, 2017). Our findings clearly link the *ATP6V1A* gene with a dominant form of encephalopathy after two biallelic homozygous missense mutations of the same gene had been related in three individuals to *cutis laxa*, a rare, severe systemic disorder, leading to early death in one of the patients and featuring, in addition to generalised skin wrinkling, marked hypotonia, dysmorphic facial features, cardiac abnormalities, structural brain abnormalities and seizures (Van Damme et al, 2017). Although comparison between our patients and the three previously reported with biallelic *ATP6V1A* mutations is only partially feasible, there is evidence that biallelic mutations cause a more complex phenotype in which severe neurological manifestations are part of a multiorgan involvement. A number of additional genetic

developmental disorders with epilepsy, including those related to *PRRT2* (Ebrahimi-Fakhari et al, 2015), *TBC1D24* (Balestrini et al, 2016), *RELN* (Dazzo et al, 2015) and *SLC2A1* (Wang et al, 2000) genes, have been associated with both autosomal dominant and more severe recessive phenotypes.

Moreover we tried to elucidate why mutations on *ATP6V1A* can impact on formation and maintenance of excitatory synapses.

V-ATPase is a proton transport important for the acidification of intracellular organelles, in particular lysosomes that have critical requirements for pH. This organelle contains enzymes active at the specific acidic pH, therefore when the lysosomal pH is not in correct range, the enzymatic function is inhibited.

Autophagy is a cellular process that degrades proteins and organelles by delivering them to the lysosome. Three distinct type of autophagy have been described: Microautophagy, chaperone-mediated autophagy and macroautophagy (Kaushik and Cuervo 2012; Mizushima and Komatsu, 2011). Macroautophagy is characterized by the formation of the autophagosome, a double-membrane vesicle. that sequesters autophagic cargo and blends with a lysosome creating the autolysosomes in which the engulfed material is degraded by lysosomal enzymes. This scenario pointed out the central role of lysosomal pH, due to the activity of v-ATPase, in the autophagic pathway.

Autophagy is an housekeeping process and it has a fundamental role in neuronal cells due to their post mitotic and long living nature. At synaptic level however the role of this catabolic process is only beginning to unravel.

The synapse is a neuronal compartment important for the communication between neurons. At presynaptic site there is the quantal release of neurotransmitters into the synaptic cleft, while the post synaptic site contains a high density of receptors active by the neurotransmitter.

Emerging evidence suggests that autophagy is a mechanism with a central role at synaptic level in order to allow the synaptic transmission. A recent work elucidated that presynaptic protein Bassoon, that is a component of the synaptic active zone and crucial for the synaptic vesicles release (Ackermann et al., 2015), is crucial to inhibit autophagy in the presynaptic zone (Okerlund et al., 2018). Loss of Bassoon causes an increased number of autophagosomes in hippocampal neurons. Okerlund et al., proposed that Bassoon inhibits autophagy by interacting with Atg5, a protein crucial for the recruitment of LC3 to autophagosomes leading to an increased presynaptic autophagy with a decreased numbers of synaptic vesicles. This evidence suggests that autophagy flux degrades synaptic vesicles or their compartments.

Recent work demonstrated autophagy plays an important role also on the postsynaptic site, especially in dendritic spines. Shehata et al. suggested autophagy locally degrades internalized AMPA receptors (Shehata et al., 2012). However it is unclear how it contributes to receptor degradation. It is possible that autophagy could degrade proteins involved for keeping receptors attached to the postsynaptic membrane.

After demonstrating an effect of pathogenic mutation affecting one of the v-ATPase's gene on synapse formation and moreover that pH homeostasis plays a fundamental role in the proper pre/postsynaptic coupling, in the last year of my PhD program we investigated on the role of v-ATPase on the autophagy and synaptic maintenance.

In order to demonstrate the role of *ATP6V1A* on neuronal development and synaptic density, we showed a decreased expression of ATP6V1A using a short-hairpin RNA again ATP6V1A both with western blot and ICC experiments. This reduced level of protein was followed by the loss of function of v-ATPase in neurons evaluated as a lower level of lysotracker intensity meaning that there was an alteration in pH and lysosomal homeostasis. This alteration of lysosomal homeostasis and pH, due to the lack of expression of ATP6V1A, followed by a loss of function of this enzyme,

significantly affects the outgrowth and branching of neuronal processes during development. A disfunction of lysosomal homeostasis and pH impacts on the autophagic flux because of the central role of lysosome on macroautophagy.

An experimental method to monitor autophagy is the detection of LC3 protein processing. LC3 proteins are specifically cleaved at the C terminus by Atg4 to become LC3-I, which then conjugates to phosphatidylethanolamine to form LC3-II (Kabeya et al., 2000). Based on the observation that LC3-II is degraded in autolysosomes, the level of LC3-II is used as a marker for the autophagic process (Klionsky et al., 2012). Autophagic flux can be detected by LC3-II turnover using Western blot analysis in the presence of lysosomal degradation inhibitors, such bafilomycin A1. The macrolide antibiotic bafilomycin A1 was among the first of this class isolated from Streptomyces gresius, and has been shown to be an inhibitor of the v-ATPase which controls pH in the lysosome (Browman et al., 1988; Yoshimori et al., 1991; Werner et al., 1984). Through this mechanism bafilomycin inhibits autophagic flux by preventing the acidification of endosomes and lysosomes (Klionsky et al.; 2008; Yamamoto et al.,1998). If autophagic flux is occurring, the level of LC3-II is increased in the presence of the lysosomal degradation inhibitor because the transit of LC3-II through the autophagic pathway is blocked. This scenario leads to a block of autophagic flux with an accumulation of LC3II signal. Moreover, during autophagy many types of cargo are degradated, P62, also known as Sequestosome‑1, is one factor that targets specific cargoes for autophagy (Lamark, 2009). When autophagy is disrupted in several model systems, p62 accumulates.

We assessed the effect of ATP6V1A loss of expression on autophagic flux and revealed strong increased level of LC3II followed by a strong increased expression of p62. We observed the same results when we treated wild type neurons with

bafilomycin. This correlation pointed out the central role of ATP6V1A on the autophagic flux in neuronal cells.

As described above, autophagy as a central role in the brain so we moved to the synaptic level to study if the block of the autophagic flux could impact on the physiology of the excitatory synapses and demonstrated that the loss of expression of ATP6V1A dramatically impair the formation and maintenance of excitatory synapses. Collectively, these results suggest that the absence of a single subunit, ATP6V1A, of v-ATPase causes a dramatic lysosomal pH-dependent dysfunction leading to a block of the autophagic flux affecting both the neurodevelopmental process and the number of excitatory contacts.

7 Future perspectives

After we published the data, many clinicians contacted Prof. Renzo Guerrini and our group to inform on additional EOEE patients harboring mutations in ATP6V1A. Now we list 17 patients with 15 different *de novo* mutations in *ATP6V1A.* We mapped all the mutations in the human ATP6V1A modeled structure and revealed that they all cluster around the A/B interface and /or the A catalytic site. In the future, we plan to proceed to functionally characterize these novel mutations in vitro using patient's cells and neuronal cells.

8 Acknowledgements

Many are the people I would like to thanks for the support and constant help given during these four long years of PhD.

In the first place, I would to thank my supervisor Anna Fassio for her precious advice and the help she gave me to develop this project .

I want also to thank Professor Fabio Benfenati for the great chance to work in its laboratory.

I want to acknowledge Professor Pasquale Striano and Professor Filippo Acconcia for their constructive comments concerning this manuscript.

I will not forget to mention my colleagues, in particular Mattia Bramini and Anna Rocchi which followed me during my first steps in the lab; Emanuele Carminati and Caterina Michetti for the funny moments we shared and all the people of our group working at NSYN.

Many thanks go Davide Aprile, Marco Nigro, Enrico Castroflorio and Stefania Criscuolo for the constant exchange of ideas and the hours passed together inside and outside the lab.

A big thank goes to my “Special People” who, leaving all behind, madly joined me in this adventure. You will always be in my heart.

Any word would be worthless expressing to my parents, my brother, Venus and grandparents the gratitude for their infinite efforts, support and love.

9 Bibliography

Ackermann F, Waites CL, Garner CC. Presynaptic active zones ininver tebrates and vertebrates. EMBO Rep. 2015, 16, 923–938

Allen AS, Berkovic SF, Cossette P, Delanty N, Dlugos D, Eichler EE, *et al*. De novo mutations in epileptic encephalopathies. Nature. 2013; 501: 217-21.

Appenzeller S, Balling R, Barisic N, Baulac S, Caglayan H, Craiu D, et al. De novo mutations in synaptic transmission genes including DNM1 cause epileptic encephalopathies. Am J Hum Genet. 2014; 95: 360-70.

Balestrini S, Milh M, Castiglioni C, Lüthy K, Finelli MJ, Verstreken P, *et al*. TBC1D24 genotype-phenotype correlation: epilepsies and other neurologic features. Neurology. 2016; 87: 77-85.

Bodzęta A, Kahms M, Klingauf J. The presynaptic v-ATPase reversibly disassembles and thereby modulates exocytosis but is not part of the fusion machinery. Cell Rep. 2017; 20: 1348-59.

Bowman, A. Siebers, K. Altendorf, Bafilomycins: a class of inhibitors of membrane ATPases from microorganisms, animal cells, and plant cells, Proc. Natl. Acad. Sci. U.S.A. 85 (21) (1988) 7972–7976.

Bowman, A. Siebers, K. Altendorf, Bafilomycins: a class of inhibitors of membrane ATPases from microorganisms, animal cells, and plant cells, Proc. Natl. Acad. Sci. U.S.A. 85 (21) (1988) 7972–7976.

Clague MJ, Urbé S, Aniento F, Gruenberg J. Vacuolar ATPase activity is required for endosomal carrier vesicle formation: J Biol Chem., 1994, p. 21-4.

Cotter K, Stransky L, McGuire C, Forgac M. Recent insights into the structure, regulation, and function of the v-ATPases. [Review] Trends Biochem Sci. 2015; 40: 611-22.

Davis-Kaplan SR, Compton MA, Flannery AR, Ward DM, Kaplan J, Stevens TH, Graham LA. PKR1 encodes an assembly factor for the yeast V-type ATPase. J Biol Chem., 2006, p. 32025-35. .

Dazzo E, Fanciulli M, Serioli E, Minervini G, Pulitano P, Binelli S, *et al*. Heterozygous reelin mutations cause autosomal-dominant lateral temporal epilepsy. Am J Hum Genet. 2015; 96: 992-1000.

Di Giovanni J, Iborra C, Maulet Y, Lévêque C, El Far O, Seagar M. Calcium-dependent regulation of SNARE-mediated membrane fusion by calmodulin.: J Biol Chem, 2010, Vol. 285, p. 23665-75.

Di Giovanni J, Boudkkazi S, Mochida S, Bialowas A, Samari N, Lévêque C, Youssouf F, Brechet A, Iborra C, Maulet Y, Moutot N, Debanne D, Seagar M, El Far O. V-ATPase membrane sector associates with synaptobrevin to modulate neurotransmitter release. 2010, Vol. 67, p. 268-79.

Ebrahimi-Fakhari D, Saffari A, Westenberger A, Klein C. The evolving spectrum of PRRT2-associated paroxysmal diseases. Brain. 2015; 138: 3476-95.

Edwards R.H. The neurotransmitter cycle and quantal size.: Neuron, 2007, Vol. 55, p. 835-858

Edwards, Thomas S. Hnasko and Robert H. Neurotransmitter Co-release: Mechanism and Physiological Role. Annu Rev Physiol., 2012, Vol. 74, p. 225–243.

Egashira Y, Takase M, Watanabe S, Ishida J, Fukamizu A, Kaneko R, Yanagawa Y, Takamori S. Unique pH dynamics in GABAergic synaptic vesicles illuminates the mechanism and kinetics of GABA loading. Proc Natl Acad Sci U S A, 2016, Vol. 113, p. 10702-7.

El Far O, Seagar M. s.l. A role for V-ATPase subunits in synaptic vesicle fusion? J Neurochem., 2011, Vol. 117, p. 603-12.

Falace A, Filipello F, La Padula V, Vanni N, Madia F, De Pietri Tonelli D, *et al*. TBC1D24, an ARF6-interacting protein, is mutated in familial infantile myoclonic epilepsy. Am J Hum Genet. 2010; 87: 365-70.

Féthière J., Venzke D., Madden D.R., and Böttcher B. Peripheral Stator of the Yeast V-ATPase: Stoichiometry and Specificity of Interaction between the EG Complex and Subunits C and H†.. 2005, Biochemistry, p. 15906–15914.

Fillingame R.H., Angevine C.H., Dmitriev O.Y. Mechanics of coupling proton movements to c-ring rotation in ATP synthase. 2003, FEBS Letters, p. 29–34.

Fischer B, Dimopoulou A, Egerer J, Gardeitchik T, Kidd A, Jost D, *et al*. Further characterization of ATP6V0A2-related autosomal recessive *cutis laxa*. Hum Genet. 2012; 131: 1761-73.

Forgac M. Vacuolar ATPases: rotary proton pumps in physiology and pathophysiology. Nat Rev Mol Cell Biol. 2007; 11: 917-29.

Frattini A, Orchard PJ, Sobacchi C, Giliani S, Abinun M, Mattsson JP, *et al*. Defects in TCIRG1 subunit of the vacuolar proton pump are responsible for a subset of human autosomal recessive osteopetrosis. Nat Genet. 2000; 25: 343-6

Füldner HH, Stadler H. 31P-NMR analysis of synaptic vesicles. Status of ATP and internal pH.: Eur J Biochem., 1982, Vol. 121, p. 519-24.

Ghosh P1, Dahms NM, Kornfeld S. s.l. Mannose 6-phosphate receptors: new twists in the tale. Nat Rev Mol Cell Biol., 2003, Vol. 4, p. 202-12.

Goo MS, Sancho L, Slepak N, Boassa D, Deerinck TJ, Ellisman MH, *et al*. Activity-dependent trafficking of lysosomes in dendrites and dendritic spines. J Cell Biol. 2017; 216: 2499-513.

Graham LA, Flannery AR, Stevens TH. Structure and assembly of the yeast V-ATPase. J Bioenerg Biomembr., 2003, p. 301-12.

Graham LA, Hill KJ, Stevens TH. Assembly of the yeast vacuolar H+-ATPase occurs in the endoplasmic reticulum and requires a Vma12p/Vma22p assembly complex. J Cell Biol., 1998, Vol. 142, p. 39-49.

Guerrini R, Noebels J. How can advances in epilepsy genetics lead to better treatments and cures? Adv Exp Med Biol. 2014; 813: 309–17.

Hiesinger PR, Fayyazuddin A, Mehta SQ, Rosenmund T, Schulze KL, Zhai RG, Verstreken P, Cao Y, Zhou Y, Kunz J, Bellen HJ. The v-ATPase V0 subunit a1 is required for a late step in synaptic vesicle exocytosis in Drosophila. Cell, 2005, Vol. 20, p. 607-20.

Hinton A, Bond S, Forgac M. V-ATPase functions in normal and disease processes. Pflugers Arch., 2009, Vol. 457, p. 589-98.

Hirata T, Iwamoto-Kihara A, Sun-Wada GH, Okajima T, Wada Y, Futai M. Subunit rotation of vacuolar-type proton pumping ATPase: relative rotation of the G and C subunits. J Biol Chem, 2003, Vol. 278, p. 23714-9.

Holliday S. Vacuolar H+-ATPase: An Essential Multitasking Enzyme in Physiology and Pathophysiology New Journal of Science, 2014.

Imamura H, Nakano M, Noji H, Muneyuki E, Ohkuma S, Yoshida M, Yokoyama K. .Evidence for rotation of V1-ATPase. Proc Natl Acad Sci U S A, 2003, Vol. 100, p. 2312–2315.

Imig C, Min SW, Krinner S, Arancillo M, Rosenmund C, Südhof TC, Rhee J, Brose N, Cooper BH. s.l. The morphological and molecular nature of synaptic vesicle priming at presynaptic active zones. Neuron, 2014, Vol. 84, p. 416–431.

Iwata M, Imamura H, Stambouli E, Ikeda C, Tamakoshi M, Nagata K, Makyio H, Hankamer B, Barber J, Yoshida M, Yokoyama K, Iwata S. Crystal structure of a central stalk subunit C and reversible association/dissociation of vacuole-type ATPase. 2004, Proc Natl Acad Sci U S A., p. 59-64.

Kabeya Y, Mizushima N, Ueno T, Yamamoto A, Kirisako T, Noda T. LC3, a mammalian homologue of yeast Apg8p, is localized in autophagosome membranes after processing. EMBO J 2000; 19: 5720–8.

Kane PM. The where, when, and how of organelle acidification by the yeast vacuolar H+-ATPase. Microbiol Mol Biol Rev., 2006, Vol. 70, p. 177-91.

Karet FE, Finberg KE, Nelson RD, Nayir A, Mocan H, Sanjad SA, *et al*. Mutations in the gene encoding B1 subunit of H+-ATPase cause renal tubular acidosis with sensorineural deafness. Nat Genet. 1999; 21: 84-90.

Kaushik S, Cuervo AM. Chaperone-mediated autophagy: a unique way to enter the lysosome world. Trends Cell Biol. 2012 Aug;22(8):407-17

Klionsky, Z. Elazar, P.O. Seglen, D.C. Rubinsztein, Does bafilomycin A1 block the fusion of autophagosomes with lysosomes?, Autophagy 4 (7) (2008) 849–850. [20] V.V. Teplova, A.A. Tonshin, P.A. Grigoriev, N.E. Saris, M.S. Salkinoja-Salonen, Bafilomycin A1 is a potassium ionophore that impairs mitochondrial functions, J. Bioenerg. Biomembr. 39 (4) (2007) 321–329.

Klionsky DJ, Abdalla FC, Abeliovich H, Abraham RT, Adeli K, Agholome L, et al. Guidelines for the use and interpretation of assays for monitoring autophagy. Autophagy 2012; 8: 1–100

Kornak U, Schulz A, Friedrich W, Uhlhaas S, Kremens B, Voit T, *et al*. Mutations in the a3 subunit of the vacuolar H(+)-ATPase cause infantile malignant osteopetrosis. Hum Mol Genet. 2000; 9: 2059-63.

Kortum F, Caputo V, Bauer CK, Stella L, Ciolfi A, Alawi M, *et al*. Mutations in KCNH1 and ATP6V1B2 cause Zimmermann-Laband syndrome. Nat Genet. 2015; 47: 661-7

Lamark, T., Kirkin, V., Dikic, I. & Johansen, T. Cell Cycle 2009. 8, 1986–1990

Laurie A. Graham, Tom H. Stevens, and Randy Schekman. s.l. Role of Vma21p in Assembly and Transport of the Yeast Vacuolar ATPase. Per Malkus, : Mol Biol Cell., 2004, p. 5075–5091.

Lemke JR, Riesch E, Scheurenbrand T, Schubach M, Wilhelm C, Steiner I, Hansen J, Courage C, Gallati S, Bürki S, Strozzi S, Simonetti BG, Grunt S, Steinlin M, Alber M, Wolff M, Klopstock T, Prott EC, Lorenz R, Spaich C, Rona S, Lakshminarasimhan M, Kröll. Targeted next generation sequencing as a diagnostic tool in epileptic disorders: Epilepsia, 2012, Vol. 53, p. 1387-98.

Li H, Durbin R. Fast and accurate long-read alignment with Burrows-Wheeler transform. Bioinformatics. 2010; 26: 589-95.

Liegeois S, Benedetto A, Garnier JM, Schwab Y, Labouesse M. The V0- ATPase mediates apical secretion of exosomes containing Hedgehog-related proteins in Caenorhabditis elegans. J Cell Biol, 2006, Vol. 173, p. 949-961.

Malkus P., Graham L.A., Stevens T.H., and Schekman R. Role of Vma21p in Assembly and Transport of the Yeast Vacuolar ATPase. : Mol Biol Cell., 2004, p. 5075–5091

Maxfield FR, McGraw TE. Endocytic recycling Nat Rev Mol Cell Biol., 2004, p. 121-32

Maxson ME, Grinstein S. The vacuolar-type H+-ATPase at a glance more than a proton pump. Journal of Cell Science, 2014, Vol. 127, p. 4987–4993.

Mei D, Parrini E, Marini C, Guerrini R. The impact of next-generation sequencing on the diagnosis and treatment of epilepsy in paediatric patients. Mol Diagn Ther. 2017; 21: 357-73.

Michaelson DM, Angel I. Determination of delta pH in cholinergic synaptic vesicles: its effect on storage and release of acetylcholine: Life Sci., 1980, Vol. 27, p. 39-44.

Mizushima N, Komatsu M. Autophagy: renovation of cells and tissues. Cell. 2011 Nov 11;147(4):728-41.

Morel N, Poëa-Guyon S. The membrane domain of vacuolar H^+ATPase: a crucial player in neurotransmitter exocytotic release. Cell Mol Life Sci. 2015; 72: 2561-73.

Morel N, Dunant Y, Israël M. Neurotransmitter release through the V0 sector of V-ATPase.. s.l. : J Neurochem., 2011, Vol. 79, p. 485-8

Nabbout R, Dulac O. Epileptic encephalopathies: a brief overview. J Clin Neurophysiol., 2003, Vol. 20, p. 393-7.

Nishi, T. and Forgac, M. The vacuolar (H+)-ATPases-nature's most versatile proton pumps 2002, Nat Rev Mol Cell Biol, p. 94-103.

Nishi S.K., Nishi T., and Michael Forgac.Arg-735 of the 100-kDa subunit a of the yeast V-ATPase is essential for proton translocation. 2001, Proc Natl Acad Sci U S A, p. 12397–12402

Ohira M, Smardon AM, Charsky CM, Liu J, Tarsio M, Kane PM. The E and G subunits of the yeast V-ATPase interact tightly and are both present at more than one copy per V1 complex. 2006, J Biol Chem., p. 22752-60.

Okerlund ND, Schneider K, Leal-Ortiz S, Montenegro-Venegas C, Kim SA, Garner LC, Waites CL, Gundelfinger ED, Reimer RJ, Garner CC. Bassoon Controls Presynaptic Autophagy through Atg5. Neuron. 2018 Feb 7;97(3):727.

Padamsey Z, McGuinness L, Bardo SJ, Reinhart M, Tong R, Hedegaard A, *et al*. Activity-dependent exocytosis of lysosomes regulates the structural plasticity of dendritic spines. Neuron. 2017; 93: 132-46.

Peters C., Bayer M.J., Bühler S., Andersen J.S., Mann M. and Mayer A. Trans-complex formation by proteolipid channels in the terminal phase of membrane fusion.: Nature, 2001, Vol. 409, p. 581-588

Poëa-Guyon S, Ammar MR, Erard M, Amar M, Moreau AW, Fossier P, Gleize V, Vitale N, Morel N. The V-ATPase membrane domain is a sensor of granular pH that controls the exocytotic machinery. J Cell Biol, 2013, Vol. 203, p. 283-98.

Sambri I, D'Alessio R, Ezhova Y, Giuliano T, Sorrentino NC, Cacace V, *et al*. Lysosomal dysfunction disrupts presynaptic maintenance and restoration of presynaptic function prevents neurodegeneration in lysosomal storage diseases EMBO Mol Med. 2017; 9: 112-32.

Shehata M, Matsumura H, Okubo-Suzuki R, Ohkawa N, Inokuchi K. Neuronal stimulation induces autophagy in hippocampal neurons that is involved in AMPA receptor degradation after chemical long-term depression. J Neurosci. 2012 Jul 25;32(30):10413-22.

Stadler H and Tsukita. Synaptic vesicles contain an ATP-dependent proton pump and show 'knob-like' protrusions on their surface. EMBO J., 1984, Vol. 3, p. 3333–3337

Steven B Vik, Julie C Long, Takaaki Wada, Di Zhang A model for the structure of subunit a of the Escherichia coli ATP synthase and its role in proton translocation. 2000, Biochimica et Biophysica Acta (BBA) - Bioenergetics, p. 457–466.

Stover EH, Borthwick KJ, Bavalia C, Eady N, Fritz DM, Rungroj N, *et al*. Novel ATP6V1B1 and ATP6V0A4 mutations in autosomal recessive distal renal tubular acidosis with new evidence for hearing loss. J Med Genet. 2002; 39: 796-803.

Südhof. The Presynaptic Active Zone. TC,: Neuron, 2012, Vol. 75, p. 11–25.

Südhof TC, Rothman JE. s Membrane fusion: grappling with SNARE and SM proteins. Science., 2009, Vol. 323, p. 474-7.

Takamori S. Presynaptic molecular determinants of quantal size. Front Synaptic Neurosci. 2016; 8: 2.

Takamori S, Holt M, Stenius K, Lemke EA, Grønborg M, Riedel D. Molecular anatomy of a trafficking organelle. Cell. 2006; 127: 831-46.

Van Damme T, Gardeitchik T, Mohamed M, Guerrero-Castillo S, Freisinger P, Guillemyn B, *et al*. Mutations in ATP6V1E1 or ATP6V1A Cause Autosomal-Recessive Cutis Laxa. Am J Hum Genet. 2017; 100: 216-27.

Verstegen AM, Tagliatti E, Lignani G, Marte A, Stolero T, Atias M, *et al*. Phosphorylation of synapsin I by cyclin-dependent kinase-5 sets the ratio between the resting and recycling pools of synaptic vesicles at hippocampal synapses. J Neurosci. 2014; 34: 7266-80

Vitavska, O., Wieczorek, H. & Merzendorfer, H. A novel role for subunit C in mediating binding of the H^+-v-ATPase to the actin cytoskeleton. J. Biol. Chem., 2003, p. 18499–18505.

Vitavska O, Merzendorfer H, Wieczorek H. The v-ATPase Subunit C Binds to Polymeric F-actin as Well as to Monomeric G-actin and Induces Cross-linking of Actin Filaments. J Biol Chem, 2005, Vol. 280, p. 1070-1076.

Wang D, Kranz-Eble P, De Vivo DC. Mutational analysis of GLUT1 (SLC2A1) in Glut-1 deficiency syndrome. Hum Mutat. 2000; 16: 224-231.

Wang D, Epstein D, Khalaf O, Srinivasan S, Williamson WR, Fayyazuddin A, Quiocho FA, Hiesinger PR. Ca2+-Calmodulin regulates SNARE assembly and spontaneous neurotransmitter release via v-ATPase subunit V0a1. J Cell Biol., 2014, Vol. 205, p. 21-31.

Werner, H. Hagenmaier, H. Drautz, A. Baumgartner, H. Zahner, Metabolic products of microorganisms. 224. Bafilomycins, a new group of macrolide antibiotics. Production, isolation, chemical structure and biological activity, J. Antibiot. 37 (2) (1984) (110–17).

Wilkens S, Inoue T, Forgac M. Three-dimensional structure of the vacuolar ATPase. Localization of subunit H by difference imaging and chemical cross-linking. 2004, J Biol Chem, p. 41942-9.

Yamagata SK, Parsons SM. Cholinergic synaptic vesicles contain a V-type and a P-type ATPase. J Neurochem, 1989, Vol. 53, p. 1354-62

Yamamoto, A., Y. Tagawa, T. Yoshimori, Y. Moriyama, R. Masaki, and Y. Tashiro. 1998. Bafilomycin A1 prevents maturation of autophagic vacuoles by inhibiting fusion between autophagosomes and lysosomes in rat hepatoma cell line, H-4-II-E cells. Cell Struct. Funct. 23:33–42

Yoshimori, A. Yamamoto, Y. Moriyama, M. Futai, Y. Tashiro, Bafilomycin A1, a specific inhibitor of vacuolar-type H(+)-ATPase, inhibits acidification and protein degradation in lysosomes of cultured cells, J. Biol. Chem. 266 (26) (1991)

Yuan Y, Zhang J, Chang Q, Zeng J, Xin F, Wang J, *et al*. De novo mutation in ATP6V1B2 impairs lysosome acidification and causes dominant deafness-onychodystrophy syndrome. Cell Res. 2014; 24: 1370-3.

Zhang Z, Nguyen KT, Barrett EF, David G. Vesicular ATPase inserted into the plasma membrane of motor terminals by exocytosis alkalinizes cytosolic pH and facilitates endocytosis. Neuron, 2010, Vol. 68, p. 1097-108.

Zhanga Z., Inoueb T., Forgac M., Wilkensa S. Localization of subunit C (Vma5p) in the yeast vacuolar ATPase by immuno electron microscopy. 2006, FEBS Letters, p. 2006-2010.

Zhao J, Benlekbir S, Rubinstein JL. Electron cryomicroscopy observation of rotational states in a eukaryotic v-ATPase. Nature. 2015; 521: 241-5.

10 Appendix

Articles published/ in publication by Alessandro Esposito during the PhD course.

Esposito A+, Fassio A+, Kato M, Saitsu H, Mei D, Marini C, Conti V, Nakashima M, Okamoto N, Olmez Turker A, Albuz B, Semerci Gündüz CN, Yanagihara K, Belmonte E, Maragliano L, Ramsey K, Balak C, Siniard A, Narayanan V; C4RCD Research Group, Ohba C, Shiina M, Ogata K, Matsumoto N, Benfenati F, Guerrini R. **De novo mutations of the ATP6V1A gene cause developmental encephalopathy with epilepsy**. Brain. 2018 Jun 1;141(6):1703-1718. + Equal contribution

Biallelic mutations of the *DMXL2* gene impair autophagy and cause early infantile epileptic encephalopathy with suppression burst (Ohtahara syndrome) with progressive course (submitted)

Alessandro Esposito[1,], Antonio Falace[1], Matias Wagner[1], Moran Gal[1], Davide Mei[,1], Valerio Conti, Tiziana Pisano, Annette Seibt, Daniella Magen, Tilman Polster, Ayelet Eran, Sarah Louise Stenton, Sarit Ravid, Ertan Mayatepek, Hava Hafner, Saskia Wortmann, Erez Y. Levanon, Carla Marini, Hanna Mandel, Fabio Benfenati, Felix Distelmaier, Anna Fassio, and Renzo Guerrini. 1 Equal contribution

Early infantile epileptic encephalopathy (EIEE) with a suppression burst electroencephalographic (EEG) pattern (also known as Ohtahara syndrome) is a severe condition with intractable seizures and profound developmental disability, starting in the first days or months of life. Using whole exome sequencing (WES), we identified homozygous and compound heterozygous mutations of the *DMXL2* gene in six children, born from one non-consanguineous and two consanguineous families, exhibiting severe EIEE phenotypes associated with deafness, peripheral polyneuropathy and dysmorphic facial features, five of whom died in childhood. DMXL2 is highly expressed in the brain, regulates v-ATPase assembly and activity and participates in intracellular signalling pathways. The DMXL2 protein was absent in patient-derived skin fibroblasts, which exhibited an increased Lysotracker signal associated with decreased endo-lysosomal markers and impaired autophagy, an evolutionarily conserved lysosomal degradation process indispensable for cell homeostasis. The phenotype was recapitulated in Dmxl2-silenced mouse hippocampal neurons and was associated with impaired neurite development.

Articles published by Alessandro Esposito during the PhD course due to previous work.

Emanuele M, **Esposito A**, Camerini S, Antonucci F, Ferrara S, Seghezza S, Catelani T, Crescenzi M, Marotta R, Canale C, Matteoli M, Menna E, Chieregatti E. **Exogenous Alpha-Synuclein Alters Pre- and Post-Synaptic Activity by Fragmenting Lipid Rafts**. EBioMedicine. 2016 May;7:191-204.

Alpha-synuclein (αSyn) interferes with multiple steps of synaptic activity at pre-and post-synaptic terminals, however the mechanism/s by which αSyn alters neurotransmitter release and synaptic potentiation is unclear. By atomic force microscopy we show that human αSyn, when incubated with reconstituted membrane bilayer, induces lipid rafts' fragmentation. As a consequence, ion channels and receptors are displaced from lipid rafts with consequent changes in their activity. The enhanced calcium entry leads to acute mobilization of synaptic vesicles, and exhaustion of neurotransmission at later stages. At the post-synaptic terminal, an acute increase in glutamatergic transmission, with increased density of PSD-95 puncta, is followed by disruption of the interaction between N-methyl-d-aspartate receptor (NMDAR) and PSD-95 with ensuing decrease of long term potentiation. While cholesterol loading prevents the acute effect of αSyn at the presynapse; inhibition of casein kinase 2, which appears activated by reduction of cholesterol, restores the correct localization and clustering of NMDARs.

Gallotta I, Mazzarella N, Donato A, **Esposito A**, Chaplin JC, Castro S, Zampi G, Battaglia GS, Hilliard MA, Bazzicalupo P, Di Schiavi E. **Neuron-specific knock-down of SMN1 causes neuron degeneration and death through an apoptotic mechanism**. Hum Mol Genet. 2016 Jun 15;25(12):2564-2577.

Spinal muscular atrophy is a devastating disease that is characterized by degeneration and death of a specific subclass of motor neurons in the anterior horn of the spinal cord. Although the gene responsible, survival motor neuron 1 (SMN1), was identified 20 years ago, it has proven difficult to investigate its effects in vivo. Consequently, a number of key questions regarding the molecular and cellular functions of this molecule have remained unanswered. We developed a Caenorhabditis elegans model

of smn-1 loss-of-function using a neuron-specific RNA interference strategy to knock-down smn-1 selectively in a subclass of motor neurons. The transgenic animals presented a cell-autonomous, age-dependent degeneration of motor neurons detected as locomotory defects and the disappearance of presynaptic and cytoplasmic fluorescent markers in targeted neurons. This degeneration led to neuronal death as revealed by positive reactivity to genetic and chemical cell-death markers. We show that genes of the classical apoptosis pathway are involved in the smn-1-mediated neuronal death, and that this phenotype can be rescued by the expression of human SMN1, indicating a functional conservation between the two orthologs. Finally, we determined that Plastin3/plst-1 genetically interacts with smn-1 to prevent degeneration, and that treatment with valproic acid is able to rescue the degenerative phenotype. These results provide novel insights into the cellular and molecular mechanisms that lead to the loss of motor neurons when SMN1 function is reduced.

Esposito A+, Di Giorgio ML+, Maccallini P, Micheli E, Bavasso F, Gallotta I, Vernì F, Feiguin F, Cacchione S, McCabe BD, Di Schiavi E, Raffa GD**. WDR79/TCAB1 plays a conserved role in the control of locomotion and ameliorates phenotypic defects in SMA models**. Neurobiol Dis. 2017 Sep;105:42-50. + Equal contribution

SMN (Survival Motor Neuron) deficiency is the predominant cause of spinal muscular atrophy (SMA), a severe neurodegenerative disorder that can lead to progressive paralysis and death. Although SMN is required in every cell for proper RNA metabolism, the reason why its loss is especially critical in the motor system is still unclear. SMA genetic models have been employed to identify several modifiers that can ameliorate the deficits induced by SMN depletion. Here we focus on WDR79/TCAB1, a protein important for the biogenesis of several RNA species that has been shown to physically interact with SMN in human cells. We show that WDR79 depletion results in locomotion defects in both Drosophila and Caenorhabditis elegans similar to those elicited by SMN depletion. Consistent with this observation, we find that SMN overexpression rescues the WDR79 loss-of-function phenotype in flies. Most importantly, we also found that WDR79 overexpression ameliorates the locomotion defects induced by SMN depletion in both flies and worms. Our results collectively suggest that WDR79 and SMN play

evolutionarily conserved cooperative functions in the nervous system and suggest that WDR79/TCAB1 may have the potential to modify SMA pathogenesis

Leo D, Sukhanov I, Zoratto F, Illiano P, Caffino L, Sanna F, Messa G, Emanuele M, **Esposito A**, Dorofeikova M, Budygin EA, Mus L, Efimova EV, Niello M, Espinoza S, Sotnikova TD, Hoener MC, Laviola G, Fumagalli F, Adriani W, Gainetdinov RR. **Pronounced Hyperactivity, Cognitive Dysfunctions, and BDNF Dysregulation in Dopamine Transporter Knock-out Rats**. J Neurosci. 2018 Feb 21;38(8):1959-1972.

Dopamine (DA) controls many vital physiological functions and is critically involved in several neuropsychiatric disorders such as schizophrenia and attention deficit hyperactivity disorder. The major function of the plasma membrane dopamine transporter (DAT) is the rapid uptake of released DA into presynaptic nerve terminals leading to control of both the extracellular levels of DA and the intracellular stores of DA. Here, we present a newly developed strain of rats in which the gene encoding DAT knockout Rats (DAT-KO) has been disrupted by using zinc finger nuclease technology. Male and female DAT-KO rats develop normally but weigh less than heterozygote and wild-type rats and demonstrate pronounced spontaneous locomotor hyperactivity. While striatal extracellular DA lifetime and concentrations are significantly increased, the total tissue content of DA is markedly decreased demonstrating the key role of DAT in the control of DA neurotransmission. Hyperactivity of DAT-KO rats can be counteracted by amphetamine, methylphenidate, the partial Trace Amine-Associated Receptor 1 (TAAR1) agonist RO5203648 ((S)-4-(3,4-Dichloro-phenyl)-4,5-dihydro-oxazol-2-ylamine) and haloperidol. DAT-KO rats also demonstrate a deficit in working memory and sensorimotor gating tests, less propensity to develop obsessive behaviors and show strong dysregulation in frontostriatal BDNF function. DAT-KO rats could provide a novel translational model for human diseases involving aberrant DA function and/or mutations affecting DAT or related regulatory mechanisms.

Conference presentations and School of Advanced Studies that Alessandro Esposito jointed during the PhD course

1) **Alessandro Esposito**, Anna Fassio, Davide Mei, Carla Marini, Valerio Conti, Luca Maragliano, Fabio Benfenati and Renzo Guerrini.
"De novo mutations of the ATP6V1A gene cause developmental encephalopathy with epilepsy".
The 11th FENS Forum of Neuroscience, Berlin 2018

2) Alessandro Esposito, Antonella Marte, Manuela Fadda, Franco Onofri, Fabio Benfenati and Anna Fassio.
"Role of Vacuolar ATPase in synapse formation and function."
XVII National Congress of the Italian Society of Neuroscience, Lacco Ameno, Ischia Island-Naples, Italy October 1-4, 2017.

3) **Alessandro Esposito**, Antonella Marte, Manuela Fadda, Elisa Belmonte, Valerio Conti, Davide Mei, Franco Onofri, Renzo Guerrini, Fabio Benfenati and Anna Fassio.
"Synaptic role for vacuolar ATPase V1A subunit."
6th EUROPEAN SYNAPSE MEETIN, Milan, Italy November 4-6, 2017.

School of Advanced Studies:
Autophagy in the healthy and diseased brain, Lake Como, Italy, October 1-4, 2018

doi:10.1093/brain/awy092 BRAIN 2018: 141; 1703–1718 | 1703

BRAIN
A JOURNAL OF NEUROLOGY

De novo mutations of the *ATP6V1A* gene cause developmental encephalopathy with epilepsy

Anna Fassio,[1,2,*] Alessandro Esposito,[1,2,*] Mitsuhiro Kato,[3] Hirotomo Saitsu,[4] Davide Mei,[5] Carla Marini,[5] Valerio Conti,[5] Mitsuko Nakashima,[4,6] Nobuhiko Okamoto,[7] Akgun Olmez Turker,[8] Burcu Albuz,[9] C. Nur Semerci Gündüz,[9] Keiko Yanagihara,[10] Elisa Belmonte,[1] Luca Maragliano,[2] Keri Ramsey,[11] Chris Balak,[11] Ashley Siniard,[11] Vinodh Narayanan,[11] C4RCD Research Group,[11] Chihiro Ohba,[6] Masaaki Shiina,[12] Kazuhiro Ogata,[12] Naomichi Matsumoto,[6] Fabio Benfenati[1,2] and Renzo Guerrini[5,13]

*These authors contributed equally to this work.

V-type proton (H^+) ATPase (v-ATPase) is a multi-subunit proton pump that regulates pH homeostasis in all eukaryotic cells; in neurons, v-ATPase plays additional and unique roles in synapse function. Through whole exome sequencing, we identified *de novo* heterozygous mutations (p.Pro27Arg, p.Asp100Tyr, p.Asp349Asn, p.Asp371Gly) in *ATP6V1A*, encoding the A subunit of v-ATPase, in four patients with developmental encephalopathy with epilepsy. Early manifestations, observed in all patients, were developmental delay and febrile seizures, evolving to encephalopathy with profound delay, hypotonic/dyskinetic quadriparesis and intractable multiple seizure types in two patients (p.Pro27Arg, p.Asp100Tyr), and to moderate delay with milder epilepsy in the other two (p.Asp349Asn, p.Asp371Gly). Modelling performed on the available prokaryotic and eukaryotic structures of v-ATPase predicted p.Pro27Arg to perturb subunit interaction, p.Asp100Tyr to cause steric hindrance and destabilize protein folding, p.Asp349Asn to affect the catalytic function and p.Asp371Gly to impair the rotation process, necessary for proton transport. We addressed the impact of p.Asp349Asn and p.Asp100Tyr mutations on ATP6V1A expression and function by analysing ATP6V1A-overexpressing HEK293T cells and patients' lymphoblasts. The p.Asp100Tyr mutant was characterized by reduced expression due to increased degradation. Conversely, no decrease in expression and clearance was observed for p.Asp349Asn. In HEK293T cells overexpressing either pathogenic or control variants, p.Asp349Asn significantly increased LysoTracker® fluorescence with no effects on EEA1 and LAMP1 expression. Conversely, p.Asp100Tyr decreased both LysoTracker® fluorescence and LAMP1 levels, leaving EEA1 expression unaffected. Both mutations decreased v-ATPase recruitment to autophagosomes, with no major impact on autophagy. Experiments performed on patients' lymphoblasts using the LysoSensor™ probe revealed lower pH of endocytic organelles for p.Asp349Asn and a reduced expression of LAMP1 with no effect on the pH for p.Asp100Tyr. These data demonstrate gain of function for p.Asp349Asn characterized by an increased proton pumping in intracellular organelles, and loss of function for p.Asp100Tyr with decreased expression of ATP6V1A and reduced levels of lysosomal markers. We expressed p.Asp349Asn and p.Asp100Tyr in rat hippocampal neurons and confirmed significant and opposite effects in lysosomal labelling. However, both mutations caused a similar defect in neurite elongation accompanied by loss of excitatory inputs, revealing that altered lysosomal homeostasis markedly affects neurite development and synaptic connectivity. This study provides evidence that *de novo* heterozygous *ATP6V1A* mutations cause a developmental encephalopathy with a pathomechanism that involves perturbations of lysosomal homeostasis and neuronal connectivity, uncovering a novel role for v-ATPase in neuronal development.

1 Department of Experimental Medicine, University of Genoa, Genoa, Italy
2 Center of Synaptic Neuroscience and Technology, Istituto Italiano di Tecnologia, Genoa, Italy
3 Department of Paediatrics, Showa University School of Medicine, Tokyo, Japan

Received August 22, 2017. Revised January 26, 2018. Accepted February 10, 2018. Advance Access publication April 13, 2018

4 Department of Biochemistry, Hamamatsu University School of Medicine, Hamamatsu, Japan
5 Pediatric Neurology, Neurogenetics and Neurobiology Unit and Laboratories, Children's Hospital A. Meyer-University of Florence, Florence, Italy
6 Department of Human Genetics, Yokohama City University Graduate School of Medicine, Yokohama, Japan
7 Department of Medical Genetics, Osaka Women's and Children's Hospital, Osaka, Japan
8 Private Clinic, Denizli, Turkey
9 Department of Medical Genetics, Pamukkale University Hospital, Denizli, Turkey
10 Department of Paediatric Neurology, Osaka Women's and Children's Hospital, Osaka, Japan
11 Center for Rare Childhood Disorders and Neurogenomics Division Translational Genomics Research Institute, Phoenix, Arizona 85004, USA
12 Department of Biochemistry, Yokohama City University Graduate School of Medicine, Yokohama, Japan
13 IRCCS Fondazione Stella Maris, Pisa, Italy

Correspondence to: Prof. Renzo Guerrini
Neuroscience Department, Anna Meyer Children's University Hospital, Florence Italy
E-mail: r.guerrini@meyer.it

Correspondence may also be addressed to: Prof. Anna Fassio
Department of Experimental Medicine, University of Genoa, Italy
E-mail: afassio@unige.it

Prof. Naomichi Matsumoto
Department of Human Genetics, Yokohama City University, Japan
E-mail: naomat@yokohama-cu.ac.jp

Keywords: developmental epileptic encephalopathy; v-ATPase; lysosomes; neurite elongation; synapse

Abbreviations: DIV = days *in vitro*; v-ATPase = v-type proton (H^+) ATPase

Introduction

V-type proton (H^+) ATPase (v-ATPase) is a multimeric complex that acts as an ATP-dependent proton pump. V-ATPase is composed of a peripheral V_1 domain that hydrolyses ATP and an integral V_0 domain that translocates protons by a rotary mechanism. V-ATPase is responsible for membrane trafficking processes such as receptor-mediated endocytosis, intracellular trafficking of lysosomal enzymes, and acidification of intracellular organelles in all eukaryotic cells (Forgac, 2007; Cotter *et al.*, 2015). Despite the ubiquitous role in pH homeostasis and intracellular signalling pathways, the v-ATPase complex is expressed at high levels in neurons where it plays additional and unique roles in neurotransmitter loading into synaptic vesicles and in regulating synaptic transmission (Morel and Poëa-Guyon, 2015; Bodzęta *et al.*, 2017).

In humans, a redundant set of subunits is encoded by 22 autosomal genes, allowing the composition of diverse v-ATPase complexes with specific properties and tissue expression. Among these, seven have been associated with human disease (Supplementary Table 1). Six subunits have been related to recessive disorders, including distal renal tubular acidosis and hearing loss (ATP6V1B1 and ATP6V0A4) (Karet *et al.*, 1999; Smith *et al.*, 2000; Stover *et al.*, 2002), osteopetrosis with macrocephaly, progressive deafness, blindness, hepatosplenomegaly, and severe anaemia (ATP6V0A3) (Frattini *et al.*, 2000; Kornak *et al.*, 2000), and cutis laxa, a systemic disease with severe neurological impairment featuring structural brain abnormalities, profound delay, and seizures (ATP6V0A2, ATP6V1E1 and ATP6V1A) (Kornak *et al.*, 2008; Fischer *et al.*, 2012; Van Damme *et al.*, 2017). Two allelic dominant disorders, Zimmermann-Laband syndrome type 2, featuring facial dysmorphisms and intellectual disability (Kortum *et al.*, 2015) and a form of congenital deafness with anonyochia, have also been described (ATP6V1B2) (Yuan *et al.*, 2014).

Through whole exome sequencing of 1444 patients with developmental encephalopathies and epilepsy, we identified in four patients heterozygous *de novo* missense mutations in *ATP6V1A* (p.Pro27Arg, p.Asp100Tyr, p.Asp349Asn, p.Asp371Gly), all involving highly evolutionarily conserved residues in functionally relevant regions of the molecule. Functional analysis conducted for the p.Asp100Tyr and p.Asp349Asn mutations demonstrated a loss-of-function mechanism involving increased ATPase degradation and lysosomal defects for the former, and a gain-of-function mechanism consisting of increased acidification of intracellular organelles for the latter. In neurons, both ATP6V1A mutants caused a defect in neurite elongation, accompanied by a significant loss of excitatory synapses, suggesting a crucial and unexplored role of v-ATPase in neuronal development and synapse formation. We provide evidence that *de novo* heterozygous *ATP6V1A* mutations cause a developmental encephalopathy with epilepsy with a pathomechanism that involves the effects of v-ATPase in lysosomal homeostasis and neuronal connectivity. This study also demonstrates that *ATP6V1A* mutations can be disease causing at the heterozygous state, although previously described biallelic phenotypes are more severe.

Patients and methods

Patients

Exome studies were conducted in three cohorts, including patients of different ethnicities (Supplementary Table 2A), with developmental delay/intellectual disability and epilepsy of presumed genetic origin. The overall series consisted of 1444 probands, most of whom were part of a trios study. Patients were assigned to eight specific epileptic encephalopathy syndromes, plus a ninth subgroup of 'unclassified' epileptic encephalopathies with mixed seizure disorders that could not be assigned to a specific syndrome (Supplementary Table 2B). All four patients with *ATP6V1A* mutations belonged to the latter subgroup.

All participants to the study had signed an informed consent for research whole exome sequencing studies. The study was approved by the Paediatric Ethic Committee of the Tuscany Region, in the context of the DESIRE project (Seventh Framework Programme FP7; grant agreement n° 602 531).

Whole exome sequencing

In 900 patients, whole exome sequencing was performed with the SureSelectXT Human All Exon v5 or v6 (Agilent Technologies). Captured libraries were sequenced using Illumina Hiseq 2500 (Illumina) with 101-base paired-end reads. Exome data processing, variant calling, and variant annotation were performed as previously described (Saitsu *et al.*, 2013). In singleton probands exhibiting *de novo* mutations, parentage was confirmed by microsatellite analysis, as previously described (Saitsu *et al.*, 2013). In 494 patients, whole exome sequencing was performed and analysed as previously described (Narayanan *et al.*, 2015). In 50 additional patients, exons were captured from fragmented genomic DNA samples using the SureSelect Human All Exon v4 (Agilent Technologies), and paired-end 90-base massively parallel sequencing was carried out on an Illumina HiSeq 2000, according to the manufacturer's protocols (Illumina). In the latter group, bioinformatics analysis was carried out using an in-house developed pipeline. Sequencing reads passing quality filtering were aligned to the human reference genome (hg19) with Burrows-Wheeler Aligner (BWA) (Li and Durbin, 2010). The Genome Analysis Toolkit (GATK) (McKenna *et al.*, 2010) was used for base quality score recalibration, indel realignment, duplicate removal, and to perform SNP and INDEL discovery and genotyping across all samples simultaneously using variant quality score recalibration according to GATK Best Practices recommendations (DePristo *et al.*, 2011; Van der Auwera *et al.*, 2013). For annotating and filtering data, the SNPeff program was used (Cingolani *et al.*, 2012). The *de novo* variants were called using the DeNovoGear tool with a 0.8 threshold at the posterior probability of the most likely *de novo* genotype configuration (Ramu *et al.*, 2013). All samples had a mean depth of target region covered at 112× and >97% of bases in the consensus coding sequences covered by at least 20 reads. We excluded variants with minor allele frequency (MAF) >1% in either the 1000 Genomes Project (1000g) or the Exome Aggregation Consortium (ExAC v0.3) databases.

In patients carrying *ATP6V1A* variants, we excluded *de novo* or recessive (MAF < 1%) variants in the well-established genes for epileptic encephalopathies (listed in Supplementary Table 3) and submitted for validation and segregation testing by Sanger sequencing of candidate *de novo* variants that were predicted to alter protein function (non-synonymous, stop-gain, stop-loss, frameshift, and splice-junction mutations).

We evaluated whether the *ATP6V1A* human protein-coding gene is likely to harbour disease-causing mutations using different gene-level prediction tools including the ExAC (Exome Aggregation Consortium) constraint metrics (Lek *et al.*, 2016), the residual variation intolerance score (RVIS; based on ExAC v2 release 2.0) (Petrovski *et al.*, 2013) and the gene damage index (GDI) (Itan *et al.*, 2015). Furthermore, to improve the use of existing variant-level methods such as the Combined Annotation Dependent Depletion (CADD) score (Kircher *et al.*, 2014) and test the four missense substitutions we identified in *ATP6V1A*, we also used the mutation significance cut-off (MSC) server (Itan *et al.*, 2016), a quantitative approach that provides gene-level and gene-specific phenotypic impact cut-off values.

We evaluated mutations' pathogenicity for the four *ATP6V1A* variants through *in silico* prediction using the dbNSFP database (v3.0a), which provides functional prediction scores on more than 20 different algorithms (https://sites.google.com/site/jpopgen/dbNSFP). To assess the effects of the four missense *ATP6V1A* substitutions, we used both the dbNSFP ensemble rank scores MetaSVM and MetaLR (Liu *et al.*, 2016). In addition, we used the scores obtained from Revel (Ioannidis *et al.*, 2016), M-CAP (Jagadeesh *et al.*, 2016) and Eigen (Ionita-Laza *et al.*, 2016), three different bioinformatics tools to evaluate the pathogenicity of rare variants.

We performed conservation analysis across species (orthologous sequences) using a multiple sequence alignment (MSA) of the ATP6V1A protein sequence. The MSA (MUSCLE algorithm) and the sequence logo consensus were generated by the Jalview software (http://www.jalview.org). Residues were coloured according to their physicochemical properties (Zappo colour scheme).

To evaluate if *de novo ATP6V1A* variants had ever been reported, either in affected individuals or controls, we interrogated the denovo-db database (Turner *et al.*, 2017).

ATP6V1A gene *de novo* mutation enrichment analysis

To assess whether in the 1444 probands cohort the *ATP6V1A* gene was enriched in missense *de novo* mutations, we used the freely available R package DenovolyzeR (Ware *et al.*, 2015) and gene-specific mutation rates originally reported by Samocha *et al.* (2014). The *ATP6V1A de novo* gene-specific *P*-value calculated by DenovolyzeR for missense variants was corrected for multiple testing (Bonferroni correction), according to the 19 618 genes for which mutation rates are available, and the number of tests (one test for the missense class). The genome-wide Bonferroni corrected *P*-value threshold at $\alpha = 0.05$ for one test was 2.55×10^{-6} [0.05/(1 × 19 168)]. We carried out the *ATP6V1A de novo* mutation enrichment analysis in the overall cohort without any stratification using the RStudio software (rstudio.com).

To rule out that the four variants could have arisen by chance, we performed the chi-squared test with Yates correction for a 2 × 2 contingency table (patients carrying the variants/mutation negative patients versus controls carrying the variants/mutation negative controls) using the QuickCalcs tool (graphpad.com/quickcalcs/contingency1.cfm). For each variant, we carried out the test on exome data of our cohort and the Genome Aggregation Database (gnomAD) cohorts, both at large and through ethnicity-matched analysis.

Structural modelling

We searched the crystal structure homologous to human ATP6V1A using the protein homology/analogy recognition engine, Phyre2 (Kelley *et al.*, 2015). We calculated the free energy change upon the Asp85Tyr mutation with the FoldX software (foldxsuite.crg.eu) using the crystal structure of the V_1 domain from *Enterococcus hirae* v-ATPase in a nucleotide-bound state (PDB code 3VR6). The molecular structures were drawn using PyMOL (Schrödinger, New York, NY). Using the same Phyre2 server, we also obtained the alignment of human ATP6V1A and *Saccharomyces cerevisiae* A subunit primary sequences. The homology model was created using I-TASSER (Roy *et al.*, 2010), with the A subunit of *S. cerevisiae* v-ATPase (PDB code 3J9T) as template.

ATP6V1A constructs

We synthesized wild-type and mutant (p.Asp100Tyr and p.Asp349Asn) human *ATP6V1A* cDNAs *in vitro* and cloned in pLVX-IRES-mCherry vector by Biomatik. We performed Sanger sequencing of all constructs to check the correct inserts orientation and validate their sequence.

Cell culture and transfection

Human embryonic kidney-derived 293T (HEK) cells were maintained at 37°C in a humidified 5% CO_2 incubator in DMEM (Life Technologies) supplemented with 10% FBS, 2 mM L-glutamine and 1% Penicillin-Streptomycin. Cells were transfected with Lipofectamine 2000 (Life Technologies) according to the manufacturer's instructions. HEK cells were starved by medium withdrawal for 2 h. Lymphoblatsts were prepared by infecting lymphocytes obtained from patients and their parents with the Epstein-Barr virus (EBV) *in vitro* using standard protocols and maintained in RPMI 20% foetal bovine serum (FBS), 1 mM L-glutamine and 10 mM D-glucose. Primary cortical neurons were prepared from embryonic Day 18 brains of Sprague Dawley rats as previously described (Verstegen *et al.*, 2014). Neurons were transfected using Lipofectamine® 2000 at 7 or 14 days *in vitro* (DIV) and analysed 3 days after transfection.

Western blotting

Protein lysates from HEK, lymphoblast and neuronal cultures were extracted in lysis buffer [50 mM Tris (pH 7.5), 150 mM NaCl, 0.1% SDS, 1% Nonidet P40, 0.2 mM phenylmethylsulfonyl fluoride, 2 µg/ml pepstatin, and 1 µg/ml leupeptin] and then separated by SDS-PAGE and assayed by immunoblotting with the following primary antibodies: anti-ATP6V1A (1:1000; #ab137574, Abcam), anti-ATP6V1B2 (1:2000; #ab73404, Abcam), anti-LAMP1 (1:1000; #ab24170, Abcam), anti-EEA1 (1:5000; #610457, BD Bioscience), LC3B (1:1000; #7543, Sigma-Aldrich), p62 (1:1000, #P0067, Sigma-Aldrich), anti-GAPDH (1/1000; #SC-25778, Santa Cruz Biotechnology), anti-VAMP2 (1:1000; #104202; Synaptic Systems); anti-V-GLUT1 (1:1000; #135304, Synaptic Systems) anti-PSD95 (1:1000; #SC-32290, Santa Cruz Biotechnology).

Degradation assay

HEK cells were transfected with ATP6V1A wild-type, ATP6V1A Asp349Asn or ATP6V1A Asp100Tyr and treated with 10 µg/ml of cycloheximide (C4859, Sigma-Aldrich) 24 h after transfection. Cells were lysed at different times after cycloheximide addition and analysed by western blotting. Protein level is expressed with respect to ATP6V1A content in the cells collected at time zero and treated with vehicle (DMSO).

Immunocytochemistry and fluorescence microscopy

Transfected primary cortical neurons or HEK cells were fixed in 4% paraformaldehyde in phosphate-buffered saline (PBS), permeabilized in 0.1% Triton™ X-100, blocked with 2% FBS/0.05% Tween-20 in PBS and incubated with the various antibodies in blocking solution. Samples were mounted in ProLong® Gold antifade reagent with DAPI (#P36935, Thermo-Fisher Scientific). Capture of confocal images was performed using a laser scanning confocal microscope (SP5, Leica) with a 40× or 63× oil-immersion objective. For LAMP1 (1:200, #L1418 Sigma-Aldrich) and EEA1 (1:500; #610457, BD Bioscience), ATP6V1B2 (1:200, #SAB1405501 Sigma-Aldrich) and LC3B (1:200, #2775 Cell Signalling) labelling, each image consisted of a stack of images taken through the *z*-plane of the cell. The co-localization of ATP6V1B2 and LC3B signals was analysed using the ImageJ intensity correlation analysis plugin to calculate Pearson's correlation coefficient. For LysoTracker® Deep Red (Molecular Probes/Life Technologies) experiments, HEK cells were incubated with 200 nM LysoTracker® for 1 h, whereas neurons were incubated with 50 nM LysoTracker® for 30 min, at 37°C in culture medium, immediately fixed and analysed within 12 h. Images were taken at either epifluorescence (Olympus 1X81) or confocal (SP5, Leica) microscope in a single plane not to fade the fluorescent signal. Settings were kept the same for all acquisitions within each experiment.

Measurement of endo-lysosomal pH

Endo-lysosomal pH was measured using a ratiometric pH indicator dye, LysoSensor™ Yellow/Blue dextran (Molecular Probes/Life Technologies), a dual excitation dye that allows pH measurement in endocytic organelles independently of dye concentration. Lymphoblasts (4×10^6) were incubated for 3 h at 37°C with 0.5 mg/ml of LysoSensor™ Yellow/Blue dextran in culture medium. Cells were divided into five samples, four to perform the calibration curve and one for the measurements. To obtain a pH calibration curve, cells were resuspended with MES calibration buffer solution

(5 mM NaCl, 115 mM KCl, 1.2 mM $MgSO_4$ and 25 mM MES, pH ranging from 3.7 to 7.6) containing 10 µM monensin (Sigma-Aldrich) and 10 µM nigericin (Sigma-Aldrich). For the pH measures, cells were resuspended in MES calibration buffer solution pH 7.7 in the absence of ionophores. Emission scans were collected at 450 nm and 528 nm with the Luminescence Spectrometer LS 50 (Perkin Elmer), using excitation at 360 nm and emission/excitation bandwidths set to 4 nm. Calibration data (ratio 450/528) were fitted to a linear regression with the software GraphPad Prism5 and the sample ratios converted into absolute pH values by interpolation in the calibration function.

Sholl analysis

Neurons were plated at low density (80 cells/mm^2), transfected at 7 DIV and analysed at 10 DIV. For analysis, neurons were fixed in 4% PFA, in PBS and decorated with βIII tubulin antibody (1:1000, #MMS-435P Covance) followed by Alexa Fluor® 488 secondary antibody to unequivocally distinguish neuronal cells. The extent of neurite arborization was evaluated using Sholl analysis as previously described (Falace *et al.*, 2010). Concentric circles with radii increasing at regular 10-µm steps were centred to the cell body and the number of intersections was automatically evaluated with the ImageJ/Sholl analysis plug-in.

Synapse quantification

Neurons, plated at low density as described above, were either transfected at 14 DIV and analysed at 17 DIV or treated at 17 DIV with 200 nM leupeptin for 3 h (#EI8, MerckMillipore; Goo *et al.*, 2017). To measure excitatory synapses, neurons were labelled with anti-V-GLUT1 (1/500, #135304; Synaptic Systems) and anti-Homer1 (1/200, #160011; Synaptic Systems) antibodies. Confocal images were acquired with a laser scanning confocal microscope (SP5 Upright, Leica) with a 40× oil-immersion objective. Each image consisted of a stack of images taken through the *z*-plane of the cell. Confocal microscope settings were kept the same for all scans in each experiment. The co-localization analysis was performed by evaluating the labelling of the VGLUT1/Homer1 synaptic protein couples. Co-localization puncta with areas of 0.1–2 µm^2 were considered *bona fide* synaptic boutons. Synaptic boutons along Cherry-positive neurites were manually counted on 30 µm puncta starting from the cell body.

Results

Identification of *ATP6V1A* mutations

Trio-based whole exome sequencing studies revealed *de novo* mutations in *ATP6V1A* (MIM 607027; RefSeq accession number NM_001690.3), encoding the ATPase H^+ transporting V_1 subunit A in three patients [Patient 1: c.298G > T (p.Asp100Tyr); Patient 2: c.1045G > A (p.Asp349Asn); and Patient 4: c.80C > G (p.Pro27Arg)]. A subsequent search for *ATP6V1A* variants in whole exome sequencing data obtained from singleton patients, identified an additional patient carrying a *de novo* heterozygous *ATP6V1A* variant [Patient 3: c.1112A > G (p.Asp371Gly)]. Patients 1–3 were identified via an ongoing collaboration matching exome data generated in Europe by the DESIRE project on rare developmental/epileptic encephalopathies (http://epilepsydesireproject.eu) with those of a comparable cohort in Japan. Patient 4 was subsequently identified through DESIRE dissemination activities, after preliminary data on the first three patients were made available in the project website. We also screened for *ATP6V1A* inherited variants with a frequency <1% in the 1000 Genomes Project (1000g) or in the Exome Aggregation Consortium (ExAC) databases, both in cases of homozygous recessive or compound heterozygous state.

None of the *de novo ATP6V1A* identified mutations was observed in the 1000g, ExAC, gnomAD or dbSNP (build 147) databases. We confirmed the mutations and their *de novo* nature on genomic DNA of probands and parents by Sanger sequencing. Patient 3 parentage was confirmed using 12 microsatellite markers.

All four highly functionally relevant *de novo* mutations caused missense substitutions at evolutionarily conserved amino acid positions (Fig. 1) and were predicted to be damaging by *in silico* methods (Supplementary Table 4A). ExAC constraint metrics indicated that *ATP6V1A* has fewer variants than expected and is intolerant both to loss-of-function (pLI = 0.99) and missense variants (Z-score = 3.03). The RVIS (RVIS score −0.7; RVIS percentile 20.93%) and the GDI (GDI score 22.7; GDI_Phred 0.76) scores also highlight *ATP6V1A* intolerance to variations. Finally, the MSC damage prediction (99% confidence interval) tool highlights the highly damaging impact the p.Pro27Arg, p.Asp100Tyr, p.Asp349Asn, and p.Asp371Gly substitutions have on the ATP6V1A protein, according to the MSC CADD corrected scores (Supplementary Table 4B).

To explore pathogenicity of the four variants further, we performed gene-specific *de novo* mutation enrichment analysis and a variant-specific chi-squared test with Yates correction for a 2 × 2 contingency table. The *ATP6V1A* missense *de novo* mutations enrichment analysis performed with DenovolyzeR ($n = 1444$, *de novo* mutations observed = 4, *de novo* mutations expected = 0.1, enrichment 79) reached genome-wide statistical significance (P-value of 2.63×10^{-7}; Bonferroni correct threshold P-value 2.55×10^{-6}). All four variants reached significant values ($P < 0.0001$) in the chi-squared test performed using the 123136 gnomAD exomes as control (Supplementary Table 5A). Performing the same analysis matching the four mutations versus ethnically matched subpopulations, all mutations maintained significant values (Supplementary Table 5B–E). These data suggest that the *ATP6V1A* mutations did not occur by chance in the cohort studied.

The denovo-db returned only five *de novo* hits (three intronic and two missense substitutions) in *ATP6V1A*. The two missense substitutions were p.Asp11Asn, identified in a male with autism spectrum disorder (Iossifov *et al.*, 2014), and p.Pro249Arg identified in another male with a

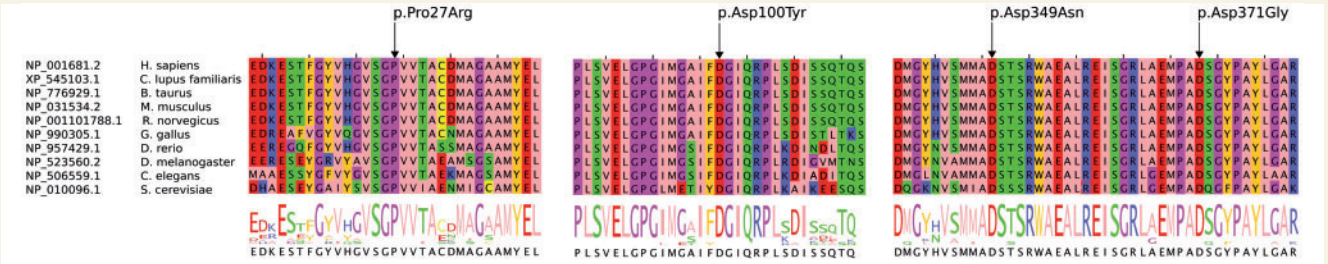

Figure 1 Multiple sequence alignment and sequences logo. Multiple sequence alignment between human ATP6V1A and orthologous sequences. Residues were coloured according to their physico-chemical properties (Zappo colour scheme). Residues affected by the missense substitutions are indicated by black arrows.

severe developmental disorder (McRae *et al.*, 2017). These two missense substitutions, however, have not been subjected to orthogonal validation and should therefore be considered as 'potential' *de novo* variants. These data further highlight how rare *de novo* mutations are in the *ATP6V1A* gene.

Clinical findings

Clinical, EEG and MRI findings observed in the four patients are summarized in Table 1 and presented in detail in the Supplementary material. In brief, early manifestations, observed in all patients, were developmental delay and febrile seizures, evolving in two patients to encephalopathy with profound delay, hypotonic/dyskinetic quadriparesis, intractable multiple seizure types and severe diffuse epileptiform EEG abnormalities (Patients 1 and 4) and to moderate delay with milder epilepsy and focal/multifocal EEG abnormalities in the other two (Patients 2 and 3).

Structural consideration of the v-ATPase mutations

We mapped the mutation sites of human ATP6V1A onto the crystal structure of the V_1 domain from a prokaryotic homologue, *E. hirae* v-ATPase, in a nucleotide-bound state (PDB code 3VR6) (Arai *et al.*, 2013). All the identified mutations fall into the A subunit of the V_1 domain (Fig. 2A).

Pro12 (Pro27 in human ATP6V1A) resides in the type I β-turn that is a part of the interaction interface between subunits A and B. Since the substitution of a proline residue with an arginine residue affects the main-chain conformation of the β-turn, the mutation may perturb the A–B interaction (Fig. 2A and B).

Asp85 (Asp100 in human ATP6V1A) makes a hydrogen bond with Arg89, a guanidium group that makes van der Waals contacts with adjacent hydrophobic side chains (Fig. 2B). As a result, the side chain of Asp85 is closely surrounded by hydrophobic residues, and its replacement with a bulkier tyrosine residue quite likely causes steric hindrance and destabilizes the protein folding. This is supported by the FoldX calculation, which predicted a significant increase in free energy (about 13 kcal/mol) upon the Asp85Tyr mutation.

Asp329 (Asp349 in human ATP6V1A) is located near a nucleotide-binding site (Fig. 2B) and its side chain is involved in water-mediated coordination with a magnesium ion, which plays a critical role in the ATPase activity (Fig. 2B). Thus, the Asp329Asn mutation possibly impairs the catalytic function.

Asp351 (Asp371 in human ATP6V1A) is located at the interface among A, B and D subunits (Fig. 2A). The D subunit rotates within the A3B3 core along with the ATP hydrolysis, and thus the rotation process may be affected by the Asp351Gly mutation. The mutation sites were also mapped on the cryo-EM structure of the human homologue v-ATPase from the eukaryotic *S. cerevisiae* (rotational state 1, PDB code 3J9T) (Zhao *et al.*, 2015). As shown in Fig. 2B, the mapped mutation sites in the *S. cerevisiae* structure overlap with those of the *E. hirae*, suggesting that the predicted impact of the mutations on the prokaryotic structure is also valid for the eukaryotic orthologues.

Finally, we generated a homology model of human ATP6V1A (Supplementary Fig. 1) using *S. cerevisiae* A subunit as template, obtaining a high-confidence result (C-score 88% and TM-score 87%). The resulting structure shows a fold similar to the template (*cf.* Supplementary Fig. 1 and 2B), and the mutation sites are in the same locations of the *E. hirae* and *S. cerevisiae* structures.

Effects of *ATP6V1A* mutations on protein expression and stability

We addressed the impact of p.Asp349Asn and p.Asp100Tyr mutations on the ATP6V1A expression and stability by analysing HEK cells overexpressing ATP6V1A. Cells were transfected with vectors driving the expression of the wild-type or mutant variants in association with a Cherry fluorescent tag for identification. Immunocytochemistry of transfected cells coupled with quantitative western blot analysis showed a decreased expression of both ATP6V1A mutants that reached significance only for the

Table 1 Summary of clinical features in four patients carrying *ATP6V1A* mutations

	Patient			
	1	2	3	4
Origin/sex	Caucasian/F	Asian/M	Caucasian/F	Latino/M
Age at follow-up	14 years	8 years	8 years	11 years
ATP6V1A mutation	c.298G>T (p.Asp100Tyr) *de novo*	c.1045G>A (p.Asp349Asn) *de novo*	c.1112A>G (p.Asp371Gly) *de novo*	c.80C>G (p.Pro27Arg) *de novo*
Clinical diagnosis	Infantile onset epileptic encephalopathy	ID/epilepsy	ID/epilepsy	Infantile onset epileptic encephalopathy
Head circumference	At birth: 32 cm = 3rd %ile (−1.9 SD); at 12 years: 44.5 cm ⩽ 1st %ile (−7 SD): microcephaly	At birth: 33 cm = 10th %ile (−1.2 SD)	Unknown	At 12 months: 43.5 cm = 1st %ile (−2.2 SD); at 11 years: 49 cm ⩽ 1st %ile (−3.2 SD): microcephaly
Age/symptoms at first clinical presentation	11 months, hypotonia, developmental delay, seizures	1 month, developmental delay, jerky movement	2 years 6 months, developmental delay, seizures	7 months, hypotonia, developmental delay
Epilepsy	+	+	+	+
Age at seizure onset	11 months	2 years 10 months	2 years 6 months	11 months
Seizures types	Convulsive seizures during fever at onset, then infantile spasms, tonic, focal clonic, focal occipital	Convulsive seizures during fever at onset, then focal occipital	Convulsive seizures during fever at onset, then generalized tonic-clonic	Convulsive seizures during fever at onset, then spasms, tonic, clonic and myoclonic
Interictal EEG	Slow background, diffuse and multifocal epileptiform discharges	Posteriorly dominant, multifocal epileptiform discharges	Anteriorly predominant multifocal epileptiform discharges	Slow background, diffuse and multifocal epileptiform discharges
Brain MRI	Hypomyelination, mild brain and cerebellar atrophy	Normal at 7 years	Normal at 7 years	Mild atrophy at 1 years 5 months and 3 years 7 months
Clinical phenotype at last follow-up	Profound delay, non-verbal, no visual fixation, hypotonic/dyskinetic quadriparesis, non-ambulatory, early puberty (9 years).	Moderate ID (FSDQ: 53), poor language, headache, amelogenesis imperfecta diagnosed at 3 years, optic atrophy	Moderate ID, poor language, mild dysmorphic features (wide forehead, deep set eyes, beaked nose), behavioural abnormalities with autistic traits, wide based gait, hypotonia	Profound delay, non-verbal, no visual fixation, coloboma of the iris, hypotonic/dyskinetic quadriparesis, non-ambulatory

F = female; FSDQ = full scale developmental quotient; ID = intellectual disability; M = male; N/A = not available.

p.Asp100Tyr variant, and no overt subcellular mislocalization of both p.Asp100Tyr and p.Asp349Asn mutants with respect to wild-type ATP6V1A (Fig. 3A and B). The expression of the molecular partner, ATP6V1B2, was not modified either by p.Asp100Tyr or p.Asp349Asn mutation (Fig. 3B). To investigate the stability of ATP6V1A protein, we performed a degradation assay by treating transfected HEK cells with the protein synthesis inhibitor cycloheximide for various times. Compared to the wild-type isoform, both mutant ATP6V1A isoforms were less stable, although degradation was significantly increased only for the p.Asp100Tyr variant (Fig. 3C).

We next asked whether these findings could also be observed in patients' cells. To this end, we analysed the expression of endogenous ATP6V1A protein in patients' lymphoblasts and compared it with the respective healthy parents' cells (Fig. 3D and E). While the expression of ATP6V1A and ATP6V1B2 was not modified in Asp349Asn proband's cells with respect to his healthy mother's cells, a significant decrease of ATP6V1A, but not ATP6V1B2, expression was observed in Asp100Tyr proband's cells. These data are in full agreement with the structural analysis prediction of a folding defect in the p.Asp100Tyr mutant (Fig. 2A) that may enhance its degradation.

ATP6V1A mutations result in lysosomal abnormalities

To examine the impact of the p.Asp349Asn and p.Asp100Tyr mutations in the regulation of pH homeostasis, we used the LysoTracker® probe to qualitatively evaluate intracellular acidic organelles in HEK cells overexpressing either pathogenic or wild-type ATP6V1A variants. Interestingly, the p.Asp349Asn mutant increased, while the p.Asp100Tyr mutant decreased, LysoTracker® fluorescence intensity (Fig. 4A). The LysoTracker® signal monitors both the actual pH of acidic organelles, namely endosomal and lysosomal compartments, and their relative abundance within the cell. Thus, we analysed in parallel the expression of the endosomal and lysosomal markers, EEA1 and LAMP1, respectively. Whereas EEA1 expression was unaltered in HEK cells expressing wild-type ATP6V1A or either pathogenic variants, the p.Asp100Tyr mutant was associated with a significant decrease of LAMP1 expression

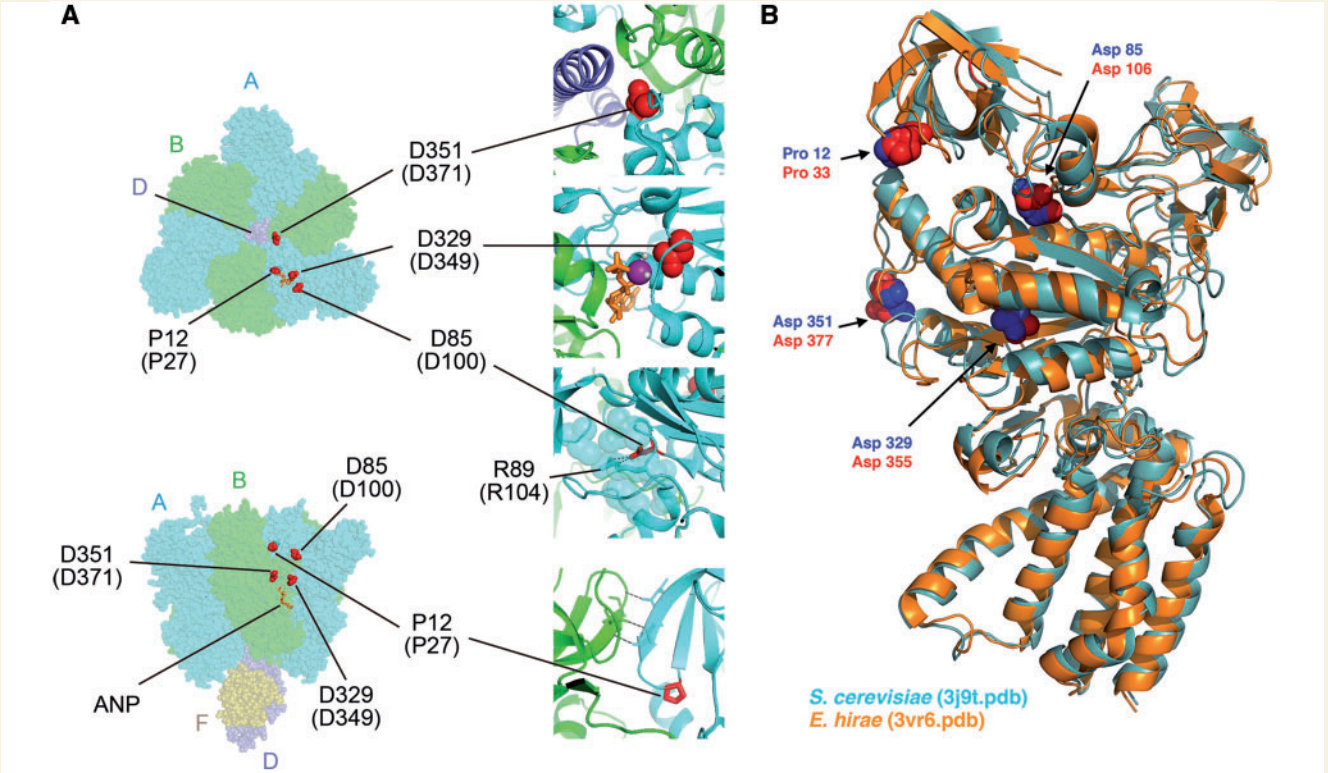

Figure 2 Structural mapping of the missense mutations in the V-ATPase. (**A**) *Left*: Crystal structure of the V_1 domain from *E. hirae* v-ATPase in a nucleotide-bound state (PDB code 3VR6), viewed from the extracellular side (*top*) and the membrane plane (*bottom*), shown as the sphere representation. The A, B, D and F subunits are coloured in cyan, green, violet and brown, respectively, and residues at the mutation sites are coloured in red. The non-hydrolyzable ATP analogue ANP (phosphoaminophosphonic acid-adenylate ester) is depicted as orange sticks. *Right*: Magnified views of the mutation sites presented in the ribbon model. Pro12 and Asp85 are depicted as red sticks, and Arg89, which makes a salt bridge with Asp85, is shown as sticks with translucent spheres. Some side chains of hydrophobic residues around Arg89 are shown as translucent spheres, and magnesium ion and its coordinated water molecules are depicted as a purple sphere and small grey dots, respectively. Black dotted lines indicate hydrogen bonds. Amino acid numbers in parentheses correspond to those of human ATP6V1A. (**B**) Crystal structures of the A subunit from *E. hirae* (orange) and the cryo-EM structure of the A subunit from *S. cerevisiae* (cyan, PDB code 3J9T) V-ATPase. Mutation sites are shown as spheres and coloured in red for *S. cerevisiae* and blue for *E. hirae*.

evaluated by both single cell immunocytochemistry (Fig. 4B) and western blotting (Supplementary Fig. 2A). The data suggest that the p.Asp349Asn mutant exacerbates the acidic pH of intracellular organelles, while the p.Asp100Tyr mutant leads to a decreased expression of LAMP1-positive lysosomal structures. Lysosomes fuse with phagosomal and autophagosomal structures to generate autolysosomes and v-ATPase also acidifies autolysosomal organelles. We therefore investigated whether pathogenic *ATP6V1A* variants affect v-ATPase translocation to LC3-positive phagosomal structures. To this aim, we measured the co-localization between the v-ATPase subunit ATP6V1B2 and LC3 in HEK cells expressing wild-type ATP6V1A or either pathogenic variant. Both p.Asp100Tyr and p.Asp349Asn resulted in a decreased co-localization coefficient with respect to wild-type ATP6V1A (Fig. 4C). However, the v-ATPase translocation induced by cell starvation was slightly impaired by p.Asp100Tyr and substantially unaffected by p.Asp349Asn (Fig. 4C). No significant changes in LC3II/LC3I ratio and p62 accumulation were observed in both experimental groups (Supplementary Fig. 2B). These data suggest a significant impact of both mutations on the recruitment of the v-ATPase to LC3-positive autolysosomal structures, with slightly impaired autophagic flux only for Asp100Tyr.

To verify whether altered lysosomal pH and levels of lysosomal markers were also present in patients, we subjected patients' lymphoblasts to the same analysis. Experiments using the ratiometric pH probe LysoSensor^{TM} Yellow/Blue dextran, revealed a significant reduction in endocytic organelle pH in the Asp349Asn patient's lymphoblasts when compared to his healthy mother's lymphoblasts, in the absence of any change in the expression of LAMP1 and EEA1 (Fig. 5). Conversely, while the pH of endocytic organelles was not modified in the Asp100Tyr patient's lymphoblasts, a significant reduction in LAMP1 expression was observed (Fig. 5). Taken together, these data suggest a gain-of-function effect for the p.Asp349Asn mutation, characterized by an increased proton pumping into intracellular organelles, and a loss-of-function effect for the

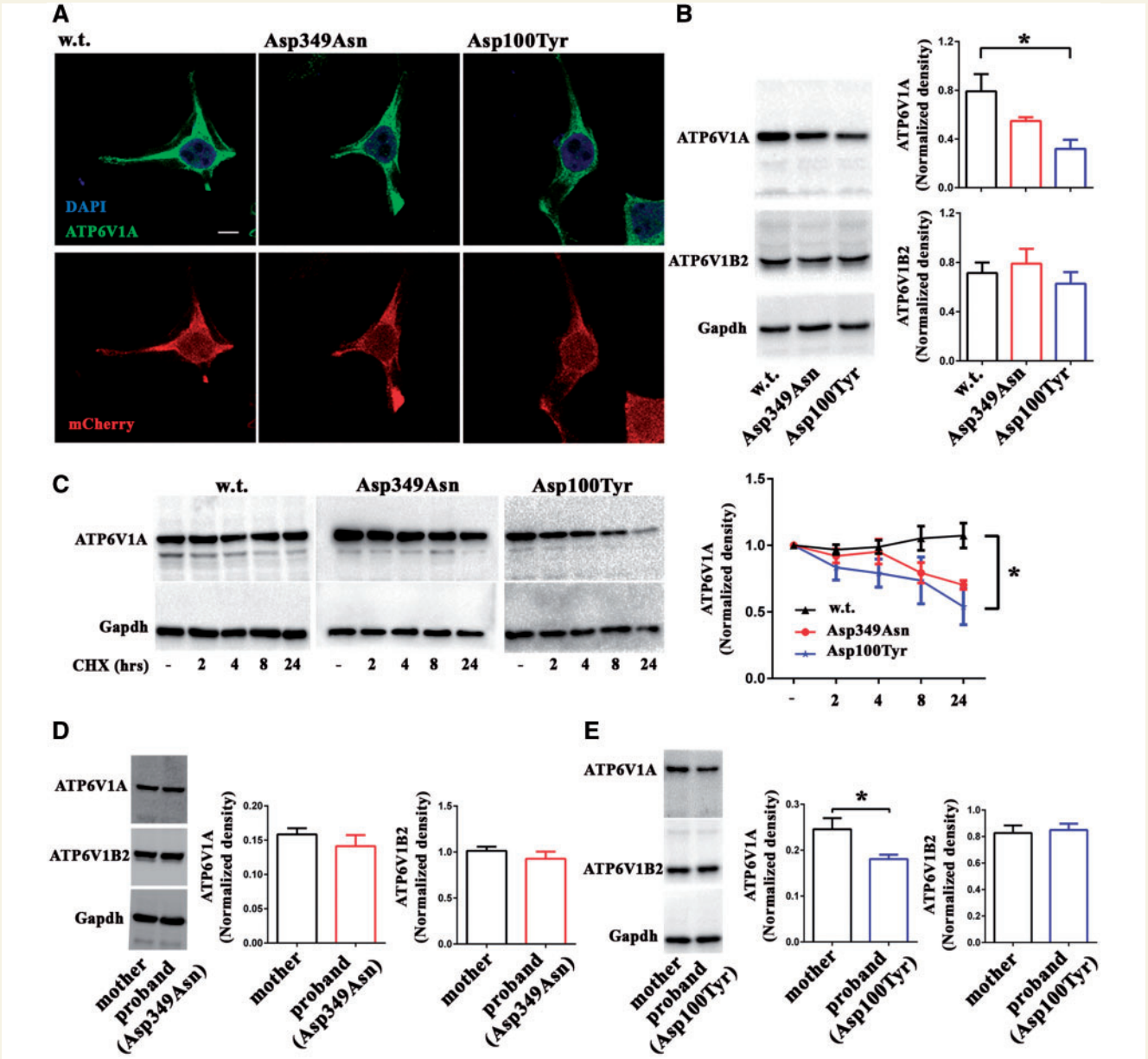

Figure 3 Impact of *ATP6V1A* mutations on protein expression and stability. (**A**) Representative images of HEK cells transfected with vectors coding wild-type ATP6V1A (w.t.), Asp349Asn ATP6V1A (Asp349Asn) or Asp100Tyr ATP6V1A (Asp100Tyr) variants. ATP6V1A immunolabelling, DAPI nuclear stain and Cherry reporter fluorescence are shown. Scale bar = 10 μm. (**B**) Representative western blot (*left*) from HEK cells transfected as above and lysed 24 h after transfection. ATP6V1A and ATP6V1B2 intensities were quantified by densitometric analysis with respect to GAPDH intensity (*right*). Data are means ± standard error of the mean (SEM) from five independent experiments. *$P < 0.05$ versus wild-type; Kruskall-Wallis/Dunn's tests. (**C**) *Left*: Representative western blots of HEK cell lysates stained with anti-ATP6V1A antibody and anti-GADPH as loading control. Cells were transfected with wild-type, Asp349Asn or Asp100Tyr ATP6V1A variants and incubated with cycloheximide for 2, 4, 8, 24 h or vehicle (DMSO; 24 h) as a control (–). *Right*: Densitometric analysis of ATP6V1A intensity with respect to GADPH expressed in percent of control samples without cycloheximide. Data are means ± SEM from four independent experiments. The areas under the respective curves were compared using the Kruskal-Wallis/Dunn's tests. *$P < 0.05$ versus wild-type. (**D**) Representative western blot from lymphoblast lysates (30 μg) of patient affected by the Asp349Asn mutation (proband) and the healthy mother. (**E**) Representative western blot from lymphoblast lysates (30 μg) of patient affected by the Asp100Tyr mutation (proband) and the healthy mother. In **D** and **E**, ATP6V1A and ATP6V1B2 intensity were quantified by densitometric analysis with respect to GADPH. Data are means ± SEM from four independent experiments. *$P < 0.05$; Mann Whitney U-test.

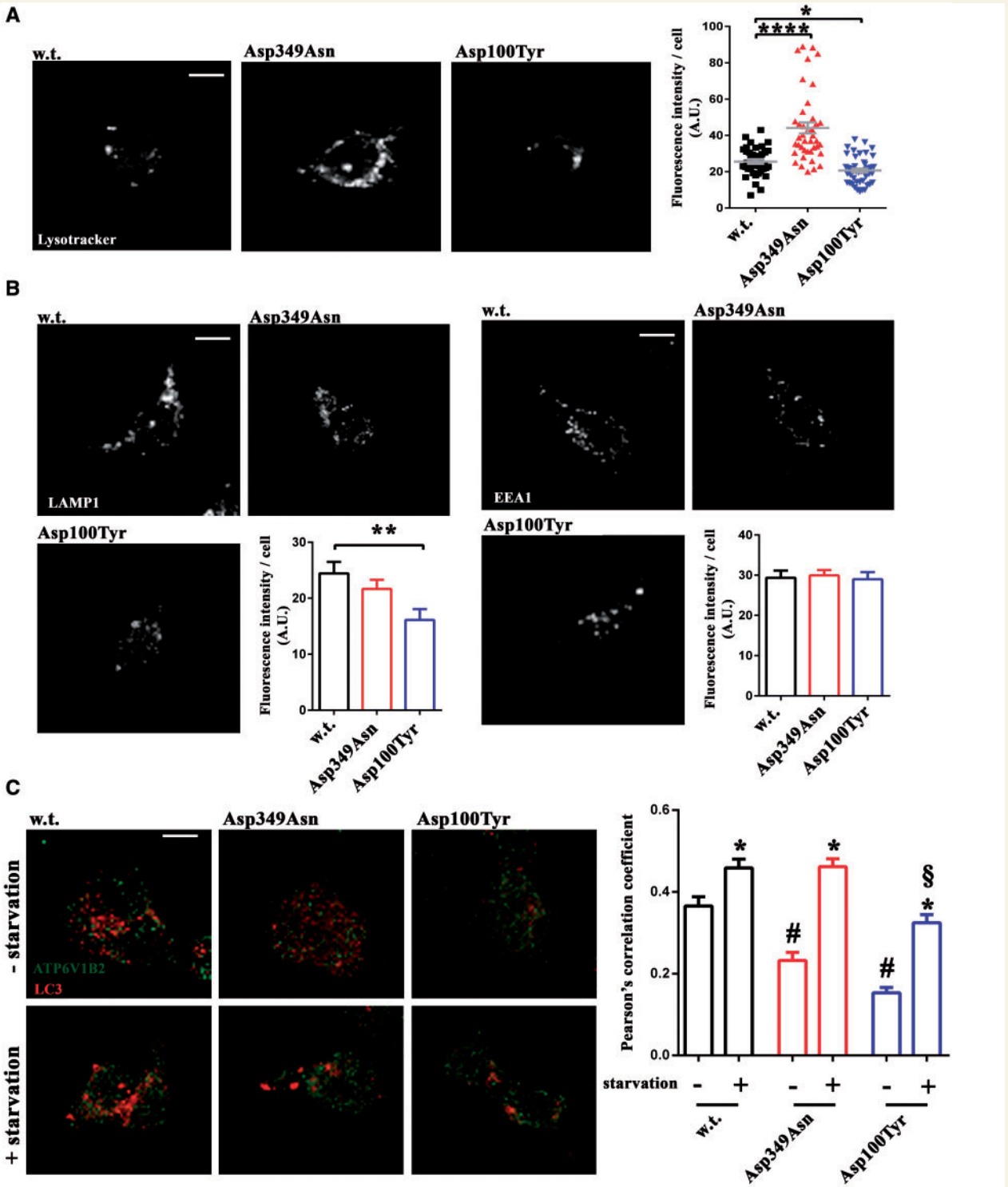

Figure 4 Effects of *ATP6V1A* mutations on endo-lysosomal markers and v-ATPase recruitment to autophagosomes.
(**A**) *Left*: Representative images of HEK cells transfected with wild-type ATP6V1A (w.t.), Asp349Asn ATP6V1A (Asp349Asn) or Asp100Tyr ATP6V1A (Asp100Tyr) variants and incubated with LysoTracker® (200 nM, 1 h). *Right*: LysoTracker® fluorescence intensity was quantified in 38 (wild-type), 41 (Asp349Asn) and 45 (Asp100Tyr) cells from three independent experiments. Individual data and means ± SEM are shown. $^{*}P < 0.05$, $^{****}P < 0.0001$ versus wild-type; Kruskall-Wallis/Dunn's tests. (**B**) Representative images and densitometric quantification from HEK cells transfected as above and immunolabelled with LAMP1 (*left*) or EEA1 (*right*). Histograms show quantification of signal intensity. Data are means ± SEM of 24–33 cells per experimental condition, from three independent experiments. $^{**}P < 0.001$ versus wild-type Kruskall-Wallis/Dunn's tests. (**C**) Representative images from HEK cells transfected as above and immunolabelled with ATP6V1B2 and LC3B under control conditions or after starvation for 2 h. Graph shows the quantification of ATP6V1B2 and LC3B co-localization using ImageJ software to determine the Pearson's correlation coefficient. Data are means ± SEM of 30 cells per experimental condition. $^{*}P < 0.05$ versus respective control; $^{\#}P < 0.001$ versus non-starved wild-type; $^{\S}P < 0.001$ versus starved wild-type. Data were analysed by two-way ANOVA/Bonferroni's tests.

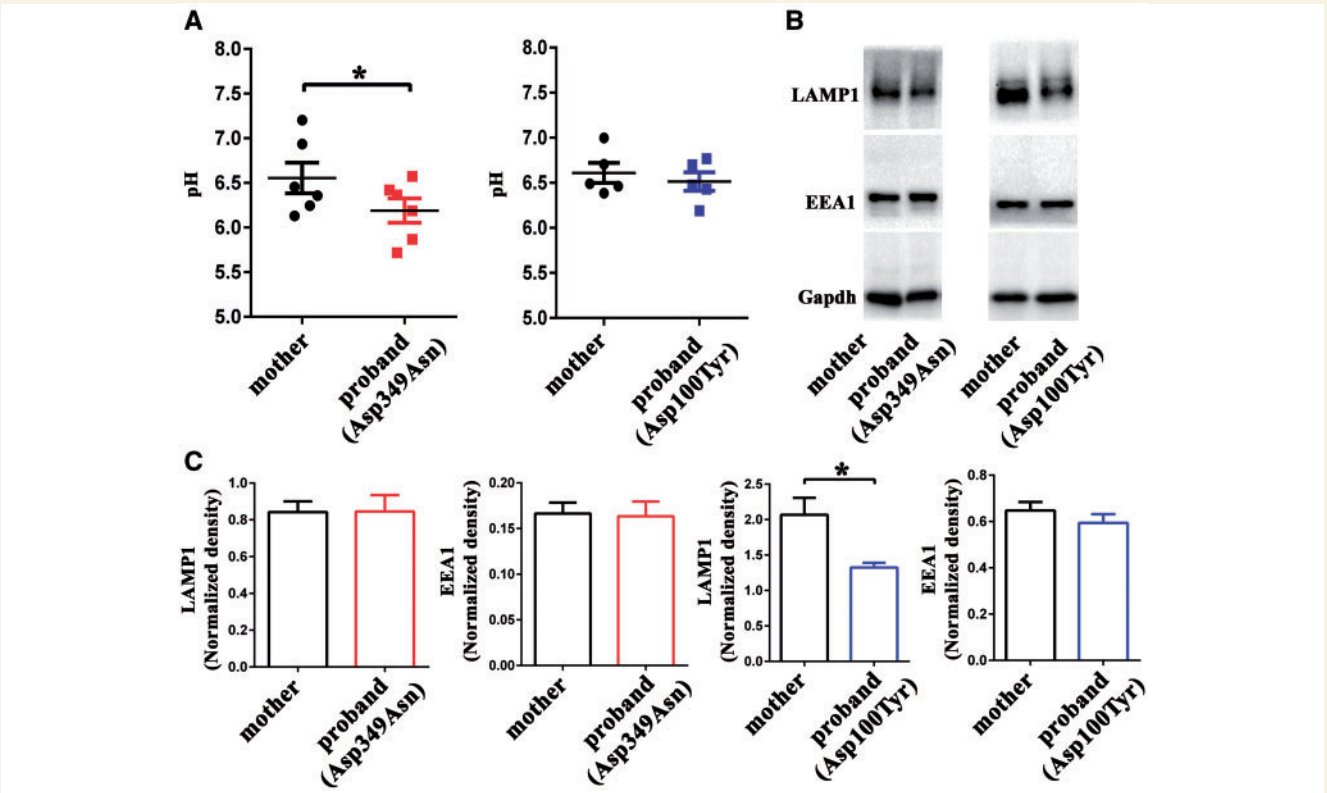

Figure 5 Effects of *ATP6V1A* mutations on intracellular organelle pH and endo-lysosomal markers in patients' cells. (**A**) Quantification of endocytic organelle pH in lymphoblasts from patients (probands) bearing either p.Asp349Asn (red) or p.Asp100Tyr (blue) mutation and the respective healthy mothers (black). Individual data and means ± SEM of five to six independent measurements are shown. *$P < 0.05$; Wilcoxon matched pairs signed rank test. (**B**) Representative western blot from lymphoblast lysates (30 μg) as defined above. LAMP1, EEA1 and GADPH as loading control is shown. (**C**) LAMP1 and EEA1 immunoreactivities were quantified by densitometric analysis and normalized to GADPH. Data are means ± SEM from four independent experiments. *$P < 0.05$; Mann-Whitney U-test.

p.Asp100Tyr mutation associated with defects in lysosomal compartments.

ATP6V1A mutations impact on neuronal pH homeostasis and neuronal development

In view of the neurodevelopmental phenotype observed in the four patients carrying *de novo* heterozygous *ATP6V1A* mutations, we investigated whether the effects on lysosomal homeostasis observed in HEK cells and patient-derived lymphoblasts were recapitulated in neurons. To address this question, we transiently expressed ATP6V1A and the pathogenic mutants thereof in rat hippocampal neuronal cultures and evaluated intracellular acidic organelles by LysoTracker® staining at the neuronal soma. As shown in Fig. 6A, neurons overexpressing p.Asp349Asn resulted in a significantly higher LysoTracker® staining as compared to wild-type ATP6V1A-expressing neurons. In contrast, p.Asp100Tyr ATP6V1A overexpression induced a significant loss of LysoTracker® staining. Thus, the expression of the two mutants in neurons precisely phenocopies the effects observed in cell lines, suggesting that such an alteration in pH and lysosomal homeostasis also occurs in brain cells.

To investigate cellular correlates of the patients' neurodevelopmental delay and explore whether the defects in LysoTracker® signal have an impact on neuronal development, we transfected rat hippocampal neurons at 7 DIV and analysed neurite elongation at 10 DIV by Sholl analysis. The analysis revealed a similar and significant loss of neurite arborization for both p.Asp349Asn- and p.Asp100Tyr-expressing neurons, indicating that both pathogenic variants significantly affect the outgrowth and branching of neuronal processes during development (Fig. 6B).

ATP6V1A mutations affect synapse formation in primary neurons

In developing neurons, neurite elongation is followed by synapse formation and stabilization. V-ATPase is a fundamental protein component of synaptic vesicles, where it allows neurotransmitter loading and regulates synaptic

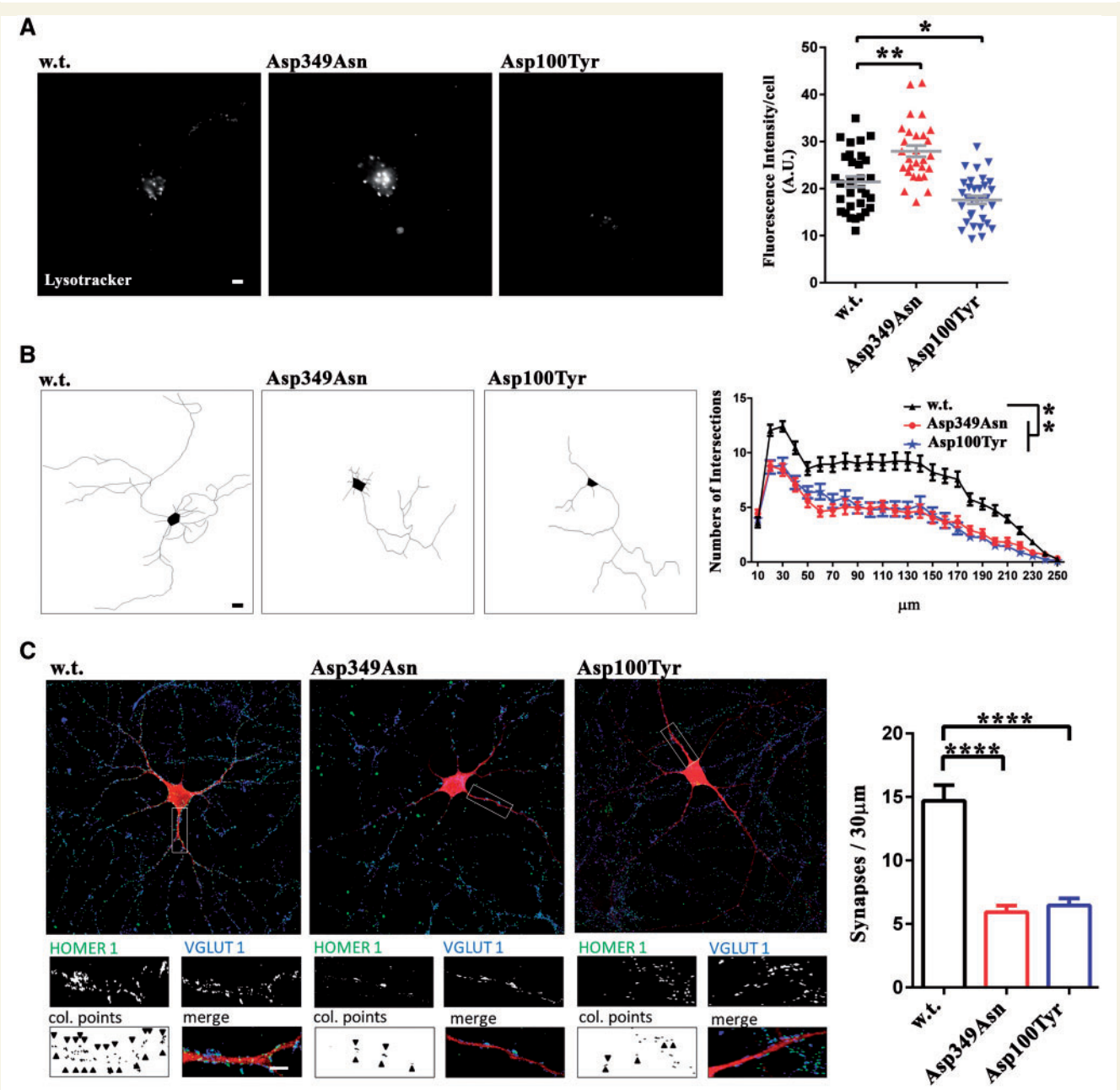

Figure 6 Effect of *ATP6V1A* mutations on pH homeostasis, development and synaptic connectivity in primary hippocampal neurons. (**A**) *Left*: Representative images of rat hippocampal neurons transfected with wild-type (w.t.), Asp349Asn (Asp349Asn) and Asp100Tyr (Asp100Tyr) ATP6V1A variants at 7 DIV and incubated with LysoTracker® (50 nM, 30 min) at 10 DIV. *Right*: LysoTracker® fluorescence intensity was quantified in 31 (wild-type), 28 (Asp349Asn) and 33 (Asp100Tyr) neurons from two independent preparations. Individual data and means ± SEM are shown. $^{*}P < 0.05$, $^{**}P < 0.01$ versus wild-type; Kruskall-Wallis/Dunn's tests. (**B**) *Left*: Representative neurite traces of 10 DIV neurons transfected as in **A**. *Right*: Sholl analysis of neurite arborization as a function of distance from the soma. Data are means ± SEM of 29–33 neurons for experimental group from three independent preparations. $^{**}P < 0.01$ versus wild-type; Kruskall-Wallis/Dunn's tests. (**C**) *Left*: Representative images of hippocampal neurons transfected with wild-type ATP6V1A (w.t.), Asp349Asn ATP6V1A (Asp349Asn) or Asp100Tyr ATP6V1A (Asp100Tyr) variants (*top*) at 14 DIV and analysed at 17 DIV. White rectangles indicate proximal dendrites shown at high magnification (*bottom*). Synaptic boutons were identified by double immunostaining for VGLUT1 (blue) and Homer1 (green). The co-localization panels (col. points) highlight the double-positive puncta (black), marked by arrowheads, corresponding to *bona fide* synapses. The merge panels show positive puncta along transfected branches. Scale bar = 10 µm. *Right*: Quantitative analysis of synaptic puncta counted on 30-µm branches starting from the cell body. Data are means ± SEM of 27–28 neurons per experimental condition, from three independent preparations. $^{****}P < 0.0001$ versus wild-type; two-way ANOVA/Bonferroni's tests.

transmission (Takamori *et al.*, 2006; Takamori, 2016). Moreover, acidic lysosomes have been recently described at excitatory postsynaptic sites (Goo *et al.*, 2017; Padamsey *et al.*, 2017). Accordingly, the expression of the v-ATPase V_1 subunits, ATP6V1A and ATP6V1B2, was found to increase with *in vitro* neuronal maturation and synaptogenesis along with the expression of pre- and postsynaptic markers (Supplementary Fig. 3A).

To study the effects of ATP6V1A mutants on synapse formation, we transfected hippocampal neurons at 14 DIV and analysed synapse density at 17 DIV. Excitatory synaptic contacts were visualized by double immunostaining with the presynaptic marker VGLUT1 and the postsynaptic marker Homer1 to identify mature excitatory synapses unambiguously. Synapse counting at 30 µm distance from the cell body revealed a significant loss of excitatory synaptic connections for p.Asp349Asn and p.Asp100Tyr overexpressing neurons, suggesting that both pathogenic variants dramatically impair the formation and maintenance of excitatory synapses (Fig. 6C). Similar effects on the density of excitatory synaptic contacts were observed after treatment of hippocampal neurons with the lysosomal enzyme inhibitor leupeptin (Supplementary Fig. 3B).

Discussion

The phenotypic features observed in the four patients reported here can be typically described as developmental encephalopathy with epilepsy and subsumed as *ATP6V1A* encephalopathy, although a larger number of observations is necessary to reveal the whole phenotypic spectrum. However, gathering a large series may take a long time because *ATP6V1A* mutations are very rare, and have not emerged before in large cohorts with epileptic and developmental encephalopathies (Allen *et al.*, 2013; Appenzeller *et al.*, 2014; McRae *et al.*, 2017); we could only identify four cases through whole exome sequencing studies on 1444 probands from three continents. Querying the denovo-db, we found only two potential *de novo* variants in the coding regions of *ATP6V1A*, thus further highlighting the rarity of *de novo* variants in this gene. Pathogenicity of the *de novo* p.Pro27Arg, p.Asp100Tyr, p.Asp349Asn and p.Asp371Gly variants could be established based on their: (i) occurrence in four patients with a developmental encephalopathy with epilepsy, the genome-wide statistical significance for missense *de novo* mutations enrichment; (ii) absence from publicly available databases; (iii) causing substitutions at highly evolutionarily conserved amino acid positions; and (iv) predicted highly damaging consequences emerging from *in silico* methods and the high intolerance of the *ATP6V1A* gene to variations. Accordingly, structural modelling allowed to localize the mutated sites in regions of ATP6V1A responsible for either the proper folding of the subunit (p.Asp100Tyr), the interaction with the V_0 B subunit (p.Pro27Arg) or the function of the v-ATPase complex (p.Asp349Asn, p.Asp371Gly).

As most causative variations occur with very low allele frequency within each gene and only account for a small fraction of epilepsy patients (Myers and Mefford, 2015) sequencing large cohorts of patients, collected through large networks and gene-matching tools has higher chances to find multiple affected individuals carrying *de novo* mutations in the same gene(s) (Hamdan *et al.*, 2017). This strategy can overcome the challenge to determine whether the candidate *de novo* mutations have a causal relationship with the disease or are found by chance. A statistical framework specifically developed to address this challenge (Samocha *et al.*, 2014), and successfully applied to developmental disorders in previous studies (Lelieveld *et al.*, 2016; McRae *et al.*, 2017), has also proved instrumental to demonstrate that *ATP6V1A* reached genome-wide statistical significance for missense *de novo* mutations enrichment in our cohort.

The Online Mendelian Inheritance in Man (OMIM) catalogue contains 59 entries for early infantile epileptic encephalopathies featuring intellectual disability and epilepsy (https://www.omim.org/entry/308350?search = EIEE&highlight = eiee) (Supplementary Table 3), caused by mutations in as many genes, and mentions that similar phenotypes are also observed in other genetic disorders, highlighting the extreme genetic heterogeneity underlying this category.

The many genes that have been associated with such complex developmental epilepsy conditions have revealed the pathogenic role of mutations affecting diverse molecular pathways that regulate ion channel functioning, membrane excitability, synaptic plasticity, neurotransmitter release, postsynaptic receptors, transporters, cell metabolism, and many formative steps in early brain development such as the proliferation and migration of neuronal precursors, dendritogenesis, synaptogenesis, cell and glial biology (Guerrini and Noebels, 2014). Our experimental work on the p.Asp100Tyr and p.Asp349Asn missense substitutions indicates that *ATP6V1A* mutations cause functional defects in v-ATPase physiology with alterations of lysosomal homeostasis associated with abnormal neuritogenesis and synaptic density.

The main function of v-ATPase is proton transport and acidification of intracellular organelles, in particular lysosomes that have critical requirements for pH. The functional experiments performed on the p.Asp100Tyr mutation, causing the more severe phenotype, demonstrated an increased degradation with impaired expression of ATP6V1A and lower lysosomal abundance. This finding was also associated with decreased recruitment of v-ATPase by autophagosomes under basal and starvation conditions, suggesting a potential impairment of the autophagic flux, as recently described in patients with mutations in the accessory v-ATPase subunit *ATP6AP2* (Rujano *et al.*, 2017). Conversely, p.Asp349Asn, which was associated with a milder phenotype, resulted in decreased endo-lysosomal pH, with no effects on either expression of the mutant

protein or lysosomal abundance, pointing to a gain-of-function effect. This variant slightly impairs v-ATPase translocation to autophagosomes under basal, but not starvation, conditions, suggesting that the formation of autolysosomes is preserved. These functional findings were supported by structural modelling results, predicting that the p.Asp100Tyr mutation decreases protein stability, whereas p.Asp349Asn affects the catalytic activity of v-ATPase.

When modelled in hippocampal neurons, these pathogenic mutations produced the same significant and divergent effects on lysosomal marker intensity and endolysosomal pH that were observed in cell lines and probands' lymphoblasts, reflecting their relevance for the CNS. Moreover, in primary neurons, both p.Asp100Tyr and p.Asp349Asn mutants induced significant and comparable defects in dendrite development and excitatory synapse formation. The neuronal phenotype of both mutants demonstrates a previously unexplored role of the v-ATPase in the processes of neuronal development and connectivity. Similarities in changes on synapse formation induced by the two tested mutations and by leupeptin, a known inhibitor of lysosomal function, suggest an important pathophysiological role of altered lysosomal homeostasis. This hypothesis is also supported by recent reports on novel roles of lysosomes at the synapse for the turnover of synaptic proteins, as well as for the plasticity of dendritic spines (Goo *et al.*, 2017; Padamsey *et al.*, 2017; Sambri *et al.*, 2017).

Although the precise molecular mechanisms through which the described *de novo* mutations result in a developmental encephalopathy with epilepsy remain to be clarified, we here propose that alteration in lysosomal homeostasis may represent a novel pathogenic mechanism for this aetiologically heterogeneous group of disorders. Further work is needed to clarify the role of v-ATPase in brain development and to precisely establish the cellular signalling pathways that can be altered by loss of lysosomal homeostasis.

It is often impossible to disentangle whether the developmental or epileptic component is more important in contributing to a patient's presentation. In the four patients described here, however, there was good correspondence between severity of epilepsy and overall neurodevelopmental impairment, which might suggest either a more severe brain dysfunction leading to both severe impairment and to the epileptic encephalopathy or a deleterious effect of early severe and long-lasting epilepsy on development.

Next generation sequencing studies have demonstrated that sporadic developmental disorders associated with epilepsy, once considered potentially recessive in nature, often arise from *de novo* mutations of dominant genes and that the same gene can be associated with a broader phenotypic spectrum than originally believed (Mei *et al.*, 2017). Our findings clearly link the *ATP6V1A* gene with a dominant form of encephalopathy after two biallelic homozygous missense mutations of the same gene had been related in three individuals to cutis laxa, a rare, severe systemic disorder, leading to early death in one of the patients and featuring, in addition to generalized skin wrinkling, marked hypotonia, dysmorphic facial features, cardiac abnormalities, structural brain abnormalities and seizures (Van Damme *et al.*, 2017). Although comparison between our patients and the three previously reported with biallelic *ATP6V1A* mutations is only partially feasible, there is evidence that biallelic mutations cause a more complex phenotype in which severe neurological manifestations are part of a multi-organ involvement. A number of additional genetic developmental disorders with epilepsy, including those related to *PRRT2* (Ebrahimi-Fakhari *et al.*, 2015), *TBC1D24* (Balestrini *et al.*, 2016), *RELN* (Dazzo *et al.*, 2015) and *SLC2A1* (Wang *et al.*, 2000) genes, have been associated with both autosomal dominant and more severe recessive phenotypes.

Acknowledgements

We thank Davide Aprile and Manuela Fadda (Department of Experimental Medicine, University of Genoa, Italy) for neuronal culture preparation and helpful discussion. The authors acknowledge the contributions of all members (current and past) of the C4RCD Research Group. This group includes the clinical team and laboratory research team involved in patient enrolment, sample processing, exome sequencing, data processing, preparation of variant annotation files, data analysis, validation of data, and return of research data to families. Candidate genes are identified and discussed at data analysis meetings of the entire group. The following members of the group (listed in alphabetical order) have contributed significantly to this work: Newell Belnap, Jason J. Corneveaux (deceased), Amanda Courtright, David W. Craig, Matt de Both, Brooke Hjelm, Matthew J. Huentelman, Ahmet Kurdoglu, Vinodh Narayanan, Keri M. Ramsey, Sampathkumar Rangasamy, Ryan Richholt, Isabelle Schrauwen, Ashley L. Siniard and Szabolcs Szelinger.

Funding

This work was supported by a grant from the EU Seventh Framework Programme FP7 under the project DESIRE (grant agreement n° 602531) and in part by grants Research on Measures for Intractable Disease (grant number 14525125); the Strategic Research Program for Brain Science (grant number 15656973); Initiative on Rare and Undiagnosed Diseases (grant number 17ek0109151h0003) from the Japan Agency for Medical Research and Development; grants-in-aid for Scientific Research (A, B and C) (grant number A: 17H01539, B: 16H05160, C: 15K10367) from the Japan Society for the Promotion of Science. The generous support of Fondazione CARIGE (Genova) for a 1-year postdoctoral fellowship and of the Mariani Foundation for promoting and organizing

the International Workshop on Epileptic Encephalopathies, Florence 2016, is also acknowledged.

Supplementary material

Supplementary material is available at *Brain* online.

References

Allen AS, Berkovic SF, Cossette P, Delanty N, Dlugos D, Eichler EE, et al. *De novo* mutations in epileptic encephalopathies. Nature 2013; 501: 217–21.

Appenzeller S, Balling R, Barisic N, Baulac S, Caglayan H, Craiu D, et al. *De novo* mutations in synaptic transmission genes including DNM1 cause epileptic encephalopathies. Am J Hum Genet 2014; 95: 360–70.

Arai, S, Saijo S, Suzuki K, Mizutani K, Kakinuma Y, Ishizuka-Katsura Y, et al. Rotation mechanism of *Enterococcus hirae* V1-ATPase based on asymmetric crystal structures. Nature 2013; 493: 703–77.

Balestrini S, Milh M, Castiglioni C, Lüthy K, Finelli MJ, Verstreken P, et al. TBC1D24 genotype-phenotype correlation: epilepsies and other neurologic features. Neurology 2016; 87: 77–85.

Bodzęta A, Kahms M, Klingauf J. The presynaptic v-ATPase reversibly disassembles and thereby modulates exocytosis but is not part of the fusion machinery. Cell Rep 2017; 20: 1348–59.

Cingolani P, Platts A, Wang le L, Coon M, Nguyen T, Wang L, et al. Program for annotating and predicting the effects of single nucleotide polymorphisms, SnpEff: SNPs in the genome of Drosophila melanogaster strain w1118; iso-2; iso-3. Fly 2012; 6: 80–92.

Cotter K, Stransky L, McGuire C, Forgac M. Recent insights into the structure, regulation, and function of the v-ATPases. Trends Biochem Sci 2015; 40: 611–22.

Dazzo E, Fanciulli M, Serioli E, Minervini G, Pulitano P, Binelli S, et al. Heterozygous reelin mutations cause autosomal-dominant lateral temporal epilepsy. Am J Hum Genet 2015; 96: 992–1000.

DePristo MA, Banks E, Poplin R, Garimella KV, Maguire JR, Hartl C, et al. A framework for variation discovery and genotyping using next-generation DNA sequencing data. Nat Genet 2011; 43: 491–8.

Ebrahimi-Fakhari D, Saffari A, Westenberger A, Klein C. The evolving spectrum of PRRT2-associated paroxysmal diseases. Brain 2015; 138: 3476–95.

Falace A, Filipello F, La Padula V, Vanni N, Madia F, De Pietri Tonelli D, et al. TBC1D24, an ARF6-interacting protein, is mutated in familial infantile myoclonic epilepsy. Am J Hum Genet 2010; 87: 365–70.

Fischer B, Dimopoulou A, Egerer J, Gardeitchik T, Kidd A, Jost D, et al. Further characterization of ATP6V0A2-related autosomal recessive *cutis laxa*. Hum Genet 2012; 131: 1761–73.

Forgac M. Vacuolar ATPases: rotary proton pumps in physiology and pathophysiology. Nat Rev Mol Cell Biol 2007; 11: 917–29.

Frattini A, Orchard PJ, Sobacchi C, Giliani S, Abinun M, Mattsson JP, et al. Defects in TCIRG1 subunit of the vacuolar proton pump are responsible for a subset of human autosomal recessive osteopetrosis. Nat Genet 2000; 25: 343–6.

Goo MS, Sancho L, Slepak N, Boassa D, Deerinck TJ, Ellisman MH, et al. Activity-dependent trafficking of lysosomes in dendrites and dendritic spines. J Cell Biol 2017; 216: 2499–513.

Guerrini R, Noebels J. How can advances in epilepsy genetics lead to better treatments and cures? Adv Exp Med Biol 2014; 813: 309–17.

Hamdan FF, Myers CT, Cossette P, Lemay P, Spiegelman D, Laporte AD, et al. High rate of recurrent *de novo* mutations in developmental and epileptic encephalopathies. Am J Hum Genet 2017; 101: 664–85.

Ioannidis NM, Rothstein JH, Pejaver V, Middha S, McDonnell SK, Baheti S, et al. REVEL: an ensemble method for predicting the pathogenicity of rare missense variants. Am J Hum Genet 2016; 99: 877–85.

Ionita-Laza I, McCallum K, Xu B, Buxbaum JD. A spectral approach integrating functional genomic annotations for coding and noncoding variants. Nat Genet 2016; 48: 214–20.

Iossifov I, O'Roak BJ, Sanders SJ, Ronemus M, Krumm N, Levy D, et al. The contribution of *de novo* coding mutations to autism spectrum disorder. Nature 2014; 515: 216–21.

Itan Y, Shang L, Boisson B, Ciancanelli MJ, Markle JG, Martinez-Barricarte R, et al. The mutation significance cutoff: gene-level thresholds for variant predictions. Nat Methods 2016; 13: 109–10.

Itan Y, Shang L, Boisson B, Patin E, Bolze A, Moncada-Vélez M, et al. The human gene damage index as a gene-level approach to prioritizing exome variants. Proc Natl Acad Sci USA 2015; 112: 13615–20.

Jagadeesh KA, Wenger AM, Berger MJ, Guturu H, Stenson PD, Cooper DN, et al. M-CAP eliminates a majority of variants of uncertain significance in clinical exomes at high sensitivity. Nat Genet 2016; 48: 1581–6.

Karet FE, Finberg KE, Nelson RD, Nayir A, Mocan H, Sanjad SA, et al. Mutations in the gene encoding B1 subunit of H+-ATPase cause renal tubular acidosis with sensorineural deafness. Nat Genet 1999; 21: 84–90.

Kelley LA, Mezulis S, Yates CM, Wass MN, Sternberg MJ. The Phyre2 web portal for protein modeling, prediction and analysis. Nat Protoc 2015; 10: 845–58.

Kircher M, Witten DM, Jain P, O'Roak BJ, Cooper GM, Shendure J. A general framework for estimating the relative pathogenicity of human genetic variants. Nat Genet 2014; 46: 310–15.

Kornak U, Reynders E, Dimopoulou A, van Reeuwijk J, Fischer B, Rajab A, et al. Impaired glycosylation and cutis laxa caused by mutations in the vesicular H(+)-ATPase subunit ATP6V0A2. Nat Genet 2008; 40: 32–4.

Kornak U, Schulz A, Friedrich W, Uhlhaas S, Kremens B, Voit T, et al. Mutations in the a3 subunit of the vacuolar H(+)-ATPase cause infantile malignant osteopetrosis. Hum Mol Genet 2000; 9: 2059–63.

Kortum F, Caputo V, Bauer CK, Stella L, Ciolfi A, Alawi M, et al. Mutations in KCNH1 and ATP6V1B2 cause Zimmermann-Laband syndrome. Nat Genet 2015; 47: 661–7.

Lek M, Karczewski KJ, Minikel EV, Samocha KE, Banks E, Fennell T, et al. Exome Aggregation Consortium. Analysis of protein-coding genetic variation in 60,706 humans. Nature 2016; 536: 285–91.

Lelieveld SH, Reijnders MR, Pfundt R, Yntema HG, Kamsteeg EJ, de Vries P, et al. Meta-analysis of 2,104 trios provides support for 10 new genes for intellectual disability. Nat Neurosci 2016; 19: 1194–6.

Li H, Durbin R. Fast and accurate long-read alignment with Burrows-Wheeler transform. Bioinformatics 2010; 26: 589–95.

Liu X, Wu C, Li C, Boerwinkle E. dbNSFP v3.0: a one-stop database of functional predictions and annotations for human nonsynonymous and splice-site SNVs. Hum Mutat 2016; 37: 235–41.

McKenna A, Hanna M, Banks E, Sivachenko A, Cibulskis K, Kernytsky A, et al. The genome analysis toolkit: a MapReduce framework for analyzing next-generation DNA sequencing data. Genome Res 2010; 20: 1297–303.

McRae JF, Clayton S, Fitzgerald TW, Kaplanis J, Prigmore E, Rajan D, et al. Prevalence and architecture of *de novo* mutations in developmental disorders. Nature 2017; 542: 433–8.

Mei D, Parrini E, Marini C, Guerrini R. The impact of next-generation sequencing on the diagnosis and treatment of epilepsy in paediatric patients. Mol Diagn Ther 2017; 21: 357–73.

Morel N, Poëa-Guyon S. The membrane domain of vacuolar H^+ATPase: a crucial player in neurotransmitter exocytotic release. Cell Mol Life Sci 2015; 72: 2561–73.

Myers CT, Mefford HC. Advancing epilepsy genetics in the genomic era. Genome Med 2015; 7: 91.

Narayanan M, Ramsey K, Grebe T, Schrauwen I, Szelinger S, Huentelman M, et al. Case report: compound heterozygous nonsense mutations in TRMT10A are associated with microcephaly, delayed development, and periventricular white matter hyperintensities. F1000Res 2015; 4: 912.

Padamsey Z, McGuinness L, Bardo SJ, Reinhart M, Tong R, Hedegaard A, et al. Activity-dependent exocytosis of lysosomes regulates the structural plasticity of dendritic spines. Neuron 2017; 93: 132–46.

Petrovski S, Wang Q, Heinzen EL, Allen AS, Goldstein DB. Genic intolerance to functional variation and the interpretation of personal genomes. PLoS Genet 2013; 9: e1003709.

Ramu A, Noordam MJ, Schwartz RS, Wuster A, Hurles ME, Cartwright RA, et al. DeNovoGear: *de novo* indel and point mutation discovery and phasing. Nat Methods 2013; 10: 985–7.

Roy A, Kucukural A, Zhang Y. I-TASSER: a unified platform for automated protein structure and function prediction. Nat Protoc 2010; 5: 725–38.

Rujano MA, Cannata Serio M, Panasyuk G, Péanne R, Reunert J, Rymen D, et al. Mutations in the X-linked ATP6AP2 cause glycosilation disorder with autophagic defect. J Exp Med 2017; 214: 3707–29.

Saitsu H, Nishimura T, Muramatsu K, Kodera H, Kumada S, Sugai K, et al. *De novo* mutations in the autophagy gene WDR45 cause static encephalopathy of childhood with neurodegeneration in adulthood. Nat Genet 2013; 45: 445–9.

Sambri I, D'Alessio R, Ezhova Y, Giuliano T, Sorrentino NC, Cacace V, et al. Lysosomal dysfunction disrupts presynaptic maintenance and restoration of presynaptic function prevents neurodegeneration in lysosomal storage diseases. EMBO Mol Med 2017; 9: 112–32.

Samocha KE, Robinson EB, Sanders SJ, Stevens C, Sabo A, McGrath LM, et al. A framework for the interpretation of *de novo* mutation in human disease. Nat Genet 2014; 46: 944–50.

Smith AN, Skaug J, Choate KA, Nayir A, Bakkaloglu A, Ozen S, et al. Mutations in ATP6N1B, encoding a new kidney vacuolar proton pump 116-kD subunit, cause recessive distal renal tubular acidosis with preserved hearing. Nat Genet 2000; 26: 71–5.

Stover EH, Borthwick KJ, Bavalia C, Eady N, Fritz DM, Rungroj N, et al. Novel ATP6V1B1 and ATP6V0A4 mutations in autosomal recessive distal renal tubular acidosis with new evidence for hearing loss. J Med Genet 2002; 39: 796–803.

Takamori S. Presynaptic molecular determinants of quantal size. Front Synaptic Neurosci 2016; 8: 2.

Takamori S, Holt M, Stenius K, Lemke EA, Grønborg M, Riedel D. Molecular anatomy of a trafficking organelle. Cell 2006; 127: 831–46.

Turner TN, Yi Q, Krumm N, Huddleston J, Hoekzema K, Stessman HAF, et al. denovo-db: a compendium of human *de novo* variants. Nucleic Acids Res 2017; 45: D804–11.

Van Damme T, Gardeitchik T, Mohamed M, Guerrero-Castillo S, Freisinger P, Guillemyn B, et al. Mutations in ATP6V1E1 or ATP6V1A cause autosomal-recessive cutis laxa. Am J Hum Genet 2017; 100: 216–27.

Van der Auwera GA, Carneiro MO, Hartl C, Poplin R, Del Angel G, Levy-Moonshine A, et al. From FastQ data to high confidence variant calls: the genome analysis toolkit best practices pipeline. Curr Protoc Bioinformatics 2013; 43: 11.10.1–33.

Verstegen AM, Tagliatti E, Lignani G, Marte A, Stolero T, Atias M, et al. Phosphorylation of synapsin I by cyclin-dependent kinase-5 sets the ratio between the resting and recycling pools of synaptic vesicles at hippocampal synapses. J Neurosci 2014; 34: 7266–80.

Wang D, Kranz-Eble P, De Vivo DC. Mutational analysis of GLUT1 (SLC2A1) in Glut-1 deficiency syndrome. Hum Mutat 2000; 16: 224–31.

Ware JS, Samocha KE, Homsy J, Daly MJ. Interpreting *de novo* variation in human disease using denovolyzeR. Curr Protoc Hum Genet 2015; 87: 7.25.1–15.

Yuan Y, Zhang J, Chang Q, Zeng J, Xin F, Wang J, et al. *De novo* mutation in ATP6V1B2 impairs lysosome acidification and causes dominant deafness-onychodystrophy syndrome. Cell Res 2014; 24: 1370–3.

Zhao J, Benlekbir S, Rubinstein JL. Electron cryomicroscopy observation of rotational states in a eukaryotic v-ATPase. Nature 2015; 521: 241–5.